

Aus dem Max-Planck-Institut für Herz- und Lungenforschung, Bad Nauheim

Am Fachbereich Biologie und Chemie  
der Justus-Liebig-Universität Gießen

---

Interferon Regulatory Factor 9 Promotes Lung Cancer Progression  
via Regulation of Versican

---

Inauguraldissertation

zur Erlangung des akademischen Grades

Doctor rerum naturalium

- Dr. rer. nat. -

Fachbereich Biologie und Chemie  
der Justus-Liebig-Universität Gießen

vorgelegt von

David Alexander Brunn

Cuxhaven 2021

Dekan: Prof. Dr. Thomas Wilke

1. Gutachter: Prof. Dr. Reinhard Dammann

2. Gutachter: Prof. Dr. Rajkumar Savai

Parts of this dissertation have been published:

Brunn, D., Turkowski, K., Günther, S., Weigert, A., Muley, T., Kriegsmann, M., Winter, H., Dammann, R. H., Stathopoulos, G. T., Thomas, M., Guenther, A., Grimminger, F., Pullamsetti, S. S., Seeger, W., Savai, R., *Interferon Regulatory Factor 9 Promotes Lung Cancer Progression via Regulation of Versican*. *Cancers (Basel)*, 2021. **13**(2):E208. Doi: 10.3390/cancers13020208

## I Table of content

I	Table of content .....	1
II	Summary .....	4
III	Zusammenfassung.....	6
1.	Introduction.....	8
1.1.	Lung cancer .....	8
1.1.1.	Classification.....	8
1.1.2.	Pathogenesis and risk factors.....	10
1.1.3.	Lung cancer therapy .....	12
1.2.	Tumour Microenvironment.....	15
1.2.1.	Characterisation and composition of the tumour microenvironment .....	15
1.2.2.	Endothelial cells.....	16
1.2.3.	Cancer-associated fibroblasts .....	16
1.2.4.	Myeloid-derived leukocytes .....	16
1.2.5.	Macrophages.....	17
1.2.6.	Lymphoid-derived leukocytes .....	17
1.2.7.	Extracellular matrix .....	18
1.3.	Interferon (IFN) .....	19
1.3.1.	Classification and canonical signalling.....	19
1.3.2.	Non-canonical type I IFN signalling .....	21
1.3.3.	Role of type I IFN in host defence .....	23
1.4.	Interferon Regulatory Factors .....	25
1.4.1.	Characterisation of IRF family members.....	26
1.4.2.	IRF9.....	28
1.5.	Versican .....	30
2.	Aims of the study .....	33
3.	Materials and Experimental Procedures.....	34
3.1.	Cell culture .....	34
3.1.1.	Cell lines and cultivation.....	34
3.1.2.	IFN stimulation .....	35
3.1.3.	Lentiviral transduction .....	35
3.1.4.	siRNA transfection.....	35
3.2.	Molecular Biology.....	36
3.2.1.	Protein Isolation and Western analysis.....	36

3.2.2.	RNA isolation and reverse transcription .....	36
3.2.3.	Quantitative real-time polymerase chain reaction (RT-qPCR) .....	37
3.2.4.	DNA isolation.....	39
3.2.5.	RNA-seq.....	39
3.2.6.	Immunocytochemistry .....	40
3.3.	Functional cell analysis.....	40
3.3.1.	Proliferation.....	40
3.3.2.	Migration.....	40
3.4.	Human data.....	41
3.4.1.	Kaplan-Meier analyses .....	41
3.4.2.	Gene expression profile using online tool USCS Xena .....	41
3.4.3.	Acquisition of human lung cancer samples.....	41
3.5.	Promoter analysis.....	42
3.5.1.	In-silico analysis of <i>VCAN</i> promoter .....	42
3.5.2.	Chromatin Immunoprecipitation .....	42
3.5.3.	Cloning.....	43
3.5.4.	Luciferase .....	44
3.6.	Histology.....	44
3.6.1.	Immunohistochemistry (IHC) .....	44
3.6.2.	Lung cancer tissue microarray (TMA) and xenograft tumours .....	45
3.6.3.	Haematoxylin & Eosin staining.....	45
3.7.	Animal experiments .....	45
3.7.1.	Mouse lines .....	45
3.7.2.	Genotyping of <i>Irf9</i> <sup>-/-</sup> mice .....	46
3.7.3.	Subcutaneous tumour model.....	46
3.7.4.	Intravenous tumour model .....	47
3.7.5.	Isolation and generation of bone marrow-derived macrophages (BMDM) .....	47
3.7.6.	Flow cytometry.....	48
3.8.	Statistical analysis.....	48
4.	Results .....	49
4.1.	IRF9 is highly expressed in human lung cancer patients.....	49
4.2.	IRF9 is highly expressed in lung and other cancer cell lines .....	52
4.3.	Stimulation with type I IFN upregulates IRF9 in cancer cells .....	54
4.4.	Characterisation of transduction of IRF9 constructs in human lung cancer cell lines .....	56
4.4.1.	Overexpression of IRF9 promotes oncogenic behaviour .....	56
4.4.2.	Knockdown of IRF9 reduces migratory and proliferative behaviour .....	58

4.5.	Characterisation of transduction of Irf9 constructs in murine lung cancer cell lines .....	60
4.6.	RNA-Sequencing of transduced cells identified VCAN as possible target of IRF9.....	62
4.7.	Evaluation of VCAN in lung adenocarcinoma in interaction with IRF9 .....	65
4.7.1.	VCAN expression correlates with IRF9 expression in lung cancer patients .....	65
4.7.2.	VCAN expression is influenced by IRF9 manipulation.....	66
4.7.3.	VCAN knockdown diminished oncogenic effect of IRF9 .....	68
4.8.	IRF9 regulates expression of VCAN .....	70
4.9.	IRF9 regulates tumour growth in vivo.....	72
4.9.1.	Subcutaneous tumour models of transduced cell lines .....	72
4.9.2.	Tumour models in global Irf9-knockout mice .....	74
5.	Discussion.....	78
5.1.	Role of IRF9 in lung cancer progression .....	78
5.1.1.	Relevance of IRF9 in cancer.....	78
5.1.2.	Non-canonical/IFN-independent upregulation of IRF9 promotes oncogenic features	79
5.1.3.	VCAN elicit oncogenic feature after IRF9 manipulation.....	83
5.2.	Relevance of IRF9 in TME .....	87
5.2.1.	Effects of IRF9 in stromal cells.....	87
5.2.2.	Effects of VCAN in stromal cells .....	88
5.3.	Conclusion .....	90
5.4.	Future Perspectives / Outlook .....	91
6.	List of Abbreviations.....	93
7.	List of Figures and Tables .....	98
7.1.	List of Figures.....	98
7.2.	List of Tables.....	99
8.	Literature.....	100
9.	Statement of Authenticity.....	111
10.	Acknowledgement .....	112
11.	Curriculum Vitae.....	113

## II Summary

Lung cancer is the leading cause of cancer-related death worldwide and accounts for more than 1.8 million deaths per year globally. It has been shown that the tumour microenvironment plays a crucial role in tumour progression and metastasis. Beside numerous cytokines, chemokines and other factors secreted by the tumour stroma, type I IFNs are strong immune modulators, showing anti-proliferative and pro-apoptotic properties. The transcription factor Interferon Regulatory Factor 9 (IRF9) is the key mediator in the canonical IFN pathway as it can bind directly to DNA at so-called interferon-stimulated response elements (ISRE).

Based on Kaplan-Meier estimators, high levels of IRF9 in lung cancer patients have been associated with a significantly lower survival. Using tissue microarrays, we could show that IRF9 is expressed in most of the lung cancer entities. In human lung cancer tissues, IRF9 is expressed in both the solid tumour part and the tumour microenvironment, where we identified strong expression of IRF9 in Tumour-Associated Macrophages. IFN treatment inhibited the proliferation of A549 and induced IRF9 expression, but it is also able to activate the expression of 2,000 other genes. To solely manipulate IRF9 expression, we used lentiviral particles to transduce the adenocarcinoma cell lines A549 and A427 to stably overexpress (A549/A427 LV IRF9) or to stably suppress IRF9 (A549/A427 shIRF9). Overexpression of IRF9 increased tumour cell proliferation and migration, whereas the knockdown of IRF9 accordingly led to a reduction. The transduction of murine lung cancer cell line CULA confirmed the oncogenic phenotype after overexpression; however, knockdown of murine *Irf9* failed to regulate tumour cell proliferation and migration. RNA-seq of transduced A549 identified 1544 regulated genes in IRF9-overexpressing cells, 662 regulated genes in IRF9-silenced cells and 117 genes that were commonly regulated, including the proteoglycan Versican (VCAN). Further analysis in human cell lines revealed a correlation between VCAN and IRF9 expression, and in silico analysis located potential ISRE in the promoter of VCAN. Chromatin-immunoprecipitation and luciferase studies proved that IRF9 binds at these sites and activates the expression of VCAN. According to the observations in transduced CULA cells, *Irf9* overexpression induced *Vcan* upregulation, whereas the knockdown of *Irf9* failed to regulate *Vcan*. Silencing of VCAN in transduced cells diminished IRF9-mediated proliferation and migration and was even stronger in IRF9-silenced cells. Additionally, we identified the tumour suppressor p21 to be affected by siVCAN transfection, indicating an IRF9-VCAN-p21 axis to regulate oncogenic behaviour in human lung adenocarcinoma.

We applied transduced cells in a subcutaneous tumour model, where increased (A549 LV IRF9) and accordingly decreased (A549 shIRF9) tumour sizes were observed. In accordance with in vitro results, CULA LV *Irf9* resulted in stronger tumour growth, but tumours from CULA sh*Irf9* did not differ from the control group. Naïve murine cancer cell line LLC1 was injected both intravenously and subcutaneously in *Irf9*<sup>-/-</sup> mice to study the role of *Irf9* in the tumour stroma. The loss of *Irf9* did not lead to changes in artificial tumour progression, but led to a reduction of macrophages, monocytes and natural killer cells within the tumour composition, indicating its beneficial influence in the tumour microenvironment.

Altogether, these results indicate that IRF9 influences tumour development and progression intrinsically and alters the cellular composition in the microenvironment. Tumour cell-specific inhibition of IRF9 provides a potential treatment for lung cancer, enabling higher specificity over a global inhibition of IFN pathway by bypassing collateral harm to beneficial stromal IFN and IRF9.

### III Zusammenfassung

Lungentumore sind weltweit die häufigste Todesursache für Krebs-bedingte Todesfälle und führen jährlich zu mehr als 1,8 Millionen Tote weltweit. Das Mikromilieu des Tumors (tumour microenvironment) nimmt maßgeblichen Einfluss auf die Tumorentwicklung und die Metastasierung. Neben zahlreichen Zytokinen, Chemokinen und weiterer Faktoren sezerniert das Tumorstroma auch Typ-I-Interferone (IFN). Sie besitzen stark immunmodulierende Eigenschaften, wirken antiproliferativ und proapoptotisch. Der Transkriptionsfaktor IRF9 (Interferon Regulatory Factor 9; Interferon-regulierender Faktor 9) nimmt im kanonischen IFN-Signalweg eine Schlüsselrolle ein. IRF9 kann dabei direkt an sogenannten ISRE (interferon-stimulated response elements; Interferon-stimulierte Reaktionselemente) in der DNA binden.

Kaplan-Meier-Kurven zeigen, dass Lungenkrebspatienten mit hoher IRF9-Expression signifikant geringere Überlebenschancen besitzen. Anhand Gewebefärbungen von Mikroarrays für IRF9 konnten gezeigt werden, dass der Transkriptionsfaktor in allen Lungenkrebstypen exprimiert wird. Weitergehende Färbungen zeigten, dass IRF9 sowohl in Krebszellen als auch im Stroma nachweisbar ist. Im Speziellen konnte es in Tumor-Assoziierten Makrophagen nachgewiesen werden. Die Stimulation von A549 mit IFN verringerte deren Proliferation und aktivierte die Expression von IRF9. Allerdings werden durch IFN etwa 2.000 verschiedene Gene hochreguliert, weshalb in der Folge ein Ansatz gewählt wurde, um die Expression von lediglich IRF9 zu verändern. Dabei wurden die Zelllinien A549 und A427 mittels lentiviraler Transduktion so verändert, dass diese nachhaltig IRF9 überexprimieren (A549/A427 LV IRF9) oder dessen Expression gemindert wird (A549/A427 shIRF9). Die Überexprimierung erhöhte die Proliferation und Migration der Tumorzellen, wohingegen diese durch den Knockdown entsprechend verringert wurden. Zusätzlich wurde die murine Zelllinie CULA transduziert, wobei die Überexprimierung ebenfalls den onkogenen Phänotyp verstärkte, der Knockdown hingegen nicht zu einer Veränderung führte. Mittels RNA-seq transduzierter A549 konnte folgende Regulation festgestellt werden: in IRF9-überexprimierenden Zellen war die Expression von 1544 Genen verändert; in Knockdown-Zellen dagegen 662 Gene; 117 Gene waren in beiden Konditionen verändert. Zu letzteren gehörte das Proteoglykan Versican (VCAN), dessen Expression mit der von IRF9 korrelierte. In-silico-Modelle lokalisierten potenzielle ISRE im VCAN-Promotor. Durch Chromatin- und Luciferase-Untersuchungen wurde die Bindung von IRF9 an diesen Stellen und die damit einhergehende Expression von VCAN bestätigt. Entsprechend den vorhergehenden Ergebnissen konnte in CULA LV Irf9 erhöhte VCAN Level nachgewiesen werden, wohingegen in CULA shIrf9 keine veränderte VCAN-Expression festgestellt wurde. Der Knockdown von VCAN verringerte die durch IRF9 induzierte Proliferation und Migration. Dieser Effekt war umso stärker, sobald IRF9 zuvor bereits verringert war. In diesen Prozessen war der Tumorsuppressor p21 involviert. Dies lässt auf eine IRF9-VCAN-p21-Achse schließen, die in humanen Lungenadenokarzinomen Einfluss auf den onkogenen Phänotyp nimmt.

Die transduzierten Zellen wurden in einem Subkutan-Tumormodell verwendet. Dabei führte die Injektion von A549 LV IRF9 zu größeren Tumoren, A549 shIRF9 zu kleineren. CULA LV Irf9 ebenfalls größere Tumore, während CULA shIrf9 sich nicht von der Kontrollgruppe

unterschied. Durch die Injektion der murinen Lungenkrebs-Zelllinie LLC1 in *Irf9*<sup>-/-</sup>-Mäuse konnte die Rolle von IRF9 im Tumorstroma untersucht werden, hier führte die Abwesenheit von Irf9 weder nach subkutaner noch nach intravenöser Injektion zu einer Zunahme der Tumorgroße oder Anzahl der Lungentumore. Die Deletion von *Irf9* führte in der Zusammensetzung der untersuchten Tumore und Lungen zu einer Abnahme an Makrophagen, Monozyten, sowie Natürlicher Killerzellen. Dies lässt auf einen positiven Einfluss von IRF9 im Tumormikromilieu schließen.

Zusammenfassend wird in dieser Arbeit der Einfluss von IRF9 auf das Tumorstromawachstum aufgezeigt, sowohl tumorzell-intrinsisch als auch innerhalb des Tumormikromilieus. Tumorzell-spezifische Inhibierung von IRF9 könnte eine potenzielle Therapie gegen Lungenkrebs darstellen, die gezielter und nebenwirkungsärmer agieren würde als eine gesamtstrome Inhibierung des grundsätzlich nützlichen IFN-Signalwegs.

## 1. Introduction

### 1.1. Lung cancer

#### 1.1.1. Classification

Tumour diseases are the leading cause of death worldwide, with increasing incidence and mortality [1]. In 112 of 183 countries, cancer is one of the main cause of death among the population (< 70 years), particularly in developed countries [1]. Although lung cancer is not the type of cancer with the highest incidence (14.3% in male, 8.4% in female; Figure 1), it is the leading cause of cancer-related deaths worldwide (21.5% in male, 13.7% in female; Figure 2) [1, 2]. In 2020, over 2.2 million cases were diagnosed, resulting in almost 1.8 million deaths [1]. In the European Union alone, tumour diseases are responsible for about one quarter of all deaths and are only exceeded by diseases of the circulatory system [3]. Lung cancer is characterised by an uncontrolled tumour cell proliferation initiating in the lung, but with progression metastases occurring at near and more distant areas within the body [2, 4]. At an early stage, symptoms of lung cancer mostly appear unsuspecting and unspecific (e.g. cough, weight loss) [5]. The occurrence and severity of symptoms grow as they are caused not only by the primary tumour (e.g. chest pain, dyspnoea, haemoptysis), but also by metastases (fatigue and weakness, bone or abdominal pain) [5].

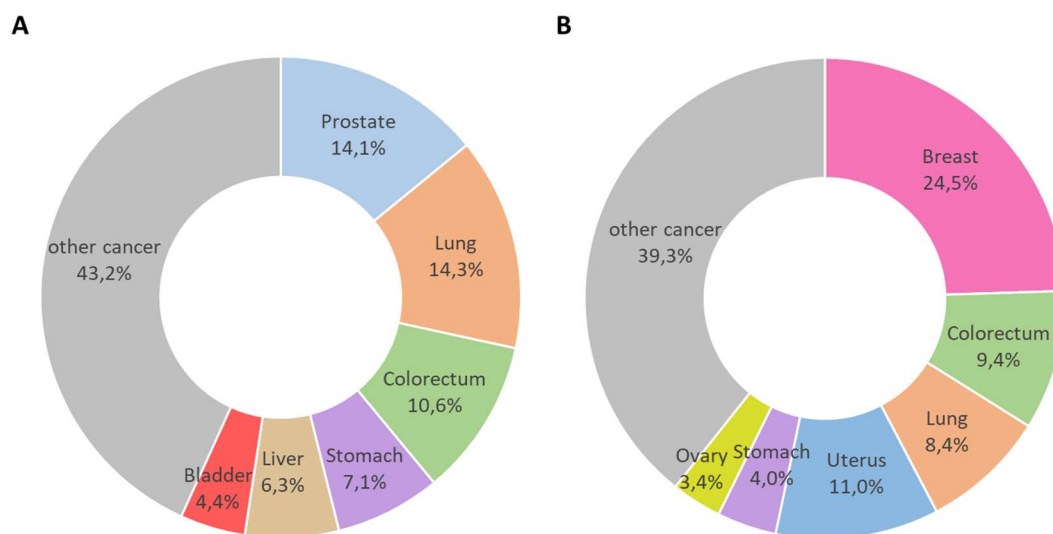


**Figure 1. Distribution of worldwide cancer incidence in 2020.** Divided in males (A) and females (B). Data are shown as percentages (adapted from Sung, H., et al., 2021 [1]).

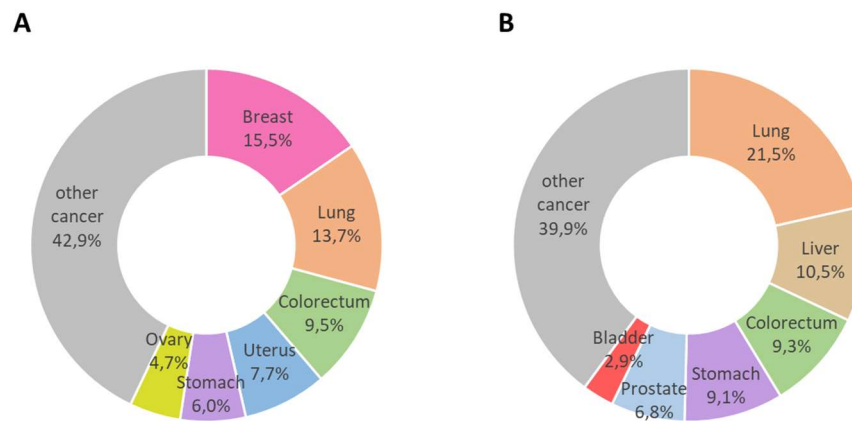


**Figure 2. Distribution of worldwide cancer mortality in 2020.** Divided in males (A) and females (B). Data are shown as percentages (adapted from Sung, H., et al., 2021 [1]).

Based on the histological type, lung cancer is classified into small-cell lung carcinoma (SCLC) and non-small-cell lung carcinoma (NSCLC), and the histology is critical to choose the most effective therapy and to estimate the individual prognosis [6].

SCLC have a prevalence of 15% and are characterised by a dense cellular appearance [6]. NSCLC account for about 80% of all lung cancers and can be subclassified further into adenocarcinoma (LUAD), squamous cell carcinoma (LUSC) and large cell carcinoma (LCC) with a prevalence of 40%, 25% and 10%, respectively [6]. Other classes, such as carcinoid lung carcinoma or bronchial gland lung carcinoma, are diagnosed comparatively rarely (< 5%) [6].

In addition to having a histological classification, tumours are classified by stages, which are defined and regularly reviewed by the Union Internationale Contre le Cancer (UICC) and the American Joint Committee on Cancer (AJCC). Staging via TNM classifies the harmonised anatomic extent of tumours, prognosis and therapy [4]. These three criteria are assessed based on (i) the extent of the primary tumour (T1–T4), (ii) the involvement of lymph nodes (N0–N3), and (iii) metastases (M0–M1) [4]. Every TNM criterion is subdivided based on size, number, region and so on (e.g. T1a–T1c, N2a1, M1a–M1c) [4]. Eventually a harmonised grouping of these criteria results in lung cancer stage reaching from IA1 (small tumour, no lymph nodes involved, no metastases) to IVB (metastases at near and distant sites, involvement of near and distant lymph nodes), which is visualised in Table 1 [4].

T/M	Label	N0	N1	N2	N3
T1	T1a	IA1	IIB	IIIA	IIIB
	T1b	IA2	IIB	IIIA	IIIB
	T1c	IA3	IIB	IIIA	IIIB
T2	T2a	IB	IIB	IIIA	IIIB
	T2b	IIA	IIB	IIIA	IIIB
T3	T3	IIB	IIIA	IIIB	IIIC
T4	T4	IIIA	IIIA	IIIB	IIIC
M1	M1a	IVA	IVA	IVA	IVA
	M1b	IVA	IVA	IVA	IVA
	M1c	IVB	IVB	IVB	IVB

**Table 1. Lung cancer stage grouping based on TNM classification, 8<sup>th</sup> Edition.** T, extent of the primary tumour. N, involvement of lymph nodes; M, distant metastases. Stages reach from I to IV with subclasses, respectively (adapted from Detterbeck, F. C., et al., 2017 [4]).

### 1.1.2. Pathogenesis and risk factors

Lung cancer prevalence increases with age, with an overall average age of 71 years at diagnosis [2]. Similar to other cancer entities, individual factors such as region and development, gender, lifestyle and environment can influence risk. The main risk factor for lung cancer is smoking, which is estimated to cause 80–90% of all cases, and it is proportional with smoking intensity and duration [6, 7]. Thereby, smoking duration has a stronger impact than intensity, with a 20- to 50-fold increased risk for long-term smokers compared to never-smokers [8]. Tobacco smoke contains over 5,000 compounds, of which 73 are identified as carcinogenic; thereby, to quit smoking is an effective way to reduce individual risk for lung cancer [9, 10].

It is notable that only about 10% of all lung cancer patients are non-smokers and mostly diagnosed with LUAD, whereas other classes are mainly associated with and found in smokers [2, 6, 10]. Since only about 15% of all smokers develop lung cancer, additional factors influence prevalence. Furthermore, environmental smoke and exposure to other carcinogens such as asbestos or radiation are known risk factors for non-smokers. Notably, not only medical radiation by radiotherapy or radiodiagnosis but also indoor exposure to radon has a significant impact on lung cancer risk [6, 7].

Chronic, non-malignant lung diseases such as chronic obstructive pulmonary disease (COPD), tuberculosis and asthma are associated with lung cancer incidence. It is suggested that chronic inflammation, together with the expression of highly inflammatory cytokines, can lead to a repetitive cycle of bronchial injury and repair. Furthermore, anti-apoptotic and pro-angiogenic

signalling are promoted with persisting inflammatory signalling, which increases the risk of an eventually malignant transformation of normal airway epithelium [8, 11].

The origin of tumours presents a distinct difference within NSCLC. LUADs presumably arise from alveolar type II cells, bronchioalveolar stem cells or Clara cells; hence, they are found at more distant locations. Conversely, LUSCs are found at proximal sites and may originate from tracheal basal cells [12].

Since it is known that genetic alterations influence the progression and classification of lung tumours, large cohort studies on frequency, influence and targeted therapies have been emerging [5, 12]. Table 2 highlights some of the most frequent and relevant mutations in lung cancer patients differentiated for the lung cancer classes LUAD, LUSC and SCLC [12, 13]. The mutation either leads to an increase in oncogenic activity (e.g. epidermal growth factor receptor [EGFR]; Kirsten rat sarcoma virus [KRAS]) or results in lost or diminished effects of tumour suppressor genes (e.g. tumour protein p53 [TP53]).

Alteration	Lung adenocarcinoma (NSCLC)	Lung squamous carcinoma (NSCLC)	Small-cell lung carcinoma
<i>EGFR</i>	14.3–39.6%	< 5%	Very rare
<i>FGFR1</i>	< 1%	20%	5–6%
<i>ALK</i>	3–13%	N/A	N/A
<i>PDGFRA</i>	6–7%	4%	N/A
<i>HER2</i>			
mutation	2–4%	Very rare	Very rare
amplification	5–10%	Very rare	Very rare
<i>KRAS</i>	14.9–32.6%	Very rare	Very rare
<i>BRAF</i>	1–2%	Very rare	Very rare
<i>NF1</i>	12%	10%	Very rare
<i>PIK3CA</i>			
mutation	4.4–6.9%	16%	Very rare
amplification	29%	30–40%	5%
<i>MYC</i>	31%	Very rare	16%
<i>TP53</i>	35.1–61.4%	81%	93.6%
<i>PTEN</i>	2.2%	8%	10%

**Table 2. Frequencies of genetic alterations in lung cancer, divided by classes.** ALK, ALK receptor tyrosine kinase; PDGFRA, platelet derived growth factor receptor alpha; HER2, erb-b2 receptor tyrosine kinase 2; BRAF, B-Raf proto-oncogene, serine/threonine kinase; NF1, neurofibromin 1; PIK3CA, phosphatidylinositol-4,5-bisphosphate 3-kinase catalytic subunit alpha; MYC, MYC proto-oncogene, bHLH transcription factor; PTEN, phosphatase and tensin homolog (adapted from Tan, W. L., et al. 2016 and Chen, Z., et al., 2014 [12, 13]).

A highly prominent mutation affects EGFR and can be found in 14.3 to 39.6% of all LUAD patients. EGFR is the receptor for various growth factors, such as the epidermal growth factor (EGF), and belongs to the receptor tyrosine kinases (RTK) amongst others (e.g. fibroblast GFR (FGFR) and vascular endothelial GFR (VEGFR)). When ligands bind to the receptor, tyrosine residues of the intracellular part become phosphorylated, which is the start of the downstream signalling cascade, inter alia, to activate cell proliferation and migration. Mutations of EGFR can result in increased amplification or gain of function. In both cases, this leads to an abnormal

oncogenic activity [13-15]. Due to the clinical relevance and the oncogenic effects of RTKs, pharmacological substances targeting these kinases have been emerging.

Another widely mutated proto-oncogene is the GTPase KRAS, which belongs to the RAS family. Active KRAS binds to GTP, where it enables signal transduction of growth factors and regulates cell proliferation. Acting as a switch, GDP-binding KRAS is inactive, and GDP needs to be replaced by GTP before KRAS can act as signal transducer again. The most relevant mutation in NSCLC occurs at codon 12, where the mutation leads to an exchange of glycine to, inter alia, cysteine (G12C), valine (G12V) or aspartic acid (G12D) and functionally results in a constitutively active KRAS form. Lung cancer patients bearing KRAS mutations face a poor prognosis [16, 17]. Another common mechanism of tumour promotion is the loss of suppressing functions by mutation. One prominent example is the tumour suppressor p53, encoded by the gene *TP53*. Often described as ‘the guardian of the genome’, p53 is a crucial tumour suppressor responsible for DNA damage repair, cell cycle arrest or induction of apoptosis. Most mutations lead to missense mutations and loss of heterozygosity rather than complete loss of p53; however, a reduction of functional p53 results in tumour development and progression and is associated with lower survival probability [18].

### 1.1.3. Lung cancer therapy

The late-stage diagnosis of lung cancer patients due to inconspicuous symptoms dramatically reduces their survival rate. In general, the overall 5-year survival rate of SCLC patients is much lower compared to NSCLC patients with only about 7% and 24%, respectively [6, 7]; as demonstrated in Table 3, this survival rate decreases in accordance with staging [4]. Depending on tumour staging and physiological condition, therapy includes surgical resection, radiotherapy and adjuvant chemotherapy.

Type	IA1	IA2	IA3	IB	IIA	IIB	IIIA	IIIB	IIIC	IVA	IVB
Clinical	92	83	77	68	60	53	36	26	13	10	0
Pathological	90	85	80	73	65	56	41	24	12	-	-

Table 3. Average 5-year overall survival of lung cancer patients [%] divided by clinical and pathological stage grouping. (adapted from Detterbeck, F. C., et al. 2017 [4]).

### Surgery/Surgical resection

Surgical resection is described as first-line therapy of NSCLC patients for the stages I and II that aims to completely remove the primary tumour. It further includes the additional removal of lymph nodes to complete patients’ staging and to evaluate metastatic events. Surgery can be highly effective for early-stage NSCLC patients but is not considered first-line therapy for SCLC. Lobectomy is performed to remove the affected pulmonary lobe completely, either by open surgery or video- or robotic-assisted surgery. Lobectomy reduces the recurrence risk compared to sublobar resection, where only affected parts are excised. However, based on physiological condition and individual risks, lobectomy is not feasible for every patient. Surgery can be included in the

therapeutic management of Stage III patients depending on the evaluation of lymph nodes, and it is an option for Stage IIIA; nevertheless, for stage IIIB and onwards and depending on the number of metastatic sites, the guidelines do not propose resections [6, 7, 19].

### **Radiotherapy**

Radiation therapy uses ionising radiation directly to the cancerous site, aiming to kill malignant cells. Radiation leads to DNA damage and eventually to cell death. In lung cancer therapy, it can be used for all stages, mostly in combination with either surgery, chemotherapy or both in a tri-modality approach. Although it is not recommended after lobectomy, radiotherapy can be beneficial after surgeries with incomplete resections or for non-operable tumours. Technical advances and accurate imaging of tumour localisation, in particular, allow a more precise delivery of radiation, thus improving radiotherapy and decreasing side effects. Stage I and II NSCLC patients benefit from stereotactic ablative body radiotherapy (SABR), where high doses of radiation are accurately delivered and healthy tissue is less affected. Another approach that can reduce side effects is intensity-modulated radiotherapy (IMRT), which uses radiation of different intensities.

SCLC patients can particularly benefit from radiotherapy; although optimal dosages and durations are subject to debate, trials have shown that durations of less than 30 days are associated with a better outcome. Alongside curative approaches, low-dose radiotherapy plays an important role at incurable stages in palliative medicine to reduce symptoms and to improve life quality [7, 19, 20].

### **Chemotherapy**

Despite the emerging role of novel targeted and immunological strategies, conservative cytotoxic chemotherapy is still critical. Guidelines recommend a platinum-based chemotherapy favouring cisplatin for younger patients and carboplatin for elder patients due to its less hazardous side effects [21]. However, when comparing cisplatin-gemcitabine, cisplatin-paclitaxel, cisplatin-docetaxel, and carboplatin-paclitaxel, other clinical trials have failed to demonstrate superiority of one or the other platinum-based agents in combination with additional substances [21, 22].

When cisplatin is taken up by the cells, it interacts with DNA and can form covalent bonds to purine bases resulting in both interstrand and intrastrand crosslinks [23]. Those platinum-DNA adducts eventually lead to a reduction of DNA replication and transcription as well as cell cycle arrest via the activation of p53. Further, caspases (CASP8, CASP9) are activated and induce apoptosis [23]. It has been reported that an increased DNA repair or a reduced cellular accumulation of cisplatin can lead to resistance in lung cancer therapy and that cisplatin can be neutralised by sulphur-containing molecules such as glutathione or metallothionein [24-26].

Paclitaxel has been approved for first-line therapy of NSCLC together with cisplatin [22]. It interferes with the  $\beta$ -tubulin subunits of microtubules, stops depolymerisation and eventually prevents cellular mitosis [27]. Although it is not fully understood how tumour cells die under paclitaxel treatment, but cell death at G1 cell cycle phase is reported as well as the activation of the

BCL2 apoptosis regulator (BCL2) [27, 28]. Chemoresistant cells show post-translational modifications of  $\beta$ -tubulin to reduce the affinity of paclitaxel [28].

The anthracycline doxorubicin intercalates into the DNA double helix and impairs DNA amplification and transcription [29]. It can bind to topoisomerase enzymes I and II and prevents resealing of DNA strands, resulting in cytotoxic DNA damage and eventually both cell cycle arrest and induction of apoptosis [29, 30]. The upregulation of ABC transporters and the increase of DNA repair mediate resistance to Doxorubicin [29]. Interestingly, NSCLC show a higher resistance in vitro and in vivo than SCLC [31].

### Targeted therapy

With the increasing knowledge about genetic alterations in lung cancer, targeted therapies have been emerging. This enables patient-fit therapeutic strategies to enhance survival and life quality but requires individual screening for potential mutations. The use of tyrosine kinase inhibitors (TKIs) stands for a targeted therapy, for instance in NSCLC patients with EGFR mutations. Exon 19 deletion or L858R point mutations are highly sensitive against TKI Erlotinib, whereas patients with T790M mutation benefit more from Osimertinib than from Erlotinib therapy [13]. The use of monoclonal antibody Cetuximab can be another option for inhibiting EGFR [32], and other TKIs such as Crizotinib or Alectinib have been approved for treating ALK-positive tumours and Dabrafenib for BRAF V600E mutations [13].

### Immunotherapy

Immunotherapy is a rising and promising approach to increase survival, particularly for patients who do not respond to conventional therapy. The regulation and interaction of programmed death receptor 1 (PD-1; encoded by *PDCD1*) and its ligand PD-L1 (*CD274*) are effective mechanisms for cancer cells to escape cell death. PD-1 is an immune checkpoint expressed by T cells to prevent excessive immune reactions such as autoimmune diseases. PD-L1 is expressed on the surface of cancer cells, where upregulation not only leads to an evasion of host immune reaction but is also associated with a lower survival of patients. When PD-L1 binds to PD-1, the antitumoural answer of T cells is reduced, and tumour cells are not attacked. Immune checkpoint inhibitors target PD-1 or PD-L1 and inhibit their interaction. Particularly in patients with high PD-L1 levels, checkpoint inhibitors reactivate an appropriate T cell answer of the immune system followed by a macrophage-mediated cell depletion. The recombinant antibodies Pembrolizumab and Nivolumab target PD-1, Atezolizumab and Durvalumab recognise PD-L1, and all four have been approved for treating NSCLC. It can be noted that immune checkpoint inhibitors are highly effective and associated with less toxic side effects [13, 33-35].

Novel approaches enhance the outcome of lung cancer therapy and can improve the life quality of patients. However, conventional approaches are the cornerstone of the therapeutic strategy eventually associated with severe side effects and therapy resistance, which remains a limiting factor in successful therapy outcome. Innovative approaches target the tumour microenvironment and its related structures, which allows to re-activate the host's defence and reduce escape or resistance mechanisms. Promising targets are such as tumour-associated macrophages (TAMs), cancer-

associated fibroblasts (CAFs), extracellular matrix (ECM) or various cytokines, growth factors, and signalling of the tumour microenvironment.

## 1.2. Tumour Microenvironment

### 1.2.1. Characterisation and composition of the tumour microenvironment

Relevant cancer research has been gradually focusing on the tumour stroma, and the amount of scientific work about the tumour microenvironment (TME) has been on a continuous increase. It was demonstrated that stromal cells influence tumour progression and development by crosstalk with cancer cells [36]. This crosstalk is already activated early, allowing the tumour to mediate a supportive environment while growing. Among other mechanisms, it includes angiogenesis to guarantee oxygen and nutrient supply and removal of cytotoxic metabolic waste [37]. TME does not consist only of resident and infiltrating stromal cells, but it also include the extracellular matrix (ECM) and all the secreted cytokines and factors within [37]. As visualised in Figure 3, the role of the TME cannot be generalised, and depending on the tumour type, both tumour-promoting and suppressive TMEs are described [37].

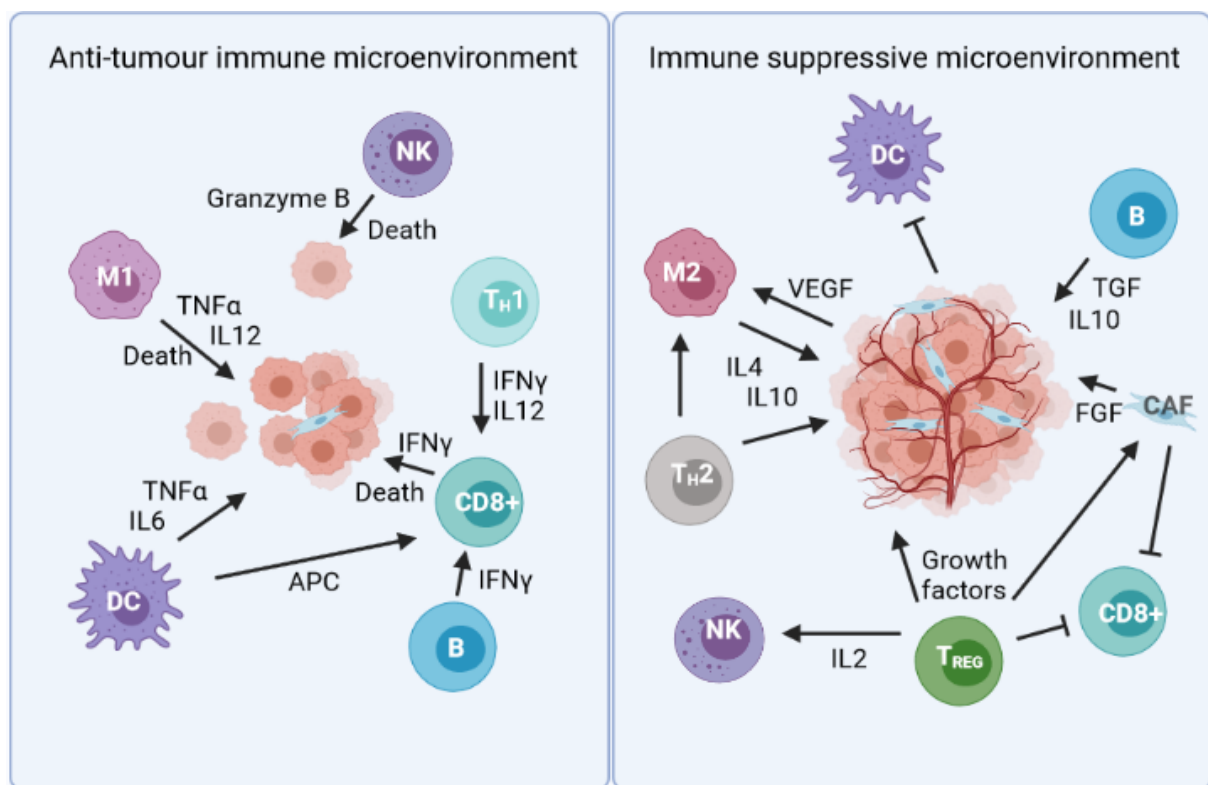


**Figure 3. Impact of microenvironmental cells on tumour development.** Immune cells influence tumour growth and development by providing either an anti-tumour or an immune suppressive environment. Natural killer cells (NK), M1 macrophages (M1) and cytotoxic T cells (CD8+) can induce cancer cell death by secretion of Granzyme B, Tumour Necrosis Factor  $\alpha$  (TNF $\alpha$ ), Interleukin 12 (IL12) or type II interferon (IFN $\gamma$ ), respectively. CD8+ cells are activated by antigen-presenting cells (APC; e.g., Dendritic cells [DC]) or via IL12 and IFN $\gamma$  (B cells [B], T helper 1 cells [T<sub>H</sub>1]). In a suppressive TME, the tumour can inhibit DC activity. Regulatory T cells (T<sub>REG</sub>) suppress the activation of CD8+ cells. Various immune cells, such as M2 macrophages (M2), T helper 2 cells (T<sub>H</sub>2), B cells, T<sub>REG</sub> and cancer-associated fibroblasts (CAF) can stimulate tumour growth by secretion of growth factors such as the transforming growth factor (TGF), fibroblast growth factors (FGF) and vascular endothelial growth factor (VEGF) or immunosuppressive cytokines (e.g. IL4, IL10, IL2; adapted from Anderson, N. M., Simon, M. C., 2020 [37]).

### 1.2.2. Endothelial cells

Endothelial cells form a monolayer, building the vascular endothelium of blood vessels and capillaries. It is a barrier between the blood and its components and the surrounding tissue, but depending on the associated tissue or organ, its permeability can vary significantly. The mechanism of endothelial cells building new vessels is called angiogenesis [37], which occurs at an early timepoint of tumour formation as a crucial process to guarantee the supply of oxygen and nutrients of the growing tumour. Hypoxia develops once the existing vasculature is not adequate to provide enough oxygen at a tumour size of 1 mm<sup>3</sup> [37, 38]. Together with other oncogenic signalling, VEGF expression – the key player of angiogenesis – is induced [39]. This process includes capillary sprouting, chemoattraction of endothelial progenitor cells and regulation of endothelial cell proliferation [37]. Due to an impaired maturation process, freshly formed vessels are highly permeable and enable the evasion and migration of tumour cells [37, 38]. Several immune cells, such as macrophages and neutrophils, can promote angiogenesis within the TME [36, 39, 40].

### 1.2.3. Cancer-associated fibroblasts

Cancer-associated fibroblasts (CAFs) are one of the most abundant cell types within the TME. They can derive from resident fibroblasts, bone-marrow derived mesenchymal cells or smooth muscle cells (myofibroblasts) and are responsible for ECM structure [41]. CAFs can secrete growth factors and other cytokines that stimulate tumour cell proliferation, such as fibroblast growth factors (FGF); with the influence on the stroma structure, CAFs promote tumour cell migration [36, 41, 42].

### 1.2.4. Myeloid-derived leukocytes

Leukocytes originating from myeloid progenitors include monocytes, macrophages, mast cells, dendritic cells, and granulocytes. Myeloid leukocytes are a major part of the immune system and host defence. Within the TME, however, they eventually support the progression and migration of tumour cells by secreting cytokines, chemokines, metalloproteinases or reactive oxygen species (ROS) [37, 43]. Mast cells, for instance, are known to release pro-tumoural cytokines such as transforming growth factor  $\beta$  (TGF $\beta$ ), interleukin 10 (IL10) and VEGF. Nevertheless, mast cells are also known to activate immune cell invasion via C-C motif chemokine ligand 5 (CCL5), induce T cell activation and secrete pro-inflammatory cytokines such as IL1 $\beta$ , IL6 and tumour necrosis factor (TNF $\alpha$ ) [44, 45]. A study with 65 NSCLC patients demonstrated that the prognosis correlated positively with the intratumoural density of mast cells [46]. Dendritic cells (DCs), as antigen-presenting cells, process and present antigens on their surface to other immune cells, such as T cell and B cells [44]. Tumour-infiltrating DCs have been described to switch their phenotype to support the immune evasion of tumour cells and suppress the T cell response via upregulation of PD-1 (programmed cell death 1) [37, 47].

### 1.2.5. Macrophages

Macrophages are a major cell type within the TME, with wide functions reaching from activating the immune response, including phagocytosis, to eventually tumour support by secretion of immune-suppressive cytokines and growth factors. Macrophages can originate from different sources: (i) most tissue macrophages arise from the yolk sac progenitors; (ii) macrophages involved in pathogen response derive from circulating bone marrow-derived monocytes; and (iii) macrophages differentiate from a splenic monocyte reservoir [48, 49]. The cytokine colony stimulating factor 1 (CSF1) is the key player in chemoattraction of macrophages to the tumour part [50]. Similar to T helper cells, tumour-associated macrophages (TAMs) show an enormous plasticity and can be polarised into tumour-suppressive M1 macrophages by stimulation with lipopolysaccharides (LPS) and IFN $\gamma$  or into tumour-promoting M2 macrophages by stimulation with IL4, IL10 and IL13 [51]. It may be noted that around 70% of TAMs are M2, and the overall TAM infiltration is associated with a poor prognosis in lung cancer [51, 52]. However, the ratio of M1/M2-TAMs, a close distance of M1-TAMs to tumour cells as well as a distant juxtaposition of M2-TAMs to tumour cells are beneficial for survival probability [51].

Even though recent studies have suggested a more distinct subclassification of macrophages, M1 and M2 phenotypes are still commonly used. M1 TAMs act as anti-tumourigenic by phagocytosis, the secretion of pro-inflammatory cytokines (e.g. TNF $\alpha$ , IL1 $\beta$ , IL12) and the release of ROS and nitric oxide (NO) [50]. The pro-inflammatory profile of M1 macrophages can also activate other immune cells such as T<sub>H</sub>1 cells and NK (Natural Killer) cells [50, 51]. In direct contrast, M2 macrophages have tumour-supporting features. With the secretion of IL4, IL10 and TGF $\beta$ , M2 TAMs suppress an adequate immune response and further activate T<sub>H</sub>2 cells. The expression of ARG1 (Arginase 1), CHIT1 (Chitinase 1) or MMP9 can influence ECM remodelling and collagen formation [37, 50]. M2 TAMs express PD-L1 and PD-L2, which further reduce the activation of cytotoxic T cell and NK cells [49]. In addition, the secretion of VEGF and platelet-derived growth factor (PDGF), amongst other growth factors, which directly promoted tumour growth and neoangiogenesis, has been demonstrated [49, 50]. Further, it has been shown that the therapeutic inhibition of VEGF can reduce macrophage infiltration [53]. PD-L1 inhibitors follow a similar approach and can restore a macrophage-mediated T cell activation [50].

### 1.2.6. Lymphoid-derived leukocytes

Leukocytes deriving from lymphoid progenitors include NK cells and T and B lymphocytes. As their name suggests, circulating NK cells can kill cells and are involved in immunosurveillance of the host's defence [37, 54]. The cytotoxic effect of NK cells is enabled via Granzyme B and death receptor signalling (e.g. TRAIL). NK cells can also activate further immune responses by secretion of pro-inflammatory molecules such as interferon  $\gamma$  (IFN $\gamma$ ), IL6 or TNF $\alpha$  [54]. However, the phenotype can switch to immunosuppressive when NK cells exit the bloodstream and infiltrate the tumour; hence, the reactivation of NK cells is a promising approach to treating NSCLC patients [54, 55].

T cell populations are classified by the expression of transmembrane receptor CD4 and CD8. CD4+ T cells with their most prominent members T<sub>H1</sub> (T helper 1) and T<sub>H2</sub> cells are subclassified based on their differentiation, where T<sub>H1</sub> differentiate upon IL12 stimulation and T<sub>H2</sub> upon IL4. Overall, it can be noted that T<sub>H1</sub> cells mediate an anti-tumour immune response, including the activation of macrophages and cytotoxic CD8+ T cells by secretion of IFN $\gamma$  and TNF $\alpha$  [37, 56]. In contrast, T<sub>H2</sub> cells secrete IL4, IL5 and IL10, thereby activating a tumour-promoting immune response of macrophages and inducing tumour cell proliferation [37, 56]. It has been shown that for the prognosis of breast cancer patients, the ratio of T<sub>H1</sub> and T<sub>H2</sub> cells is more relevant than the overall infiltration of CD4+ lymphocytes [57]. Moreover, research addressing other T helper cells besides well-characterised T<sub>H1</sub> and T<sub>H2</sub> cells has been emerging. Upon tumour-secreted IL9 or IL17, T helper cells differentiate into T<sub>H9</sub> and T<sub>H17</sub> cells, respectively, which have been shown to promote tumour cell proliferation and enhance migration in lung cancer [58]. Another subtype of T cells are regulatory T cells (T<sub>REG</sub>), which, in addition to CD4, also express FOXP3 [56]. It has been demonstrated that within the TME, T<sub>REG</sub> modulate NK cell activity and suppress cytotoxic CD8+ T cells [37, 56]; in NSCLC patients, the prognosis worsens with an increased amount of infiltrating T<sub>REG</sub> cells [59].

As previously described, cytotoxic T cells (CD8+) are activated by antigen-presenting cells and T<sub>H1</sub> cells to promote an anti-tumour response [37, 56, 60]. Like NK cells, cytotoxic T lymphocytes can kill unfamiliar cells by Granzyme B and Perforin secretion [56, 60]. The complex interaction between T cells and tumour cells is not fully understood; however, that between tumoural PD-L1 and PD-1 of cytotoxic T cells can reduce cytotoxic function and eventually induce T cell apoptosis, which is why aforementioned checkpoint inhibitors represent a promising therapeutic approach [33, 60].

### 1.2.7. Extracellular matrix

The extracellular matrix (ECM) provides the surrounding structure of cellular compartments and is a non-cellular component of the microenvironment. It includes collagens, proteoglycans, fibronectin, elastin, laminin and hyaluronan (HA). The composition varies based on the function and localisation of the tissue. Within cancer entities, solid tumours consist of up to 50% of ECM depending on their site and stage. CAFs are the predominant cell type contributing to the ECM [61], which was mistakenly believed not to play a role in tumour progression for a long time; however, recent studies have demonstrated a negative correlation between large collagen amounts and a poor prognosis of breast cancer patients [37]. Since the ECM holds back a massive amount of cytokines, chemokines and growth factors, its proteolytic degradation can release these factors and thereby boost tumour cell proliferation and migration [37, 61]. The ECM degradation further assists cancer cells in evading the solid tumour and enhances metastasis [61], which explains why the enrichment of matrix metalloproteases (MMP) is associated with lower survival [62]. Interestingly, a stiff ECM structure promotes tumour cells to reduce epithelial features and switch to a mesenchymal phenotype – the so-called epithelial-mesenchymal transition [61]. Furthermore,

it was shown that by regulation of integrins and protein tyrosine kinase 2 (FAK), the ECM increases tissue stiffness and facilitates chemoresistance [61, 62].

### 1.3. Interferon (IFN)

Beside numerous cytokines, chemokines and other factors secreted by microenvironmental cells and tumour cells, Interferons (IFNs) are a major cytokine class; typically, they modulate the host defence response against pathogens, predominantly viral infections [63]. The scientists Isaacs and Lindenmann discovered that an IFN is released upon influenza exposition and interferes with viral replication, hence why it was named it Interferon [64]. IFNs are classified into three main types (type I-III IFN) based on their signalling and on the respective receptors they address.

#### 1.3.1. Classification and canonical signalling

##### Type I IFN

Type I IFNs commonly bind to the IFN $\alpha$ / $\beta$  receptor complex (IFNAR), which consists of IFNAR1 and IFNAR2 [65]. Members are predominantly IFN $\alpha$  (13 subtypes) and IFN $\beta$  (2 subtypes) as well as IFN $\epsilon$ , IFN $\kappa$ , IFN $\omega$ , IFN $\delta$ , IFN $\zeta$ , and IFN $\tau$  [65]. When type I IFNs bind to one of the IFNAR, the remaining IFNAR is recruited to form a ternary complex inducing downstream signalling [66]. This spatial proximity enables tyrosine kinases that are associated with the cytosolic domain of the receptors to transphosphorylate each other; tyrosine kinase 2 (TYK2) is associated with IFNAR1 and Janus kinase 1 (JAK1) with IFNAR2 (Figure 4) [66, 67]. Phosphorylation of the kinases creates docking sites for members of the STAT family (signal transducer and activator of transcription), which are eventually phosphorylated [67]. Phosphorylated STAT1 and STAT2 can build dimers or a trimeric complex together with IRF9 (interferon regulatory factor 9) – the so-called interferon-stimulated gene factor 3 (ISGF3), which can translocate to the nucleus (Figure 4) [67] and activates the transcription of over 2,000 interferon-stimulated genes (ISG) [67]. Within the transcription factor complex ISGF3, IRF9 is the DNA-binding part, and the binding DNA sequences are called interferon-stimulated response elements (ISRE) with the consensus sequence of 5'-AGTTT(NNN)TTTC-3' [67, 68]. STATs can recruit additional cofactors to the promoter, inducing the transcription of target genes specifically [67]. Since the members of ISGF3 themselves are genes induced by IFNAR stimulation, the negative feedback is crucial to eliminate IFN signalling and prevent overreactions; this includes the internalisation and degradation of IFNAR and the dephosphorylation of activated STATs or the recruitment of protein inhibitors of activated STATs (PIAS) to interrupt protein-DNA interaction [67, 69]. Particularly, members of the SOCS family (suppressor of cytokine signalling) are known to be upregulated after IFN stimulation and inhibit further signalling by the inactivation of Janus kinases, which results in a reduced STAT activation [70].

Most leukocytes can produce type I IFN to enable a rapid antiviral response, with DCs and fibroblasts as main sources for IFN $\alpha$  and IFN $\beta$ , respectively [71]. Interestingly, it is believed that all human cells express IFNAR [67].

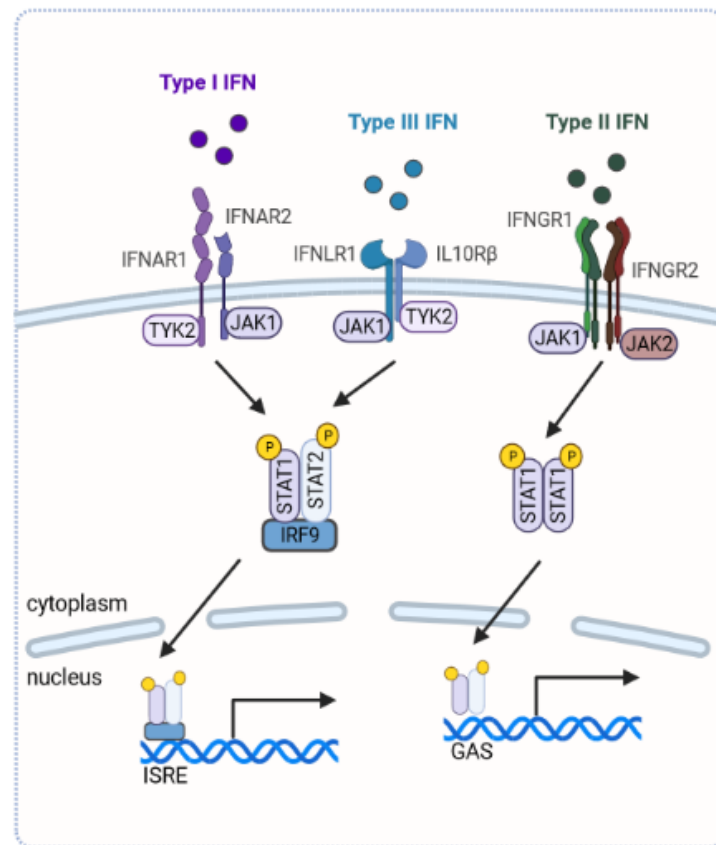


**Figure 4. Canonical signalling of interferon types I, II and III.** Upon stimulation of the respective receptor, the associated kinases JAK1, JAK2 or TYK2 are phosphorylated and activate STAT1 and STAT2 by phosphorylation. Associated with IRF9, the trimeric complex ISGF3 is formed and translocates to the nucleus binding at ISRE to activate gene expression. Phospho-dimer of STAT1 bind to GAS (adapted from Majoros, A. et al., 2017 [72]).

### Type II IFN

Type II IFN is also known as IFN $\gamma$  and binds to its respective receptor (IFNGR), which is composed of the subunits IFNGR1 and IFNGR2 [65]. The kinases JAK1 and JAK2 are associated with IFNGR and similar to type I signalling, and the binding of IFN $\gamma$  results in phosphorylation of, predominantly, STAT1. STAT1 forms independently from IRF9, a homodimer named IFN $\gamma$ -activated factor (GAF) that translocates to the nucleus [65, 67]. GAF is able to bind to the DNA, and the consensus sequence 5'-TTN<sub>2-4</sub>GAA-3' is called IFN $\gamma$ -activation sites (GAS; Figure 4) [67].

The main sources of IFN $\gamma$  are NK cells and T cells to induce antiviral host defence. By polarising CD4<sup>+</sup> cells and macrophages towards the active T<sub>H</sub>1 and M1 phenotype, respectively, IFN $\gamma$  activates a pro-inflammatory immune effect [65]. For instance, in macrophages, it induces phagocytosis as well as the production and release of NO, ROS, and pro-inflammatory cytokines (IL12, TNF $\alpha$ , IL1 $\beta$ ) [49, 65]. However, the antiviral effects of IFN $\gamma$  seem inferior to those of type I IFNs and act in a more immunoregulatory way to prevent an over-reactive immune response [65].

### Type III IFN

Type III IFNs consist of four subtypes known as IL29 (IFN $\lambda$ 1), IL28A (IFN $\lambda$ 2), IL28B (IFN $\lambda$ 3) and IFN $\lambda$ 4, of which the latter is considered a pseudogene [66]. Type III IFNs are mainly produced and secreted by DCs, and they all bind to the interferon lambda receptor complex (IFNLR), which is a heterodimer formed by IFNLR1 and IL10R $\beta$  [66, 73]. Similar to type I IFN signalling, the binding of IFN $\lambda$  leads to activation of JAK1 and TYK2, subsequently recruiting ISGF3 to eventually enhance the transcription of pro-inflammatory ISGs, including type I and III IFNs [66, 73]. Interestingly, IFNLR1 is mainly expressed on epithelial cells that function as barriers for pathogens, such as respiratory or gastrointestinal cell types, which is why IFN $\lambda$  is important for an initial antiviral host defence and to enhance type I IFN response. Even though both IFNAR and IFNLR recruit ISGF3 canonically, the expression signatures differ slightly, most likely through different cofactors guiding ISGF3 to distinct gene promoters (Figure 4) [66, 73, 74].

Type III IFNs are not used or approved as therapeutics; recent research has suggested that type III IFNs produce similar effects as type I IFNs, including viral eradication, antiproliferative effects and beneficial activation of the TME, without the harsh side effects [75]. Particularly in a lung tumour model, overexpression of IFN $\lambda$ 2 in LUAD cells led to a reduction in tumour growth supported by an increase in apoptosis and in the activation of NK cells and CD4 $^+$  and CD8 $^+$  T cells [76].

Known to be involved in immune cell activation and modulation, IFNs in TME mostly act as tumour-suppressing, anti-angiogenic and pro-apoptotic cytokines both directly targeting tumour cells and enhancing response of other stromal cells [14, 77-80]. Clinically used IFNs are mostly approved as adjuvant therapy for malignant melanoma, follicular lymphoma or chronic myelogenous leukaemia, for instance; however, novel therapies and harsh side effects have gradually supplanted IFNs to second line or maintenance therapy [80, 81].

#### 1.3.2. Non-canonical type I IFN signalling

As described, the recruitment of transcription factor complex ISGF3 follows the stimulation of type I IFN. It has been shown that not only the direct effects of IFN are responsible for the induction of downstream gene expression. The vanishing of IFN and the dephosphorylation of STAT1 (U-STAT1) by SOCS1 do not necessarily lead to an absolute interruption of type I IFN signalling, and the importance of ISGF3 with unphosphorylated STATs (U-ISFG3) and a non-canonical IFN signalling was first confirmed by the work of two groups in 2009. Cheon et al. demonstrated that after IFN treatment, the expression of genes activated at an early time point differed from those at a later time point, when phosphorylation of STAT1 was no longer detectable [82]. At the same time, Lou et al. could demonstrate that independently from phosphorylation, IRF9 and STAT2 could form an active complex without STAT1 involvement [83]. Even before, a non-canonical signalling was observed, where IRF9 could build a transcriptionally active trimeric complex with a STAT2-homodimer without STAT1 involvement; however, an IFN signalling

outside phosphorylated ISGF3 was not considered at that time [84]. Sequencing revealed the distinct expression pattern between ISGF3 and U-ISGF3 [85].

Both U-STAT1 and U-STAT2 were reported to occupy promoters of ISGs and contribute to their basal expression, thereby providing a vigilant host defence [82, 86]. This is even more interesting considering that unlike STAT1, STAT2 has no DNA-binding capabilities and is dependent on cofactors such as STAT1 and IRF9 [67]. Accordingly, U-ISGF3, U-STAT1 homodimers, U-STAT2 dimers together with IRF9, or heterodimers of U-STAT1 and U-STAT2 were reported to activate the expression of IFN-associated genes apart from the canonical cascade [84, 87-89]. IRF9 overexpression studies suggested that IRF9 was able to activate signalling transduction independently from STAT1 or STAT2, but they did not clarify which cofactors were involved [90]. Interestingly, STAT1 seems to be more important in type II than in type I signalling, which was demonstrated when STAT1, unable to bind DNA, massively reduced type II response [91]. Furthermore, this study revealed that, in ISGF3, IRF9 was the main DNA-binding part and DNA-unbindable STAT1 did affect type I IFN response only marginally (Figure 5) [91].

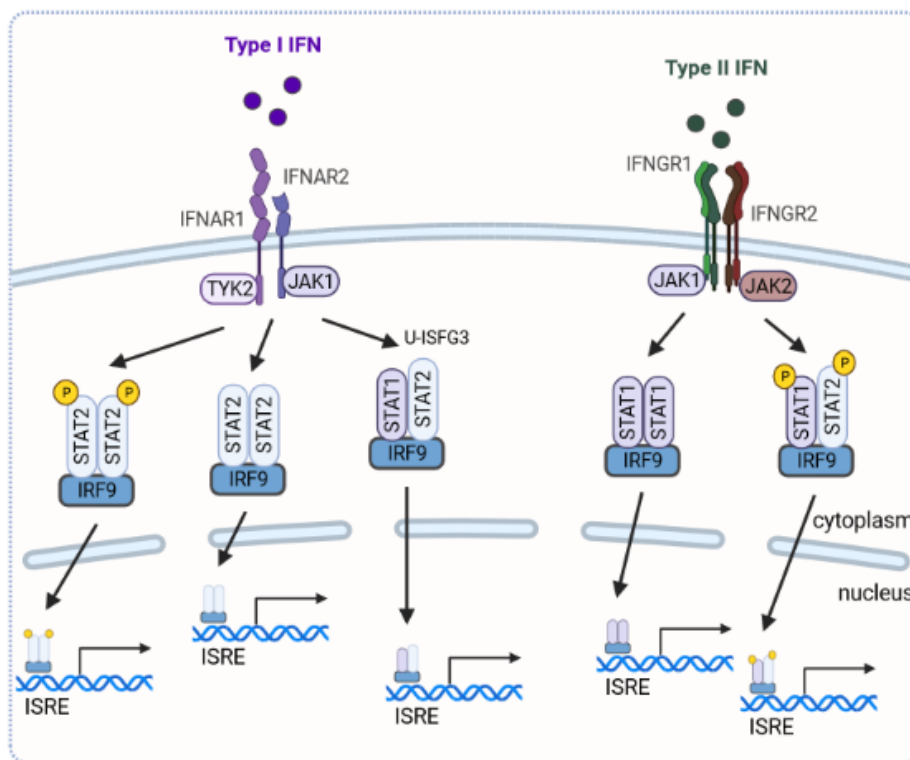


**Figure 5. Non-canonical signalling of type I and type II interferons.** Stimulation of the respective receptor leads to recruitment of STAT complexes independently of phosphorylation status. For non-canonical type I IFN signalling, complexes with IRF9 are formed with either STAT2-, phospho-STAT2-homodimers or STAT1-STAT2-heterodimer (U-ISGF3). For non-canonical type II IFN signalling, ISGF3 and complexes with IRF9 are formed with STAT1-homodimer. IRF9 is responsible for binding to ISRE elements and activating further gene expression (adapted from Majoros, A. et al., 2017 [72]).

### 1.3.3. Role of type I IFN in host defence

The release of IFN after the detection of pathogens is mainly mediated through Toll-like receptors (TLR) or cytosolic receptors such as RIG-I (retinoic acid-inducible gene I, also known as DDX58; DExD/H-box helicase 58) or MDA5 (melanoma differentiation-associated protein 5, also known as IFIH1; interferon induced with helicase C domain 1). The members of the TLR family are extensively expressed on leukocytes and can detect distinct patterns such as nucleic acids (e.g. TLR3, TLR9) and viral or bacterial components, which eventually leads to the release of type I IFN and other pro-inflammatory cytokines [92, 93]. Once viruses infect cells, the helicases RIG-I and MDA5 can detect viral double-stranded RNA in the cytosol and are eventually able to activate the expression of type I IFNs [63, 92]. Therefore, IFNs act in both an autocrine and a paracrine manner.

The antiviral properties upon IFN secretion include apoptosis and degradation of infected cells to prevent viral spreading. Examples are oligoadenylate synthases (e.g. OAS1); these are strongly upregulated, and their products activate ribonuclease L (RNase L), which is able to degrade cellular RNA. This does not only result in the degradation and apoptosis of infected cells but also in a release of viral RNA fragments that again increase IFN secretion, as previously mentioned [92, 94]. Another antiviral step is the activation of protein kinase RNA-activated (PKR) to inhibit translation initiation and thereby block the viral replication of infected cells [92, 95]. It is also known that tumour suppressor p53 is activated upon IFN signalling and that it induces the expression of other ISGs and apoptosis of infected and infectious cells. When p53 was inhibited, the transcription of important antiviral genes (RIG-I, OAS1, IRF9) was reduced, and viral clearance failed [96].

In addition to cell-based effects, type I IFNs enable an adequate immune response as they are key mediators for T cells to differentiate into functional cytotoxic T cells [60, 92, 97]. In addition, NK cells are activated upon IFN stimulation [98]. IFN increases the expression of IL15, which is involved in the activation of both cell types [97, 98]. Another affected cell type are DCs, known to differentiate upon IFN stimulation and present antigens to other immune cells to prime host defence [71]. CD4<sup>+</sup> cells are polarised towards T<sub>H</sub>1 cells, which then secrete IFN $\gamma$  and thereby prolong immune response [71, 99].

It is notable that type I IFNs can also have detrimental effects on the host defence. A long-term stimulation leads to a desensitisation of IFNAR and a reduced expression of ISGs. In some cases, it can even suppress the immune system – for instance, by apoptosis of immune cells or the expression of suppressive genes such as IL10, PD-1 and PD-L1 [71, 100, 101].

Acting as immunomodulatory cytokine, recombinant IFN $\beta$  has been approved for the treatment of multiple sclerosis. Its way of action might not be fully understood, but it includes the regulation and suppression of overactive T cells, monocytes and antigen-presenting cells [102].

Beside their importance in antiviral clearance, type I IFNs also influence tumour development and progression by affecting tumour cells intrinsically and through the TME. Some mechanisms concur with antiviral responses, whereas others differ. Similar to pathogen recognition in

infections, it is believed that functional DCs can recognise and present antigens of malignant cells to the host defence and themselves provide a source of IFNs at an early time point [103]. Further, fragments of injured, apoptotic or necrotic cells activate IFN release via TLRs and RIG-I [103]. Antiproliferative properties were shown for several subtypes, when IFN treatment results in cell cycle arrest, *inter alia*, via upregulation of cyclin dependent kinase inhibitor 1A (CDKN1A, also known as p21) [103, 104]. Beside the regulation of caspases, IFNs also induce apoptosis in tumour cells – similar to the processes in viral clearance – by the induction of p53 as well as the regulation of OAS1 and RNase L [105, 106]. When it comes to the effect of the environment, type I IFN might influence all cell types; as mentioned, it can activate DCs to further increase immune response [71, 103]. The release of pro-inflammatory cytokines (e.g. IL15) activates NK cells and T<sub>H</sub>1 cells, which further activate the polarisation of macrophages towards an M1 phenotype [97, 98]. IFN $\alpha$  stimulation reduced the expression of VEGF in cancer cell lines, which resulted in lower VEGF plasma levels of cancer patients, indicating a direct antiangiogenic effect [107].

Several animal models included the injection of IFN-overexpressing cells or the administration of an IFN-overexpressing source. Overall, it can be noted that tumour development and progression were reduced when IFN $\beta$  was overexpressed. Further, IFN $\beta$  directly inhibited cancer cell growth, led to the activation of NK, CD4<sup>+</sup> and CD8<sup>+</sup> T cells and diminished vascularisation [108, 109]. In addition to the release of type I IFNs, the expression of IFNAR is important to elicit beneficial effects. For instance, the absence of IFNAR1 in colorectal cancer patients, correlated with a negative prognosis and tumour studies in *Ifnar*-deficient mice, resulted in stronger tumour growth [110, 111].

Type I IFNs limit cancer cell proliferation and apoptosis, the activation of tumour-fighting immune cells and the inhibition of neovascularisation; however, there are negative effects that facilitate the development and growth of malignancies. With cancer progression, tumour cells developed desensitisation for IFN, resulting in a decrease of IFN signalling, which was more prominent in cancer cells from distant metastatic sites [112, 113]. This was mediated by downregulation of IRF7, a transcription factor known to be expressed upon IFN stimulation to transduce IFN signalling and to correlate with IFNAR1 expression in cancer [111, 113]. In various cancer types, it could be demonstrated that impaired TLR signalling led to a reduction of IFN secretion and that leukocytes – particularly tumour-infiltrating DCs – failed to secrete type I IFNs [103, 114]. Furthermore, this disability of DCs in breast cancer patients was associated with reduced survival prognosis [103, 115]. In macrophages, IFN $\alpha$  was responsible for upregulating PD-1, a potential mechanism to suppress the host defence [100].

For cancer treatment, type I IFNs are approved in malignant melanoma patients as the only solid tumour form and as adjuvant therapy for follicular lymphoma or chronic myelogenous leukaemia, for instance [80, 81]. Clinical studies with lung cancer patients investigating the benefits of adjuvant type I IFN therapy were not able to confirm efficacy in NSCLC [116]. However, low dose IFN $\alpha$  as post-chemotherapy and maintenance therapy showed a better survival outcome among SCLC patients [117]. Even though the therapeutic potential of IFNs is relevant to target

tumour and stromal cells, novel therapies and harsh side effects have gradually supplanted IFNs to second line or maintenance therapy, and large comprehensive studies are missing [80, 81].

#### 1.4. Interferon Regulatory Factors

The family of IRFs consists of nine members (IRF1-9) that play important roles in numerous processes such as inflammation, antiviral response, cell development and oncogenesis beside IFN signalling [118, 119]. Figure 6 visualises the structure and homology of the family members. An N-terminal DNA-binding domain (DBD) with five serial tryptophan-rich repeats is well conserved in all IRFs; further, they share IRF-associated domains (IAD), whereby IRF1-2 and IRF3-9 contain distinct domains with IAD1 and IAD2, respectively. IAD1 and IAD2 allow interaction with other structures, such as proteins and nucleic acids. Prominent interaction partners are members of the STAT family, PU.1 and other IRFs [118, 119].

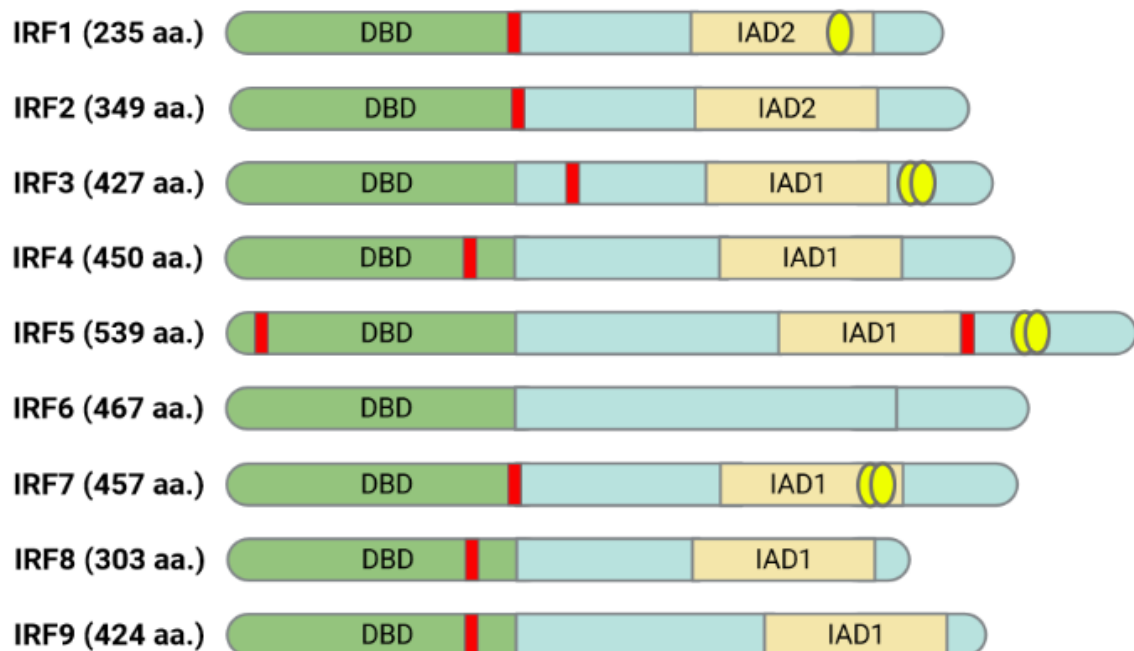


**Figure 6. Structure of IRF family members IRF1-9.** All IRFs contain an N-terminal DBD. IRF1 and IRF2 contain an IAD2 domain, and IRF4, IRF5, IRF7-9 contain an IAD1 domain. Except for IRF6, all IRFs comprise at least one nuclear localisation signal (red). Some family members contain a phosphorylation site influencing the activity (yellow circles). The size of each IRF is indicated by the number of amino acids (aa.; adapted from Yanai H. et al., 2012; Chistiakov D. A. et al., 2018 [119, 120]).

### 1.4.1. Characterisation of IRF family members

#### IRF1

IRF1 was the first member of the IRF family described in 1988. It is highly associated with type I IFN, and it is shown to activate the expression of type I IFN as well as to be increased after IFN stimulation itself. The induction of type I IFN expression after the activation of RIG-I and MAD5 is mediated by IRF1. Within the host defence, IRF1 is important for the maturation of DCs, and the loss of IRF1 suppresses their activity by high IL10 and TGF $\beta$  expression. Further, IRF1 is involved in the development of CD8+ T cells and NK cells.

In cancer research, IRF1 is well characterised as tumour suppressor able to regulate cell cycle and apoptosis. Together with p53, IRF1 directly induces the expression of cyclin-dependent kinase inhibitor (p21) resulting in cell cycle arrest, for instance after DNA damages. In a similar way, IRF1 – independently as well as together with p53 – induces apoptosis after DNA damage. The role of IRF1 and its loss of function, whether by mutation, post-translational modification or mis-splicing, has been investigated extensively. Therefore, it was described that heterozygous *IRF1* deletion is associated with a poor outcome in patients with various types of cancer, such as breast cancer, gastric cancer and leukaemia. Recent studies have demonstrated the tumour-suppressing functions of IRF1 in patients affected by lung cancer [118, 119, 121, 122].

#### IRF2

IRF2 is induced by IFN stimulation but acts as counterplayer of IRF1 and IRF9, thereby balancing and reducing type I IFN response. Further, IRF2 is involved in the development of myeloid cells, and it impairs the activation of CD8+ T cells, which is an important mechanism to prevent hyper-reactive T cells. The loss of IRF2 was shown to reduce the activity and lifetime of macrophages and to impair the development of NK cells.

IRF2 is widely associated with oncogenesis as it attenuates the function of IRF1 by interfering at the same ISREs. It was shown to activate oncogenic genes or inhibit the activity of tumour suppressors such as histone H4 and N-RAS. However, IRF2 is also involved in p53 activation, for instance in hepatocellular carcinoma patients, where the loss of IRF2 impairs both p53 expression and function. The expression of *IRF2* in pancreatic cancer patients is associated with a highly proliferative phenotype. In lung cancer, IRF2 reduction was shown to reduce tumour cell proliferation in vitro and in vivo [118, 119, 123-125].

#### IRF3

IRF3 is characterised as transcriptional activator of type I IFN and pro-inflammatory genes (e.g. CXCL10). Upon viral infection or recognition of foreign nucleic acids, IRF3 is phosphorylated, allowing to form homo- or heterodimers with IRF7 and to translocate to the nucleus, eventually activating the expression of IFN. In this manner, the heterodimer has a stronger activity than the homodimer.

Overall, IRF3 is characterised as tumour suppressor. It was demonstrated that it induces apoptosis by activating TRAIL, an important mechanism upon DNA damage and chemotherapy response. It was further shown that IRF3 inhibits tumour cell proliferation *in vitro* and *in vivo*. In NSCLC patients, *IRF3* expression is associated with a better outcome; however, the effect of mutations leading to a reduced phosphorylation – particularly in LUSC patients – is yet to be determined [118, 119, 126, 127].

#### **IRF4**

IRF4 is characterised as regulatory factor in myeloid cell development. Competitively, IRF4 and IRF5 are involved in the polarisation of macrophages. Via IRF4 upregulation, IL4 and M-CSF independently induce polarisation towards the M2 phenotype and induce immunosuppressive genes such as Arg1, IL10 and even IL4. The absence of IRF4 leads to elevated pro-inflammatory genes by an increased TLR-signalling (e.g. IL6, TNF $\alpha$ ). IRF4 is further able to antagonise the IRF5-induced macrophage polarisation towards M1. It is also a critical factor for T<sub>H</sub> cell polarisation; similar to macrophages, the loss of IRF4 inhibits T<sub>H</sub> cells' production of IL4 and other cytokines relevant for T<sub>H</sub>2 activation. Additionally, IRF4 and IRF8 are crucial for the regulation and differentiation of B cells and plasma cells.

In malignancies, it was observed that this mechanism is involved in the pathogenesis of leukaemia, particularly with low *IRF4* expression in CML patients. However, increased *IRF4* expression is observed in T cell leukaemia, believed to inhibit cell cycle arrest via Cyclin B1. In myeloma cancer cells, IRF4 interacts with the oncogene MYC, and the expression correlates with poor prognosis in patients. Elevated expression levels are also observed in NSCLC tumour tissue, and *in vitro* silencing reduced cancer cell proliferation [51, 118, 120, 128].

#### **IRF5**

As previously mentioned, IRF5 is highly involved in pro-inflammatory pathways and M1 macrophage activation. It is induced by RIG-I and TLR signalling as well as by GM-CSF, resulting in the production of inflammatory cytokines such as TNF $\alpha$ , IL6 and IL12. IRF1 and type I IFN were shown to increase IRF5 expression and improve macrophage activation. M1 macrophages still express IRF5 at high levels, maintaining their phenotype and cytokine secretion. The loss of IRF5 leads to defective type I IFN production upon viral infections as well as other cytokines such as IL6 and CXCL2.

In malignancies, IRF5 shows tumour suppressing properties. Upon DNA damage, p53 directly regulates IRF5 expression to induce apoptosis. However, p53-independent mechanisms for apoptosis have been reported in p53-deficient cancer cells via FAS signalling. Furthermore, overexpression of IRF5 reduces the proliferation of lymphoma cells [51, 118-120, 127].

#### **IRF6**

IRF6 is the only family member that is not involved in the immune system, but it is highly associated with connective tissues as it is a crucial factor for keratinocyte differentiation. Pathophysiologically, two diseases are known to be caused by *IRF6* mutations: van der Woude

syndrome and popliteal pterygium syndrome. These are often related to cleft palates or heart malfunction as well as to limbs, genitals or face dysplasia. IRF6 is described as tumour suppressor known to induce cell cycle arrest upon overexpression. Nevertheless, increased IRF6 expression was recently found in NSCLC tissues, and in vitro experiments revealed oncogenic features in lung cancer cell lines [119, 129, 130].

### **IRF7**

As previously described, IRF7 is strongly involved in the induction of type I IFN. It is expressed at low levels in the cytoplasm but is intensely induced by type I IFN stimulation. This indicates the importance of a loop mechanism to allow rapid IFN secretion and signalling when required. IRF7 is phosphorylated and thereby activated by TLRs, RIG-I and viral infections, and its loss dramatically reduces type I IFN production, resulting in suppression of the immune system, particularly via DCs and monocytes.

IRF7 was shown to negatively regulate metastasis-related genes in breast cancer. High expression of IRF7 is associated with a better prognosis in breast cancer patients and a prolonged metastasis-free survival. It was also associated with a better survival of colorectal patients, mainly by upregulation of IFNAR1. Nevertheless, upregulated RIG-I and IRF7 were involved in lung cancer invasion and metastasis [111, 113, 131].

### **IRF8**

IRF8 is mainly involved in the development of myeloid cells and inflammation. It is induced by LPS and TLR9 activation and induces proinflammatory cytokines, such as type I IFN and IL12. DCs highly express IRF8, which is required for both DC differentiation and type I IFN secretion upon viral infection, confirmed by *IRF8*-depletion experiments in vitro. In monocytic progenitors, IRF8 drives the differentiation towards macrophages and is further involved in M1 polarisation to enhance the expression of type II IFN-induced genes. IRF8 is further involved in the activation of T<sub>H</sub> cells, where it acts as a counterplayer of IRF4. The deletion of IRF8 impairs the ability of T<sub>H</sub> cells to fully polarise to T<sub>H</sub>1 cells. Interestingly, the loss of IRF8 is associated with the development of CML and other malignancies as it represses the expression of BCL2 and can induce cell death via FAS. The manipulation of IRF8 in lung cancer cells demonstrated its properties as tumour suppressor and is further associated with the outcome in patients [118, 120, 132].

#### **1.4.2. IRF9**

As previously described, IRF9 is part of the trimeric ISGF3 complex and activates the expression of ISGs to mediate type I IFN signalling. The alternative names p48 and ISGF3 $\gamma$  are based upon its molecular weight and its role within ISGF3, respectively and are currently rarely used [133]. Considering the structure of IRF9, it consists of a DNA-binding domain (DBD) with tryptophan-rich repeats at the N-terminal end. The DBD also contains a bipartite basic nuclear localisation signal which allows IRF9 to migrate between cytosol and nucleus. The C-terminal IRF-associated domain (IAD) is well conserved among IRFs and essential for the interaction with other proteins (Figure 6) [118, 134]. Even though IRF9 is the main DNA-binding part, the

interaction with STAT1 and STAT2 is needed to navigate the transcription complex towards the target genes and increase binding affinity [84]. IRF9 was also shown to bind to phosphorylated STAT2 and STAT6 specifically in B cells. However, other binding partners remain unknown [135].

IRF9 expression is upregulated upon type I and type III IFN stimulation. Moreover, IL6 was able to induce IRF9 expression and enhance IFN response presumably by involving ISREs [136, 137]. In leukemic cell lines, retinoic acid led to cell differentiation by the induction of ISGF3 [138]. In progressing renal cancer, several factors were identified that induced IRF9 and STATs expression. The suppressor and deubiquitinating enzyme (BAP1) protects IRF9 from degradation, and the loss of BAP1 led to a reduction in IRF9 levels [139]. In the same study, the overexpression of hypoxia-inducible factor-2 $\alpha$  (HIF-2 $\alpha$ ) resulted in both IRF9 expression and ISGF3 activity [139]. The manipulation of lysine demethylase 5C (KDM5C) indicated the influence of methylation on IRF9 expression when the knockdown of KDM5C resulted in IRF9 overexpression [139]. Even if one study suggested that methylation could increase IRF9 expression, methylation studies are needed to determine whether the upregulation of IRF9 is a secondary effect or one directly resulting from methylation.

In mice and respective knockout mice, *Irf9* was described as a direct target of miRNA93, which could inhibit the expression of *Irf9* [140]. Similarly, miRNA302d could directly reduce IRF9 expression in human patients with autoimmune disease lupus [141].

Within the host defence, IRF9 is the main key player to elicit the antiviral features of type I IFN. Animal models with mice deficient in *Irf9*, *Stat1* or *Stat2* demonstrated that all three parts of ISGF3 were important; for instance, *Stat1* deficiency was lethal in the case of lymphocytic choriomeningitis virus (LCMV) infection, whereas the immune system of *Irf9*- or *Stat2*-depleted animals, even though not lethal, failed for viral clearance. In the case of *Irf9*-knockout mice, the LCMV infection persisted for their lifetime. The presence of IRF9 is thus significant to provide a functional antiviral response of type I IFNs and to prompt cytotoxic T cell activation [99, 142]. The absence of IRF9 resulted in a different gene transcription signature upon IFN stimulation with genes that were typically expressed upon IFN $\gamma$  stimulation most probably due to STAT1 dimerisation [143, 144]. Interestingly, a medical case report described that inherited IRF9-deficiency in a child was associated with life-threatening pneumonia caused by impaired IFN signalling after influenza infection [145].

It was demonstrated that IRF9 prevented the neuronal structures from the pathological side effects of IFN, which did occur when IRF9 was deleted [146]. Additionally, high IRF9 levels were detected in patients with neuronal infections and those with multiple sclerosis. Since a decrease of *IRF9* mRNA under IFN $\beta$  therapy could be observed, it is assumed that IRF9 might play a role in autoimmune diseases and could serve as a biomarker [144, 147].

So far, the role of IRF9 in the development and progression of cancer – and particularly lung cancer – has been poorly investigated. When it comes to the antiproliferative effects of type I IFN, IRF9 is the crucial part, and the loss of IRF9 diminished that effect completely, as demonstrated in ovarian adenocarcinoma cell line OVCAR3 [148]. This was confirmed in the case of prostate

cancer, where pro-inflammatory IL6 upregulated the expression of IRF9 and sensitised cancer cells for IFN [137]. It is known that IRF9 can influence the cell cycle by the inhibition of sirtuin 1 (SIRT1), which leads to an increased acetylation of p53. In acute myeloid leukaemia, IRF9 acted as tumour suppressor and was expressed at low levels, and its restoration suppressed SIRT1 expression and restored more active p53 [106, 149]. In a xenograft model with renal cancer cells, IRF9 silencing increased tumour growth, and co-overexpression with STAT2 diminished cancer progression accordingly [139]. In other malignancies, IRF9 acted as oncogene. In the case of lung cancer, IRF9 recruited STAT2 and p65 to bind at the promoter of IL6 and enabled the oncogenic features of IL6 in vitro [68]. The knockdown of IRF9 in cell culture studies reduced cancer cell proliferation and migration [68, 150]; further, IRF9 was upregulated in breast cancer cells after cell crowding in vitro. This resulted in a strong resistance against chemotherapy, which was also observed in other IRF9-overexpressing studies and could be explained by increased repair mechanisms after DNA damage and reduced apoptosis [90, 151].

Another interesting aspect of IRF9 is the involvement in vascularisation and induction of apoptosis after cell injury. In murine vascular smooth muscle cells (VSMCs), the deletion of *Irf9* reduced migration and proliferation by *Sirt1* regulation, which resulted in impaired repair after vascular injury, whereas the overexpression promoted VSMC activity [152]. In contrast, *Irf9* inhibition led to a stronger M2-like polarisation in macrophages and eventually to an increase in angiogenesis [140]. In several mouse models with induced injuries, *Irf9*-mediated apoptosis was responsible for functional failure. This principle was confirmed in myocardial cells, neurons or hepatocytes, where the loss of *Irf9* protected the cells from injury in their respective mouse model (myocardial; cerebral or hepatic ischemia – reperfusion injury, respectively), which was even more pronounced when *Sirt1* was additionally blocked or deleted [153-155].

Important studies on IRF9 in the tumour environment are still missing, and its relevance could only be a product of speculation. However, the significance of IRF9 in host defence and vascularisation should encourage further investigation addressing TAMs, T cells and neoangiogenesis.

## 1.5. Versican

Versican (VCAN), a large proteoglycan, is widely expressed and one of the main components of the ECM. Together with aggrecan, brevican and neurocan, it belongs to the group of lectican proteins [156]. As visualised in Figure 7, its structure consists of an N-terminal G1 domain which is able to bind to hyaluronan (HA); a G2 domain with glycosaminoglycan binding regions (GAG $\alpha$ , GAG $\beta$ ); and a G3 domain that contains two EGF-like repeats, among others (Figure 7) [156, 157]. Four different splicing isoforms exist, with VCAN [V0] as longest variant. VCAN [V1] lacks the GAG $\alpha$  domain, whereas VCAN [V2] does not contain GAG $\beta$ , and VCAN [V3] is missing both. Since chondroitin sulphate chains are connected to GAG domains, the numbers of chains differ in the splice variants and lack in VCAN [V3] [158-160]. The phenotypes of VCAN variants have been studied and reviewed intensely. VCAN [V1] clearly promotes tumour cell proliferation, inhibits apoptosis and can activate EGFR signalling, whereas VCAN [V2] shows opposite effects,

with a reduction in proliferation and downregulation of EGFR signalling [159]. It was also described that upon VCAN [V1] overexpression, tumour suppressor p53 was inactivated, and cell cycle inhibitor p21 was almost erased [161]. However, both isoforms VCAN [V0] and [V1] are the predominant variants in human malignancies, and no study could clarify whether these variants differ in their oncogenic phenotype [162]. The G1 domain is known to regulate cell adhesion and, more importantly, migration via the interaction with other adhesion proteins (e.g. integrins, CD44, hyaluronan) [158, 163]. Although VCAN [V3] is the least investigated isoform, studies suggest that it plays a dual role as inhibitor of cell proliferation and inducer of migration [159, 162].

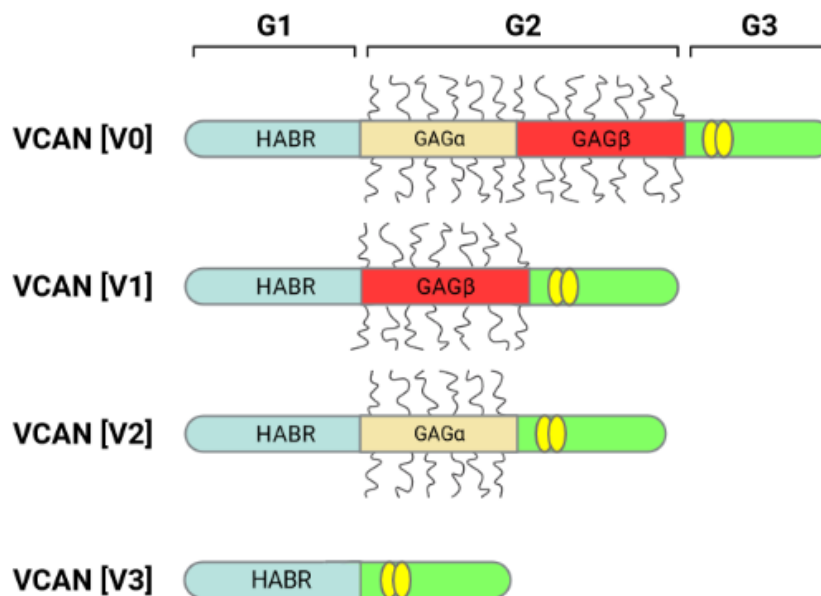


**Figure 7. Structure of Versican splicing variants.** VCAN [V0] is the longest isoform comprising G1 domain with hyaluronan binding region (HABR), G2 domain with GAG $\alpha$  and GAG $\beta$ , and G3 domain including two EGF-like elements (yellow circles). Chondroitin sulphate chains are connected to GAG elements (black lines). VCAN [V1] lacks GAG $\beta$ , VCAN [V2] lacks GAG $\alpha$ , and VCAN [V3] lacks both GAG elements (adapted from Wight, T. N. et al., 2014) [164].

Notably, VCAN was demonstrated to take a part in IFN signalling (i) when it was upregulated in macrophages upon type I IFN stimulation and (ii) when the depletion of VCAN reduced pathogen-induced IFN $\beta$  synthesis [160]. Other cytokines, such as TGF $\beta$ , PDGF or EGF, can also induce VCAN expression [162, 165].

A study with NSCLC patients revealed that VCAN was expressed predominantly in the TME as well as in cancer cells, and the intensity of VCAN staining was associated with both high abundance of HA and tumour dedifferentiation [166]. The interaction with HA, in particular, promotes the high migratory effect of VCAN and is associated with a poor outcome [162, 163, 167].

The role of VCAN in angiogenesis is mediated mainly by isoform VCAN [V2]. Even though endothelial cells did not express VCAN, TAMs – particularly the ones close to endothelial cells and vessels – expressed it highly. It is believed that stromal- or tumour cell-derived VCAN could attract and activate endothelial cells and enhance angiogenesis by facilitating cell–cell contact [168,

169]. VCAN is often cleaved by proteases like ADAMTS (a disintegrin and metalloproteinase with thrombospondin motif), but whether VCAN cleavage terminates or even enables angiogenesis remains elusive, and given the altered ADAMTS in many malignancies, it requires intense research [62, 162, 168].

## 2. Aims of the study

Lung cancer is the main cause of cancer-related deaths worldwide. Due to late-stage diagnosis, missing prevention strategies and failure of targeted therapies, the overall survival of lung cancer patients is low. As a main cytokine of the tumour stroma, IFN influences cancer cells as well as immune cells; however, underlying mechanisms and relevance in lung cancer remain elusive.

This study aims to elucidate the role of the main key player in IFN signalling, IRF9, in lung cancer oncogenesis and tumour microenvironment. It was demonstrated that IRF9 is a crucial regulator to elucidate anti-proliferative properties within the IFN pathway and that it is associated with a better outcome in leukaemia patients. However, IRF9 is highly expressed in lung cancer patients and associated with a poor prognosis. Its regulation and underlying mechanism are not understood.

To investigate the role of IRF9 in tumour development, the following approaches were taken:

1. Role of IRF9 in non-canonical IFN signalling in lung cancer:
  - 1.1. Evaluation of human lung cancer data
  - 1.2. Analysis of cell-dependent effects of IFN
  - 1.3. Generation and characterisation of IRF9-overexpressing and IRF9-knockdown lung cancer cell lines
  - 1.4. Analysis of IRF9-mediated gene regulation via RNA-seq
  - 1.5. Investigation of IRF9 in VCAN regulation by promoter analyses
  - 1.6. Evaluation of tumour models with IRF9-transduced cells lines
2. The influence of IRF9 in the tumour microenvironment was studied by:
  - 2.1. Evaluation of *Irf9*-deficient mice including tumour models and cellular composition of tumours and lungs
  - 2.2. Isolation and analysis of macrophages from *Irf9*-deficient mice

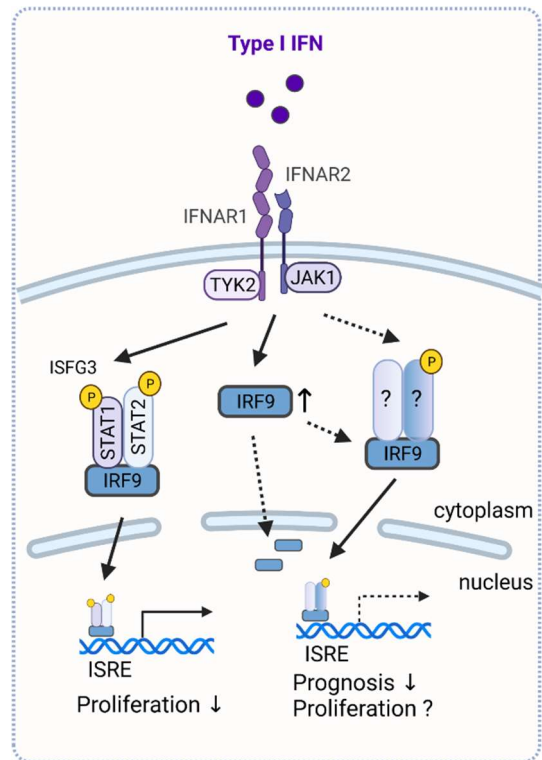


**Figure 8. Hypothesis and aim of the study.** IRF9 is the key player in elucidating the anti-proliferative effects of IFN. How does the increase of IRF9 lead to opposite effects and worsen the prognosis of lung cancer patients?

### 3. Materials and Experimental Procedures

#### 3.1. Cell culture

##### 3.1.1. Cell lines and cultivation

Human cancer cell lines HepG2 (hepatocellular carcinoma; ATCC, HB-8065), HCT116 (colorectal carcinoma; ATCC, CCL-247), MIA-PaCa2 (pancreatic carcinoma; ATCC, CRL-1420), MCF7 (breast carcinoma; ATCC, HTB-22), DU145 (prostate carcinoma; ATCC, HTB-81) and HEK293T (human embryonic kidney; ATCC, CRL-11268) were purchased from ATCC. Human LUAD cell lines A549 (ATCC, CCL-185), A427 (ATCC, HTB-53) and H1650 (ATCC, CRL-5883); human LUSC cell lines H520 (ATCC, HTB-182) and H226 (ATCC, CRL-5826); the human large cell carcinoma cell line H460 (ATCC, HTB-177); and the human small cell carcinoma H82 (ATCC, HTB-175) were purchased from ATCC. Human LUSC cell line HCC15 was purchased from DSMZ (DSMZ, ACC 496), and HBEC (Human bronchial epithelial cells; PromoCell, C-12640) were obtained from PromoCell.

The cell lines HepG2, MIA-PaCa2, MCF7, DU145, HEK293T, A549 and A427 were cultured in DMEM (Gibco, 41965-039), supplemented with 10% foetal calf serum (FCS; Gibco, 16140071) and 1 U/ml Penicillin-Streptomycin (Gibco, 15140122). H226 were cultured in DMEM/F-12 (Gibco, 31330-038), supplemented with 10% FCS and 1 U/ml Penicillin-Streptomycin. The cell lines HCT116, H1650, H520, HCC15, H460 and H82 were cultured in RPMI (Gibco, 12633-012), supplemented with 10% FCS and 1 U/ml Penicillin-Streptomycin. HBEC were cultured in provided Airway Epithelial Cell Growth Medium (PromoCell, C-21160).

The murine lung cancer cell line LLC1 was obtained from ATCC (ATCC, CRL-1642) and cultured in RPMI (Gibco, 11879-020), supplemented with 10% FCS and 1 U/ml Penicillin-Streptomycin. CULA (C57BL/6 Urethane-induced Lung Adenocarcinoma) cells were generated, characterised, provided from Stathopoulos laboratory and cultured in DMEM (Gibco, 41965-039), supplemented with 10% FCS and 1 U/ml Penicillin-Streptomycin [170, 171].

All cells were cultured at 37°C and 5% CO<sub>2</sub> in an incubator (Heracell 240i), and medium was replaced by fresh medium regularly every two to three days. Once grown to a monolayer of 70-80%, cells were washed with 1X phosphate buffered saline pH 7.4 (1X PBS; Gibco, 10010056) followed by treatment with 0.05% Trypsin-EDTA (Gibco, 25300-054) at 37 °C. After successful detachment, cells were resuspended in full medium and plated at a ratio of 1:5. For cryo-preservation, cell pellet was resuspended in cryo-medium containing 10% dimethyl sulfoxide (DMSO; Sigma, D8418) and 20% FCS and cooled down in isopropanol freezing container at -80 °C. Frozen cryo-vials were stored in liquid nitrogen tank for further use.

### 3.1.2. IFN stimulation

When indicated, cells were stimulated with type I IFN (pbl assay science, 11200-2). Therefore, IFN was applied up to desired concentration (50-200 U/ml), and cell were stimulated for indicated time (5 min to 72 h). When cells were stimulated longer than 24 h, medium was replaced with freshly prepared medium after each 24 h. We used 1X PBS as a control and used same volume as IFN.

### 3.1.3. Lentiviral transduction

HEK293T cells were co-transfected with the lentiviral overexpressing or silencing plasmid, the envelope plasmid pMD2.G and the packaging plasmid pCMV $\Delta$ R8.2 (both addgene) using Fugene HD (Promega, E2311) and reduced medium. After 24 h, medium was replaced by full medium, and viral particles were harvested after additional 24h to transfect cells using final concentration of 8  $\mu$ g/ml Polybrene (Merck KGaA, TR-1003-G) twice after 6 h. To select and culture transduced cells, Puromycin (Gibco, A1113803) was used in concentrations from 4  $\mu$ g/ml (A549) to 2  $\mu$ g/ml (A427 and CULA).

Lentiviral constructs for IRF9 overexpression (pLV IRF9) and knockdown (pLKO.1 shIRF9) in human cell lines A549 and A427 as well as respective vector controls (pLV EV; pLKO.1 sh scr) were generously gifted from George R. Stark's lab (Cleveland Clinic Lerner Research Institute, OH) [85]. The target sequence against human IRF9 was 5'-CCG GGC CAT ACT CCA CAG AAT CTT ACT CGA GTA AGA TTC TGT GGA GTA TGG CTT TTT-3' [85]. The overexpressing plasmid (pLV Irf9) and the control (pLV EV) for the transduction of murine Irf9 was custom designed from VectorBuilder including murine Irf9 cDNA. To knockdown Irf9 in CULA, we obtained plasmids from RNAi consortium's shRNA library (Broad Institute) enabling to validate five different pLKO.1 shRNA based plasmids containing following sequence against Irf9; Plasmid 1: 5'-CCG GCA GTG GGA GTT GAT TGA GAA ACT CGA GTT TCT CAA TCA ACT CCC ACT GTT TTT G-3'; Plasmid 2: 5'-CCG GGC AGA CTT GTT GAG GAT ACT TCT CGA GAA GTA TCC TCA ACA AGT CTG CTT TTT G-3'; Plasmid 3: 5'-CCG GCC CTA CAA AGT ATA TCG AAT ACT CGA GTA TTC GAT ATA CTT TGT AGG GTT TTT G-3'; Plasmid 4: 5'-CCG GGC TCT TCA AGA CCA CCT ACT TCT CGA GAA GTA GGT GGT CTT GAA GAG CTT TTT G-3'; Plasmid 5: 5'-CCG GCC CGA CAT TTA CTG GAG AAG ACT CGA GTC TTC TCC AGT AAA TGT CGG GTT TTT G-3'.

### 3.1.4. siRNA transfection

FlexiTube siRNA against VCAN (Qiagen ID: SI04948587; target sequence 5'-CAT GCG CTA CAT AAA GTC AAA-3') and AllStars Negative Control siRNA were ordered from Qiagen. The day before transfection, cells were seeded to a confluence of 60–70%. SiRNA and control were diluted using OptiMEM (Gibco, 11058021) prior to adding transfection reagent Hiperfect (Qiagen, 301707). After 5 minutes of incubation, the transfection mix was added to the wells containing full medium. A final siRNA concentration of  $2.5 \cdot 10^{-9}$  mol/l and a final ratio of 1.2  $\mu$ l Hiperfect per

$10^{-9}$  mol siRNA was used. For RNA isolation, cells were harvested two days after transfection. For transwell membrane migration, cells were starved one day after transfection and after one additional day seeded for migration. For proliferation assay, starvation medium was used for transfection, replaced by full medium after one day, and the measurement was performed after one additional day.

## **3.2. Molecular Biology**

### **3.2.1. Protein Isolation and Western analysis**

Cells were washed with ice-cold 1X PBS pH 7.4 (Gibco, 10010056) prior to harvesting by scraping directly with RIPA Lysis Buffer (SCBT, sc-24948) supplemented with cOmplete Protease Inhibitor Cocktail (Roche, 11697498001),  $0.2 \cdot 10^{-3}$  mol/l PMSF (Sigma-Aldrich, 93482-250ML-F) and  $0.1 \cdot 10^{-3}$  mol/l Sodium Orthovanadate (NEB, P0758S), whereas tumour tissue was disrupted with ceramic beads. Cell lysates were centrifuged to remove cell debris. Protein concentration was measured according to the supplier's instructions (DC Protein Assay Kit I; BioRad, 5000111), diluted and denatured by heat and 2-Mercaptoethanol (Carl Roth, 4227.1). Cell lysates were separated on handmade 11% polyacrylamide gels and blotted on Nitrocellulose or Immun-Blot PVDF Membrane (Bio-Rad, 1620112; 1620177) followed by 1 h blocking in either 5% skimmed milk (Roth, T145.2) or 5% bovine serum albumin (BSA, Sigma-Aldrich, A2153) in tris-buffered saline with Tween (TBST) at room temperature. After incubation with primary antibodies at 4°C overnight and an additional 1 h incubation with Anti-Rabbit or Anti-Mouse IgG (H+L) HRP-Conjugate (Promega, W4011; W4021), detection was performed using WesternBright ECL (Biozym, 541005X) and ImageQuant device (GE Healthcare). Antibodies were purchased and diluted in 5% skimmed milk or 5% BSA in TBST as indicated: IRF9 1:500 (SCBT, sc-365893); STAT1 1:1000 (BD, 610185), Phospho-STAT1 (Tyr701) 1:1000 (CST, 9167), STAT2 1:1000 (SCBT, sc-1668), Phospho-STAT2 (Tyr689) 1:1500 (Merck Millipore, 07-224), MMP7 1:1000 (CST, 3801), PCNA 1:2000 (SCBT, sc-7987), VCAN 1:2000 (abcam, ab19345), ACTB 1:3000 (abcam, ab6276).

### **3.2.2. RNA isolation and reverse transcription**

Cells were washed with 1X PBS pH 7.4 prior to being harvested by scraping directly with TriZOL reagent (Ambion, 15596018). RNA isolation was performed according to the manufacturer's protocol. Briefly, 200  $\mu$ l 1-Bromo-3-chloropropane (Sigma-Aldrich, B62404) was added per 1 ml TriZOL, mixed vigorously and incubated for 3 min at room temperature. After centrifugation for 15 min at +4 °C, the aqueous phase was collected and precipitated with isopropanol. The precipitate was washed with 75% DEPC-ethanol twice and resuspended in DEPC-treated water (Diethyl-pyrocabonate; Sigma-Aldrich, 1609-47-8) when air-dried. Concentration and purity of RNA was measured using NanoDrop 2000 (PeqLab Biotechnologie GmbH), and integrity was monitored by separation on handmade 3% agarose gels.

Subsequently, 1000 ng of total RNA were transcribed into cDNA using a High-Capacity cDNA Reverse Transcription Kit (Fisher Scientific, 4368813) according to the manufacturer's instructions. As control, DEPC-treated water was used instead of RNA and later as NTC (non-template control) in RT-qPCR. CDNA was diluted in a ratio of 1:5 before use in RT-qPCR.

### 3.2.3. Quantitative real-time polymerase chain reaction (RT-qPCR)

Quantitative real-time polymerase chain reaction (RT-qPCR) of diluted cDNA and analysis were performed using a StepOnePlus Real-Time PCR System (Fisher Scientific) with PowerUp SYBR Green Mastermix (Fisher Scientific, A25778). The SYBR Green Mastermix was prepared according to the supplier's instructions to a final volume of 10  $\mu$ l and a final concentration of  $0.25 \cdot 10^{-6}$  mol/l or  $0.5 \cdot 10^{-6}$  mol/l of primers. Table 4 and Table 5 list all used primer pairs, their sequence as well as the used annealing temperature in RT-qPCR. All primer pairs were verified with the NCBI primer BLAST tool (<https://www.ncbi.nlm.nih.gov/tools/primer-blast/>) and purchased from Sigma-Aldrich. To confirm primer specificity, a melt curve after RT-qPCR was performed, and the PCR products were separated on a handmade 1% agarose gel to confirm one product band only and the absence of primer dimers. NTC was used in every RT-qPCR. The following conditions were included in RT-qPCR: 2 min at 50 °C, 2 min at 95 °C, followed by 40 cycles of 15 s at 95 °C and 1 min at annealing temperature. Ct values were extracted from StepOnePlus software, and *HPRT* and *Hprt* respectively were used as housekeeping genes. The level of mRNA expression was calculated as follows:  $\Delta Ct = Ct$  value of housekeeping gene – Ct value of gene of interest;  $\Delta\Delta Ct = \Delta Ct$  of condition (e.g. LV EV siVCAN; shIRF9 si neg; LV IRF9) -  $\Delta Ct$  of Control condition (e.g. LV EV si neg; sh scr si neg; LV EV) [172]. Knockdown efficiency was calculated as  $100 \cdot 2^{-\Delta\Delta Ct}$  and displayed as percentage of control condition.

Table 4. List of primers used for RT-qPCR of human mRNA.

Gene symbol	NCBI RefSeq	Primer Sequence (5' – 3')	Annealing temperature [°C]	Final concentration [ $10^{-6}$ mol/l]	PCR product size [bp]
<i>ADGRL3</i>	NM_001322402.3	FP: TGCGGACTAGGATAAAGAGTGG RP: CCCATCGGTAAGGGGAGGTAT	60	0.25	75
<i>CDKN1A</i>	NM_000389.5	FP: AGTCAGTTCCTTGTGGAGCC RP: GCATGGGTTCTGACGGACAT	58	0.5	109
<i>CDKN1B</i>	NM_004064.5	FP: ATCACAAACCCTAGAGGGCA RP: GGGTCTGTAGTAGAACTCGGG	58	0.5	77
<i>CLDN1</i>	NM_021101.5	FP: TGGAAGACGATGAGGTGCAGAAAGA RP: CAACTAAAATAGCCAGACCTGCA	58	0.5	84
<i>DUSP26</i>	NM_024025.3	FP: TAACTGGCTTTGGGCTTCTATG RP: GATGTTGAACGTTGGCATCT	60	0.25	110
<i>EGFR</i>	NM_005228.5	FP: GCGTTCGGCACGGTGTATAA RP: GGCTTTCGGAGATGTTGCTTC	60	0.5	102
<i>EMP1</i>	NM_001423.3	FP: TCTGATTCCCTTCATTGTGTGA RP: TCCAAATCAAACCTGATAGGCAGC	60	0.25	107

<i>GRHL3</i>	NM_021180.4	FP: CAGGAGTCGATGCTCTTCCC RP: CCCAGGGTGTATTCAAAGTCAC	60	0.25	101
<i>HPRT</i>	NM_000194.3	FP: TGACACTGGCAAAAACAAT RP: GGTCCTTTTCACCAGCAA	60	0.5	94
<i>IGFBP5</i>	NM_000599.4	FP: TGACCGCAAAGGATTCTACAAG RP: CGTCAACGTACTIONCATGCCT	60	0.25	119
<i>IRF9</i>	NM_001385400.1	FP: CCATCAAAGCGACAGCACAG RP: GAGCACAGAGGGACTGAGTG	60	0.5	90
<i>PADI2</i>	NM_007365.3	FP: ACAAAGTGGGCGTGTCTACG RP: CCACCCGTGTACTIONGACCA	60	0.25	103
<i>PCNA</i>	NM_002592.2	FP: TTTTCTGTACCAAATTTGTACCTC RP: CTGCATTTAGAGTCAAGACCCTTT	60	0.5	203
<i>SERPINI1</i>	NM_005025.5	FP: GGTAAGTCTAAAGAGAGCCAAT RP: CGGCTACATTTTGACTIONGAAGTCC	60	0.25	152
<i>SH3TC2</i>	NM_024577.4	FP: GGTACTIONGGTGCAGCCTTGG RP: CCTGGCTCATAACCCGTCAA	60	0.25	159
<i>STAT1</i>	NM_139266.3	FP: ATCAGGCTCAGTCGGGGAATA RP: TGGTCTCGTGTCTCTGTCTTCT	58	0.25	186
<i>STAT2</i>	NM_005419.4	FP: CTGCTAGGCCGATTACTIONACCC RP: TCTGATGCAGGCTTTTTGCTG	58	0.5	87
<i>TP53</i>	NM_000546.6	FP: CAGCACATGACGGAGTTGT RP: TCATCCAAATACTIONCCACACGC	60	0.25	125
<i>TRIM29</i>	NM_012101.4	FP: CAAGCACCTGCGATGGA RP: GTTGGTGGTCTTGGCATIONCCTT	60	0.25	145
<i>VCAN</i>	NM_004385.5	FP: GAATGTCACTIONCTAATCCCTGTC RP: TGTCTCGGTATIONCTTGCTCAC	60	0.25	117
<i>VCAN</i> [V1]	NM_001164097.2	FP: AGGTGGTCACTIONTGGGGTGA RP: TCACTIONCATTCGACGTTTAAAGCA	60	0.25	108

Table 5. List of primers used for RT-qPCR of murine mRNA.

Gene symbol	NCBI RefSeq	Primer Sequence (5' – 3')	Annealing temperature [°C]	Final concentration [10 <sup>-6</sup> mol/l]	PCR product size [bp]
<i>Arg1</i>	NM_007482.3	FP: GGTTCTGGGAGGCCTATCTT RP: CACCTCTCTGCTGTCTTCC	58	0.5	127
<i>Ccl2</i>	NM_011333.3	FP: CTACAAGAGGATCACCAGCAG RP: TTCTGATCTATTTGGTTCCGA	60	0.25	145
<i>Cd274</i>	NM_021893.3	FP: GCTCAAAGGACTTGTACGTG RP: TGATCTGAAGGGCAGCATIONTC	60	0.25	238
<i>Chit1</i>	NM_027979.2	FP: CCCTGGGTCTCGAGGAAGCCC RP: GCAGCCTTGGAACTIONGCTTTCTCCAC	58	0.5	113
<i>Hprt</i>	NM_013556.2	FP: GCTGACCTGCTGGATTACAT RP: TTGGGGCTGTACTIONGCTTAAC	60	0.5	242
<i>Il1b</i>	NM_008361.4	FP: TTTGACAGTGATGAGAATGACC RP: AATGAGTGATACTIONGCTGCC	60	0.25	162
<i>Il10</i>	NM_010548.2	FP: CAGAGAAGCATGGCCCAGA RP: TGCTCCACTGCTTGTCTTAA	58	0.5	130

<i>Irf9</i>	NM_001159417.1	FP: GGGGTATGGTAAGGAGAAGGATG RP: ATGGTCTTGGCTGCATCGTC	60	0.25	130
<i>Nos2</i>	NM_010927.4	FP: CACCAAGCTGAACTTGAGCG RP: CCATAGGAAAAGACTGCACCG	58	0.25	105
<i>Pcna</i>	NM_011045.2	FP: GGGTTGGTAGTTGTCGCTGT RP: TCCAGCACCTTCTTCAGGAT	60	0.5	172
<i>Pdcd1</i>	NM_008798.3	FP: CAGCTTGTCCTCAACTGGTCG RP: GCTCAAACCATTACAGAAGGCG	60	0.25	100
<i>Pdgfra</i>	NM_011058.3	FP: TCCATGCTAGACTCAGAAGTCA RP: TCCCGGTGGACACAATTTTTC	60	0.25	140
<i>Stat1</i>	NM_009283.4	FP: GCTGCCTATGATGTCTCGTTT RP: TGCTTTTCCGTATGTTGTGCT	60	0.25	124
<i>Stat2</i>	NM_019963.2	FP: GGCAGCGAATCACTCAAAGC RP: CACCAGAGTCAAGAAGCCGA	60	0.5	159
<i>Tnf</i>	NM_013693.3	FP: GTCCCAAAGGGATGAGAAGT RP: TTTGCTACGACGTGGGCTAC	60	0.25	124
<i>Vcan</i>	NM_001081249.1	FP: GAAGGGAACAGTTGCTTGCG RP: TTAGGCATTGCCCATCTCCC	60	0.25	177

### 3.2.4. DNA isolation

DNA was isolated from A549 using TriZOL reagent according to the manufacturer's protocol. Briefly, after centrifugation of mixed TriZOL-cell-lysate and 1-Bromo-3-chloropropane, the aqueous phase was removed, and 100% ethanol was added and inverted to mix. Precipitated DNA was gained by centrifugation followed by washing steps. The air-dried DNA was resuspended in  $8 \cdot 10^{-6}$  mol/l sodium hydroxide (NaOH) solution, and the concentration and purity of DNA was measured using NanoDrop 2000.

### 3.2.5. RNA-seq

For RNA-sequencing (RNA-seq), RNA was isolated from three independent viral transductions of each construct (A549 LV EV; A549 LV IRF9; A549 sh scr; A549 shIRF9) using the miRNeasy micro Kit (Qiagen) combined with on-column DNase digestion (DNase-Free DNase Set, Qiagen) to avoid contamination by genomic DNA. RNA and library preparation integrity were verified with LabChip Gx Touch 24 (Perkin Elmer). 3  $\mu$ g of total RNA was used as input for the Truseq Stranded mRNA Library preparation following the low sample protocol (Illumina). Sequencing was performed on the NextSeq500 instrument (Illumina) using v2 chemistry, resulting in a minimum of 25M reads per library with 1x75bp single end setup. The resulting raw reads were assessed for quality, adapter content and duplication rates with FastQC [173]. The trimmomatic version 0.36 was employed to trim reads after a quality drop below a mean of Q20 in a window of 10 nucleotides [174], and only reads between 30 and 150 nucleotides were cleared for further analyses. Trimmed and filtered reads were aligned versus the Ensembl human genome version hg38 (GRCh38) using STAR 2.6.0c mapped length to 10% and parameter '—outFilterMultimapNmax to 999' to allow mapping in multiple positions [175]. The number of reads aligning to genes was counted with the featureCounts 1.6.0 tool from the Subread package [176].

Only reads mapping at least partially inside exons were admitted and aggregated per gene, whereas reads overlapping multiple genes or aligning to multiple regions were excluded. Differentially expressed genes were identified using DESeq2 version 1.18.1 [177]. Only genes with a maximum  $p$  value of 0.05 and a minimum combined mean of 5 reads were deemed to be significantly differentially expressed. The Ensembl annotation was enriched with UniProt data (release 06.06.2014) based on Ensembl gene identifiers [178].

### **3.2.6. Immunocytochemistry**

For immunocytochemistry (ICC), cells were seeded in 8-well glass chamber slides (Sarstedt) and allowed to grow to a confluence of 70%. Cells were then washed with 1X PBS pH 7.4, fixed with 4% PFA (Sigma-Aldrich, 158127), and treated with 0.3% Triton X-100 (Carl Roth, 3051.3). After blocking with 1% BSA for 1 h, IRF9 antibody (1:100; SCBT, sc-10793) or mouse IgG (1:250 CST, 5415) was applied for 90 min, cells were thoroughly washed, and then the secondary antibody Donkey anti-mouse IgG Alexa Fluor 488 (1:1000; ThermoFisher, R37114) was applied for 1 h. Slides were washed, and nuclei were stained by DAPI Mounting Medium (dianova, 038448). The slides were visualised under a confocal microscope (Zeiss LSM 710) using Zen 2011 software.

## **3.3. Functional cell analysis**

### **3.3.1. Proliferation**

Proliferation was assessed using a BrdU incorporating colorimetric cell proliferation ELISA (Roche, 11647229001), according to the manufacturer's instruction. ELISA was measured in a microplate reader Infinite M200 PRO (Tecan). To compare proliferation, the same number of cells was seeded in a 96-well plate and starved in serum-free medium for 24 h. After adding full, medium-reduced or conditioned medium for additional 24 h, proliferation was assessed.

### **3.3.2. Migration**

For migration, similar numbers of previously serum-starved cells were seeded in a transwell membrane insert with reduced medium (8  $\mu$ m pore size; Falcon, 353097) and allowed to migrate for 6 h towards the lower compartment filled with full medium. Afterwards, migrated cells were fixed with methanol, stained with 10% crystal violet (Sigma-Aldrich, V5265), excised and then fixed onto slides using Pertex mounting medium (Medit Service AG, LEIC811). Slides were scanned using NanoZoomer slide scanner (Hamamatsu Photonics), and the number of migrated cells were quantified with Fiji software and macro ITCN (NIH).

### 3.4. Human data

#### 3.4.1. Kaplan-Meier analyses

For the Kaplan-Meier analysis, we used online available data from a total of 1,926 lung tumours which had been profiled by Affymetrix microarray analysis (www.kmplot.com) [179]. By this, the *IRF9* (probe set ID: 203882-at), *STAT1* (probe set ID: 200887\_s\_at), *STAT2* (probe set ID: 2253636\_at) and *VCAN* (probe set ID: 204620\_s\_at) expression levels were divided at the median into high vs low subgroups. Overall survival analyses by Kaplan-Meier and Cox Proportional Hazard for all lung tumours, LUAD and LUSC were performed and displayed together with the number of usable samples.

#### 3.4.2. Gene expression profile using online tool USCS Xena

To acquire gene expression from a large cohort of human lung cancer patients, we used USCS Xena, which is available online. Data from TCGA TARGET GTEx study were used as DESeq2 standardised expression for *IRF9*, *STAT1*, *STAT2* and *VCAN* and allowed to compare expression in non-tumour lungs and lungs affected by cancer, which was further distinguished in LUAD or LUSC [180]. We performed and displayed the calculation of the correlation coefficient of *IRF9* with either *STAT1*, *STAT2* or *VCAN* expression of each individual.

#### 3.4.3. Acquisition of human lung cancer samples

RNA and protein samples from human LUAD tissue were obtained from the Lungbiobank Heidelberg, member of the Biomaterialbank Heidelberg and the Biobank platform of the German Center for Lung Research. Formalin-Fixed Paraffin-Embedded (FFPE) lung tissue specimen were obtained from the Institute for Pathology (Giessen, Germany). Lung cancer tissue microarray (TMA) LUC1501 contains 150 cores from normal/benign (3 cases) and cancer (70 cases with grading and TNM staging data) duplicated cores per case, which were purchased from Pantomics, Inc. (Cat no. LUC 1501; Richmond, CA, USA). The tumour specimens were presented in duplicates for internal control and to assess tumour heterogeneity. In addition, a pathologist validated the tumours in the cores. The study protocol for tissue donation was approved by the Ethics Committee ('Ethik-Kommission des Fachbereichs Medizin der Justus-Liebig-Universität Giessen') of the University Hospital Giessen (Giessen, Germany) in accordance with the national law and 'Good Clinical Practice/International Conference on Harmonisation' guidelines. Written informed consent was provided by each patient or their next of kin (AZ 58/15).

### 3.5. Promoter analysis

#### 3.5.1. In-silico analysis of *VCAN* promoter

To study the promoter of *VCAN* and extract the binding motif of IRF9 at ISRE, we used the online tool HOMER v4.10 ([homer.ucsd.edu/homer/](http://homer.ucsd.edu/homer/)) [181]. The sequence of the *VCAN* promoter was extracted from the online tool Eukaryotic Promoter Database ([epd.epfl.ch](http://epd.epfl.ch)) spanning from -1000bp to +100bp [182]. To calculate possible binding of IRF9 and to identify potential ISREs in the *VCAN* promoter, we used FIMO (Find Individual Motif Occurrences) from online tool MEME Suite 5.1.1 ([meme-suite.org/tools/fimo](http://meme-suite.org/tools/fimo)) and considered results with  $p < 0.001$  for further analysis [183].

#### 3.5.2. Chromatin Immunoprecipitation

A549 cells were cross-linked using 1% Formaldehyde (Sigma-Aldrich, F8775) for 10 min and quenched using a final concentration of  $125 \cdot 10^{-3}$  mol/l Glycine (Carl Roth, 0079.1) for 5 min. All the following steps were carried on ice and pre-chilled buffers and solutions used, supplemented with cOmplete Protease Inhibitor Cocktail (Roche, 11697498001),  $0.2 \cdot 10^{-3}$  mol/l PMSF (Sigma-Aldrich, 93482-250ML-F) and  $0.1 \cdot 10^{-3}$  mol/l Sodium Orthovanadate (NEB, P0758S). After intense washing with 1X PBS pH 7.4 (Gibco, 10010056), cells were lysed in L1 lysis buffer to separate nuclei, which were harvested by centrifugation. Nuclei were resuspended in L2 buffer and sonicated by 3 cycles of 5 s with tip sonicator (Bandelin Sonopuls) followed by 20 cycles of 30 s on / 30 s off with Bioruptor Pico (Diagenode). After centrifugation, a fragment size between 200 and 500 bp was confirmed by agarose electrophoresis, and soluble chromatin was diluted in dilution buffer and immunoprecipitated using specific antibodies against Histone H3 (abcam, ab12079), IRF9 (SCBT, sc-365893 X) and IgG1 as a control (CST, 5415). Chromatin-antibody complexes were further bound to BSA-blocked Protein G Agarose beads (Sigma-Aldrich, 16-201). The purification of chromatin-antibody-beads complexes was assured by mild inverting with high/low salt buffer and LiCl buffer. Chromatin was eluted with elution buffer, followed by RNase (ThermoFisher, EN0531) and Proteinase K (Sigma-Aldrich, P2308) treatment to avoid any contamination. Table 7 shows the composition and concentration of the used buffers.

Table 6. List of primers used for RT-qPCR of human promoter sequences.

Gene promoter	Region spanned by primer	Primer Sequence (5' – 3')	Annealing temperature [ °C]	Final concentration [ $10^{-6}$ mol/l]	PCR product size [bp]
<i>ACTB</i>	-751 to -670	FP: AACCGGACCGCCGTG RP: TCGCGCCTCCGAAC TG	60	0.25	82
<i>VCAN</i>	-670 to -531	FP: CATTGGGCAGTTCCTGG RP: CTTGCCTGTCCCATCAAAGG	60	0.25	140

DNA was purified using a QIAquick PCR purification kit (Qiagen) according to the supplier's instruction and subjected to RT-qPCR. Promoter enrichment was calculated as percentage of input:  $100 \cdot 2(-\Delta CT)$  [ $\Delta CT = CT_{ChIP} - (CT_{Input} - \log_2 \text{dilution factor})$ ]. Table 6 lists the sequence of used primers, and the promoter's region was spanned.

**Table 7. List and composition of used buffers for Chromatin Immunoprecipitation.** Supplier and respective ordering number are indicated in brackets.

Buffer	Final concentration	Composition
L1 lysis buffer	50·10 <sup>-3</sup> mol/l 2·10 <sup>-3</sup> mol/l 0.2% 10%	Tris-HCl pH 8.0 (Roth, 9090.3) EDTA pH 8.0 (Roth, 8043.1) IGEPAL (Sigma-Aldrich, I8896-50ML) Glycerol (Roth, 4043.1)
L2 buffer	50·10 <sup>-3</sup> mol/l 5·10 <sup>-3</sup> mol/l 1%	Tris-HCl pH 8.0 EDTA pH 8.0 Sodium dodecyl sulfate (Sigma-Aldrich, 436143-100G)
Dilution buffer	50·10 <sup>-3</sup> mol/l 5·10 <sup>-3</sup> mol/l 0.5% 0.2·10 <sup>-3</sup> mol/l	Tris-HCl pH 8.0 EDTA pH 8.0 IGEPAL Sodium chloride (NaCl; Roth, 3957.1)
Low salt washing buffer	20·10 <sup>-3</sup> mol/l 2·10 <sup>-3</sup> mol/l 1% 0.1% 0.15·10 <sup>-3</sup> mol/l	Tris-HCl pH 8.0 EDTA pH 8.0 IGEPAL Sodium dodecyl sulfate (SDS; ) NaCl
High salt washing buffer	20·10 <sup>-3</sup> mol/l 2·10 <sup>-3</sup> mol/l 1% 0.1% 0.5·10 <sup>-3</sup> mol/l	Tris-HCl pH 8.0 EDTA pH 8.0 IGEPAL SDS NaCl
LiCl washing buffer	10·10 <sup>-3</sup> mol/l 1·10 <sup>-3</sup> mol/l 1% 1% 0.25 mol/l	Tris-HCl pH 8.0 EDTA pH 8.0 IGEPAL Sodium deoxycholate (Sigma-Aldrich, D6750-100G) Lithium chloride
Elution buffer	10·10 <sup>-3</sup> mol/l 1·10 <sup>-3</sup> mol/l 0.1·10 <sup>-3</sup> mol/l 0.1%	Tris-HCl pH 8.0 EDTA pH 8.0 NaHCO <sub>3</sub> SDS

### 3.5.3. Cloning

An 818 bp segment of the upstream promoter sequence of human VCAN, including potential ISREs, was amplified from human A549 DNA using Phusion High-Fidelity DNA Polymerase (NEB, M0530L) and specific primers with an overhanging sequence for restriction enzymes: FP: 5'-ATA TTA CTC GAG GAC TGA AGG AAA GGA AGA ACG AAG-3' (XhoI); RP: 5'-ATT TAA GCT TTC AGA GCC GAG GAG GAG ACT CA-3' (HindIII). PCR products were

separated on handmade 1% agarose gels, and excised bands were purified with GenElute (Sigma-Aldrich, NA1020). The PCR construct and pGL3 basic (Promega) vector were restricted with the aforementioned enzymes; the paternal plasmid was digested with DpnI; ligation was conducted with T4 DNA ligase in a ratio of 1:3 before transformation into 10-beta competent *Escherichia Coli* (all NEB: R0176; M0202S; C3019H) and finally incubated overnight on agar plates containing 100 mg/l ampicillin (Roche, A0166) at 37 °C. Clones were screened via PCR using the recommended primer pair GLprimer2: 5'-CTT TAT GTT TTT GGC GTC TTC CA-3'; RVprimer3: 5'-CTA GCA AAA TAG GCT GTC CC-3'. The used primers included the restriction site; it was thus possible to identify positive insertion by respective PCR product length after agarose gel electrophoresis. Positive clones were cultured in LB broth (Roth, X964.1) containing 100 mg/l ampicillin overnight at 37°C. Plasmids of positive clones were purified with peqGOLD Plasmid Miniprep (VWR, #13-6943-02) according to manufacturer's protocol and confirmed by test restriction and sequencing via Eurofins (Cologne).

### 3.5.4. Luciferase

To assess luciferase activity, a Dual-Glo Luciferase Assay System (Promega, E2920) was used according to the manufacturer's instructions. Therefore, cells were co-transfected with the firefly luciferase plasmids pGL3 basic, pGL3 VCAN 818 bp, or pGL4.45 together with the renilla luciferase plasmid pCMV-RL (Promega, E2261); the latter was used as internal control. pGL4.45 was purchased from Promega; it sequentially contains five ISREs prior to a minimal promoter and the luc2P gene.

Naïve or transduced A549 were seeded in 48-well plates and grown to a confluence of 70%. Next, 250 ng of firefly luciferase plasmid, together with 5 ng pCMV-RL, were mixed in OptiMEM prior to the addition of Fugene HD in a ratio of 1:3 to obtain mastermix, which was gently mixed and incubated for 5 minutes and then added to the cells. After 24 h, medium was refreshed, or, when indicated, type I IFN or 1X PBS was applied. After an additional 24 h, cells were washed intensely and lysed with passive lysis buffer. Cell lysates were transferred to white 96-well plates, LAR II was applied, and firefly luciferase was measured using an Infinite M200 PRO microplate reader (Tecan). STOP & Glo was applied, and Renilla luciferase was measured accordingly. Luciferase activity of non-transfected controls was used as negative control. Renilla luciferase activity was used to normalise the activity of firefly luciferase.

## 3.6. Histology

### 3.6.1. Immunohistochemistry (IHC)

For IHC, FFPE tissue specimen from characterised human LUAD patients or murine tissues were trimmed to 4 µm sections. Sections were deparaffinised and rehydrated by a serial xylol-ethanol-isopropanol treatment. Next, slides were heated for 30 min in citrate buffer 6.0 to retrieve antigens, followed by washing and blocking with 5% BSA for 1 h at room temperature. Primary

antibodies were applied overnight at +4 °C: IRF9 (1:100; SCBT, sc-10793); IBA1 (1:120; Wako, 019-19741); pan-Cytokeratin (1:800; Dako, Z0622); PCNA 1:200 (SCBT, sc-7987); CD68 1:100 (abcam, ab125047); VCAN 1:150 (abcam, ab19345); mouse IgG (CST, 5415); rabbit IgG (SCBT, sc-66931). After intense washing, secondary antibodies were applied for 1 h at room temperature: Donkey anti-mouse IgG Alexa Fluor 488 (1:1000 ThermoFisher, R37114); Goat anti-rabbit IgG Alexa Fluor 555 (1:1000 ThermoFisher, A27039). The slides were washed, and the nuclei were stained by DAPI Mounting Medium (dianova, 038448). The slides were visualised under a fluorescence microscope (Leica Microsystems) using LAS software.

### **3.6.2. Lung cancer tissue microarray (TMA) and xenograft tumours**

In preparation for IHC staining, 3 µm TMA and 4 µm xenograft tumour sections were rehydrated, and antigen-retrieval was achieved with citrate buffer, as previously described [44, 184]. Then, the sections were blocked and incubated with IRF9 1:100 (SCBT, sc-10793) and VCAN 1:150 (abcam, ab19345) primary antibody overnight. A ZytoChem Plus (AP) Polymer Kit (Zytomed Systems, POLAP-100) was used for detection, following the manufacturer's instructions. Sections were embedded with Pertex and scanned using a NanoZoomer slide scanner (Hamamatsu Photonics).

### **3.6.3. Haematoxylin & Eosin staining**

FFPE mouse lung sections were deparaffinised and rehydrated by a serial xylol-ethanol-isopropanol treatment. After washing with deionised water, sections were incubated with Mayer's Haematoxylin (AppliChem, AP254766.1610) for 10 min at room temperature followed by washing under running water for 5 min. Next, slides were incubated with Eosin Y (AppliChem, AP253999.1210) for 2 min at room temperature followed by a short washing step with deionised water. After a serial ethanol-xylol treatment, slides were mounted with Pertex and analysed using a Nanozoomer slide scanner [58].

## **3.7. Animal experiments**

All animal studies were approved by the competent authority (Regierungspräsidium Darmstadt, Hessen, Germany; approval no. B2/1062) and performed in accordance with German animal protection law (TierSchG). Mice were kept under specific pathogen-free conditions in individual ventilated cages (IVC).

### **3.7.1. Mouse lines**

Wildtype C57BL/6N mice (WT) were purchased from Charles River Laboratories (Sulzfeld, Germany). BALB/c nude mice lack a thymus, are unable to produce T cells and are therefore immunodeficient. Nude mice were purchased from Charles River Laboratories and were used for mouse models with human cells.

C57BL/6N *Irf9<sup>tm1Tg</sup>* (*Irf9* targeted mutation 1 by Tadatsugu Taniguchi; *Irf9<sup>-/-</sup>*) were provided by Magdalena Huber's lab (University Marburg, Germany) and had been previously characterised. The mutation in the *Irf9* sequence targets two exons encoding for the DNA binding domain, which were replaced by a neomycin cassette [133, 142].

### 3.7.2. Genotyping of *Irf9<sup>-/-</sup>* mice

Tail tip samples were collected from new-born mice and lysed in 200  $\mu$ l lysis buffer (50 $\cdot$ 10<sup>-3</sup> mol/l Tris pH 8.0; 50 $\cdot$ 10<sup>-3</sup> mol/l EDTA; 0.5% SDS; 0.5 g/l Proteinase K) at 56°C for 4-12 h. Debris and particles were removed by centrifugation, and supernatants were collected. The lysates were diluted 1:10 and thereof 1  $\mu$ l used as DNA template in PCR with REDTaq ReadyMix (Sigma-Aldrich; R2523-100RXN). The mastermix was used according to the manufacturer's instruction with a total volume of 20  $\mu$ l, supplemented with 0.3125 $\cdot$ 10<sup>-6</sup> mol/l MgCl<sub>2</sub> and the primers Neo p48, E3G and ISGF3G, as indicated in Table 8. The following conditions were used in PCR: 3 min at 94°C, followed by 35 cycles of 30 s at 94°C, 30 s at 60°C and 90 s at 72°C, completed by a final 5 min at 72°C. The PCR products were detected on handmade 1% agarose gels with sizes of 950 bp for WT and 700 bp for *Irf9<sup>-/-</sup>*, respectively (visualised in Figure 9).

**Table 8.** List of primers used for mouse genotyping.

Primer	Primer Sequence (5' – 3')	Final concentration [10 <sup>-6</sup> mol/l]
Neo p48	TCAATGTTCCGATGTGGCAGTTCAAAGGATC	0.125
E3G	TATCGAATACTGCCAGCAGGAACCC	0.25
ISGF3G	TCCTGCTTTACGCTATCGCCGCTCCCGATT	0.375

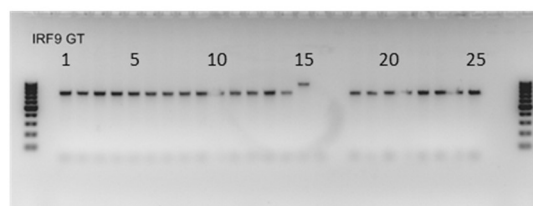


**Figure 9.** Genotyping of *Irf9<sup>-/-</sup>* offspring. Lysed mice tail tips were genotyped for *Irf9* mutation. As example: Individual 15 is homozygous wildtype for *Irf9*; Individual 20 is homozygous *Irf9*-deleted.

### 3.7.3. Subcutaneous tumour model

Subcutaneous tumour models were performed as described previously [185]. Tumour cells were resuspended in a final volume of 100  $\mu$ l 0.9% NaCl (B.Braun, 02159621) and injected with 24G Sterican needle (B. Braun, 02050841) subcutaneously into the flank of the mice. Mice were monitored daily and the tumour volume was measured every 4 days using calipers [volume = (width<sup>2</sup> x length)/2]. At the endpoint, animals were euthanised, and subcutaneous tumours were excised, photographed and weighed; then, perfused lungs were extracted and photographed. All

organs were fixed in 4% PFA and dehydrated for further IHC. Tumour parts were stored at -80 °C for further molecular biology or processed as single cell suspension for flow cytometry directly after excision.

### **Subcutaneous xenograft model**

$3 \times 10^6$  A549 IRF9 cells were injected into each BALB/c nude mouse. In total, 10 mice per condition were injected; A549 LV IRF9 were compared with A549 LV EV and A549 shIRF9 with A549 sh scr, respectively. The endpoint was reached 32 days after injection.

### **Subcutaneous syngeneic model**

For the injection of transduced CULA Irf9 cells,  $1 \times 10^6$  cells were injected into each C57BL/6N mouse. In total, 6 mice per condition were injected; CULA LV Irf9 were compared with CULA LV EV and CULA shIrf9 with CULA sh scr, respectively. The endpoint was reached 20 days after tumour formation.

For the injection of LLC1,  $1 \times 10^6$  cells were injected into either C57BL/6N or *Irf9*<sup>-/-</sup> mice. In total, 12 mice per condition were injected; *Irf9*<sup>-/-</sup> mice were compared with C57BL/6N mice, and the endpoint was reached 20 days after injection.

#### **3.7.4. Intravenous tumour model**

$1 \times 10^6$  LLC1 cells were resuspended in a final volume of 200  $\mu$ l 0.9% NaCl and injected into the tail vein of either C57BL/6N or *Irf9*<sup>-/-</sup> mice. In total, 12 mice per condition were injected and monitored daily. The endpoint was reached 16 days after injection: animals were euthanized; lungs were perfused, excised and photographed; tumour nodules were counted macroscopically; lungs were fixed in 4% PFA and dehydrated for further IHC. One part of the lung was stored at -80 °C for further molecular biology.

#### **3.7.5. Isolation and generation of bone marrow-derived macrophages (BMDM)**

Femur and tibia were prepared from 8–12 weeks old wildtype C57BL/6N or *Irf9*<sup>-/-</sup> mice. The bones were opened and flushed with 1X PBS pH 7.4, and the extracted bone marrow was filtered through 40  $\mu$ m cell strainer (Sarstedt, 83.3945.040) to remove bone and muscle debris. Erythrocytes were lysed incubating RBC lysis buffer (Invitrogen, 00-4300-54) for 5 min and removal by centrifugation. After two washing steps with 1X PBS pH 7.4, cells were resuspended in culture medium for macrophages, consisting of RPMI 1640 (Gibco, 11879-020), supplemented with 10% FCS, 1 U/ml Penicillin-Streptomycin and 40 ng/ml recombinant murine M-CSF (R&D systems, 416-ML-500). Cells were seeded into 6-well plates (Sarstedt), and fresh culture medium was replaced every 3 days. After 10–14 days, monocytes differentiated to macrophages and were ready to use. Macrophages were polarised by adding 100 ng/ml LPS (Sigma-Aldrich, L2630-100MG) and 100 U/ml IFN $\gamma$  (R&D systems, 485-MI-100) for M1 phenotype and 20 ng/ml IL4 (R&D systems, 404-ML-025) for M2 phenotype. Twenty-four hours after polarisation, cells were washed, and

culture medium without cytokines was added, collected after additional 24 h and used as conditioned medium in further experiments according to the phenotype of macrophages. Together with conditioned medium, macrophages were harvested and used for further analyses.

### 3.7.6. Flow cytometry

To analyse the cell composition of tissues, we prepared single cell suspension. Standardised amounts of solid tissues, such as subcutaneous tumours or lungs, were fragmented using scalpels to allow enzymatic digest. Then, tissue was incubated in RPMI 1640 (Gibco, 11879-020), supplemented with 1 U/ml Penicillin-Streptomycin, 10 µg/µl deoxyribonuclease (Thermo Scientific, EN0525) and 5 µg/µl Collagenase (Gibco, 17101015) for 30 min at room temperature under mild conversion. To remove debris, the mixture was filtered through a 100 µm (Sarstedt, 83.3945.100) and 40 µm cell strainer followed by incubation with RBC lysis buffer for 5 min at room temperature. Cells were washed twice with 1X PBS pH 7.4 and resuspended in 0.5% BSA in 1X PBS pH 7.4. After blocking FcγR for 15 minutes, the cells were stained for 15 minutes at 4 °C with the following antibodies: CD1c-PE/Dazzle594 (Biolegend, 331531), CD15-FITC (BD, 560997), CD33-BV510 (BD, 563257), CD45-AF700 (Biolegend, 368514), CD326-FITC (Biolegend, 324203), HLA-DR-APC/Fire750 (Biolegend, 307658), MerTK-BV421 (Biolegend, 367603), CD14 PerCP-Cy5.5 (BD, 561116) and CD64 BV605 (BD, 740406). Flow cytometry-based cell analysis was performed using an LSR II/Fortessa flow cytometer (BD Biosciences) and analysed using FlowJo software 7.6.1 (Treestar, Ashland, OR, USA), as previously described [44, 186]. All antibodies and secondary reagents were titrated to determine optimal concentrations. Antibody-capturing CompBeads (BD Biosciences) were used for single-color compensation to create multicolour compensation matrices, and fluorescence minus one (FMO) controls for gating. Instrument calibration was controlled using Cytometer Setup and Tracking beads (BD Biosciences).

### 3.8. Statistical analysis

Statistical analysis was performed with the GraphPad Prism 8 software. Ordinary one-way analysis of variance (ANOVA) was used to compare the means of individual groups to those of the control group. To compare two independent groups, we used an unpaired t test when standard deviation was assumed to be same. If standard deviation was not the same, we used Welch's t test. All sample sizes were tested for Gaussian distribution and subjected to Grubbs' outlier test. Data are expressed as mean ± SEM, and *p* value denoted statistical significance as follows: \* *p* ≤ 0.05; \*\* *p* ≤ 0.01; \*\*\* *p* ≤ 0.001; \*\*\*\* *p* ≤ 0.0001.

## 4. Results

### 4.1. IRF9 is highly expressed in human lung cancer patients

It is of great interest to determine the risk of lung cancer patients over the expression of IRF9 and its known binding partners STAT1 and STAT2. Therefore, we analysed Kaplan-Meier curves for the survival of lung cancer patients as well as of LUAD and LUSC patients, respectively.

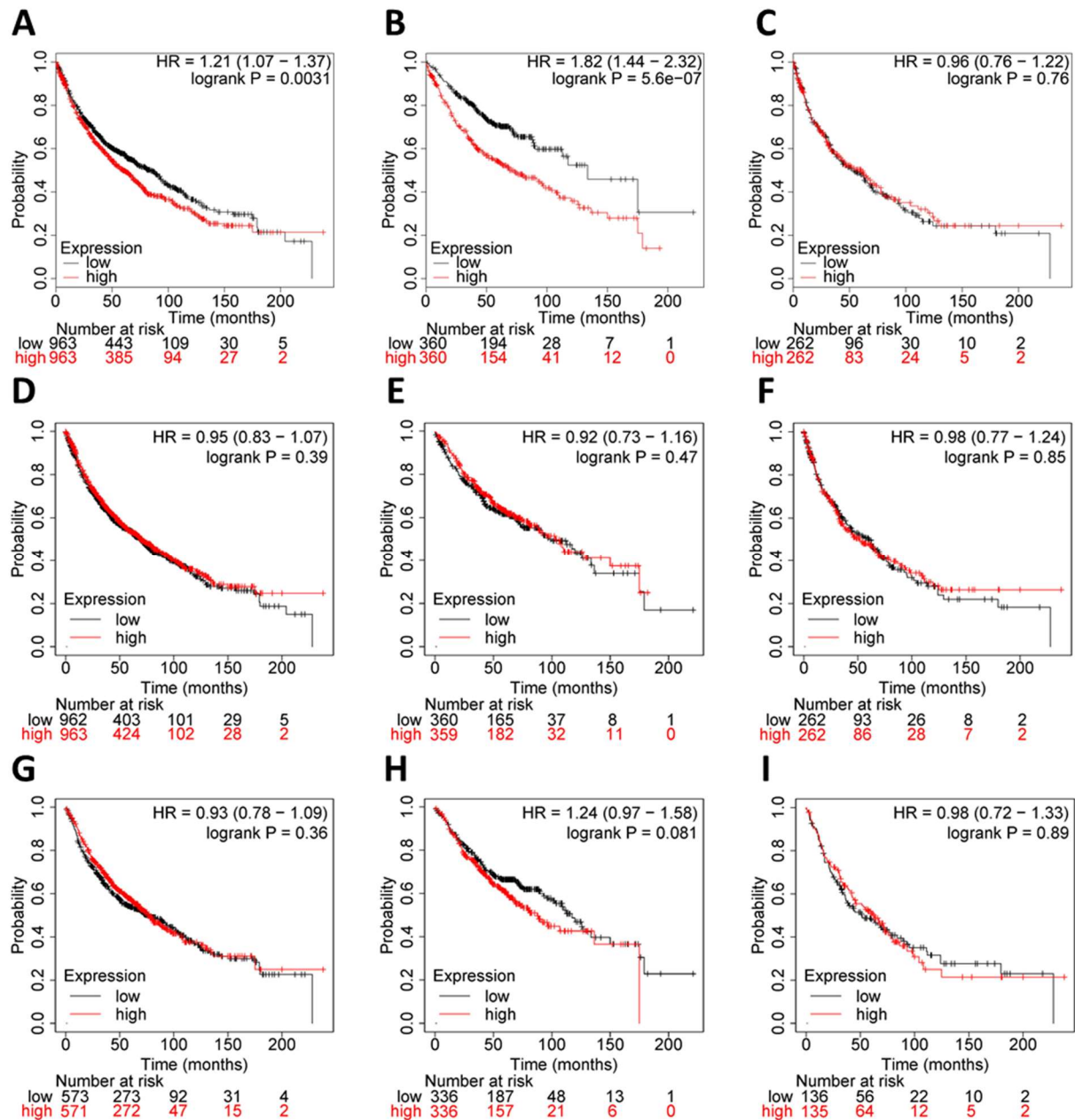


**Figure 10.** IRF9 expression is associated with a decreased survival in lung cancer patients. (A-I) Kaplan-Meier curves for *IRF9* levels over the survival of (A) all classes of lung cancer ( $n = 1926$ ), (B) LUAD ( $n = 720$ ), (C) LUSC ( $n = 524$ ) patients; *STAT1* levels over the survival of (D) all classes of lung cancer ( $n = 1925$ ), (E) LUAD ( $n = 719$ ), (F) LUSC ( $n = 524$ ) patients; *STAT2* levels over the survival of (G) all classes of lung cancer ( $n = 1144$ ), (H) LUAD ( $n = 672$ ), (I) LUSC ( $n = 271$ ) patients. Patients were divided by median into high and low expression.

High *IRF9* expression levels were associated with a lower overall survival in lung cancer patients (Figure 10 A; HR = 1.21,  $P = 0.0031$ ) and even lower survival in LUAD patients (Figure 10 B; HR = 1.82,  $P = 5.6 \cdot 10^{-7}$ ). In LUSC patients, we observed no differences in survival over the expression level (Figure 10 C; HR = 0.96,  $P = 0.76$ ). Interestingly, for both *STAT1* and *STAT2* the expression levels were not associated with changes in survival (Figure 10 D-I), and we only detected a slight tendency towards a lower survival over high *STAT2* expression in LUAD (Figure 10 H; HR = 1.24,  $P = 0.081$ ).

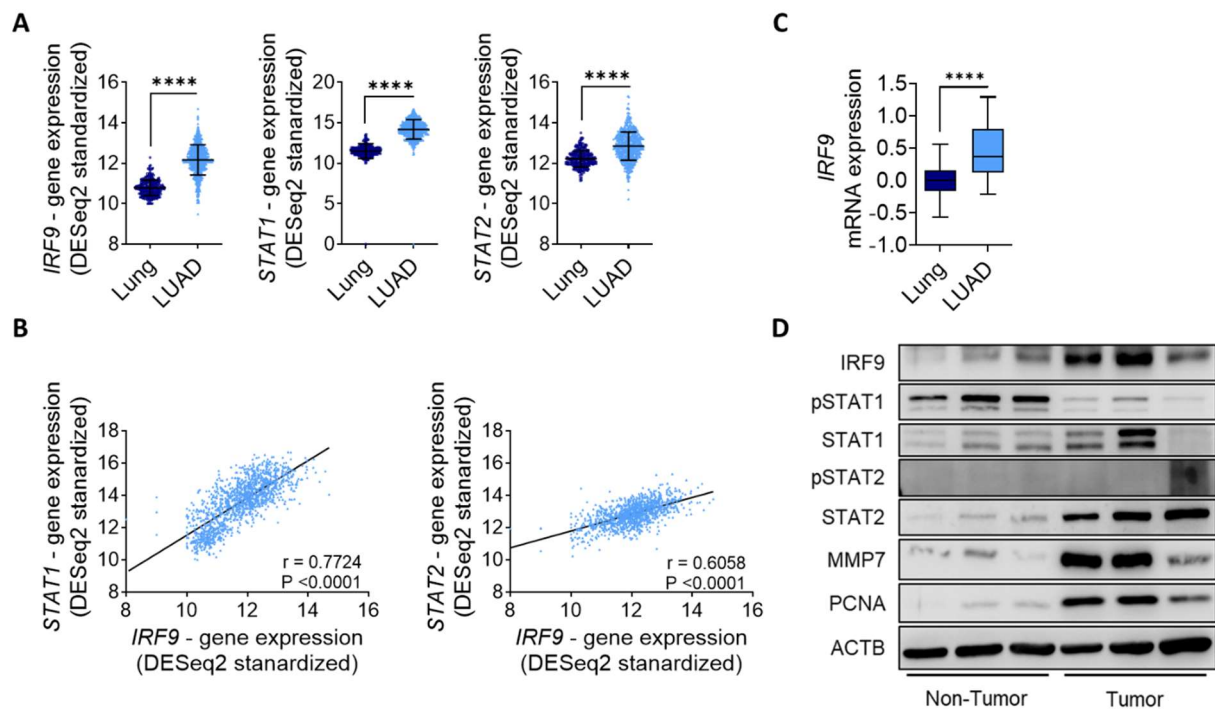


**Figure 11. Expression of U-ISGF3 members is upregulated and correlated in human lung cancer patients.** (A) Gene expression profiles of *IRF9*, *STAT1* and *STAT2* in non-tumour lung tissue ( $n = 287$ ) and LUAD patients ( $n = 573$ ) from the TCGA TARGET GTEx study. (B) Scatter plots show the correlation of *IRF9* expression with *STAT1* or *STAT2* expression in 1122 lung tumour samples from a TCGA dataset.  $R$  value and two-tailed  $p$  value was calculated via Pearson's ranking correlation coefficient. (C) mRNA expression of *IRF9* from LUAD patients and adjacent non-tumour tissue ( $n = 11$ ). (D) Protein expression from tumour and adjacent non-tumour tissue ( $n = 3$ ). Data represent mean  $\pm$  SEM; \*\*\*\*  $p < 0.0001$ ; LUAD was compared to non-tumour tissue, respectively.

By analysing the public TCGA database, we compared the expression levels of *IRF9* and its known binding partners in lung cancer patients with the levels in lung tissue. We used the TCGA TARGET GTEx study, which allows to compare expression between cancer tissue and non-tumour tissue, and observed high levels of *IRF9* as well as of *STAT1* and *STAT2* in LUAD patients (Figure 11 A). Moreover, *IRF9* levels were positively correlated with levels of *STAT1* and *STAT2* in lung cancer patients (Figure 11 B). Additionally, we had the opportunity to analyse the RNA expression of LUAD patient samples that were available at our institute and could confirm high *IRF9* levels in cancer tissue compared to adjacent non-tumour tissue (Figure 11 C).

Next, we studied the expression on the protein levels, where we detected high levels of *IRF9* together with established tumour markers *MMP7* and *PCNA* (Figure 11 D). Remarkably, we could observe differences in the expression and phosphorylation levels of

STAT1 and STAT2, with greater expression in the tumour part but stronger phosphorylation of STAT1 in the non-tumour part (Figure 11 D).

To determine where IRF9 expression is located, FFPE tissue specimen of LUAD tissue were stained for both IRF9 and Cytokeratin. Since Cytokeratin is found in epithelial cells, the staining allows to differentiate the sections between tumour stroma and solid tumour tissue, where Cytokeratin is expressed strongly. In LUAD, IRF9 was expressed in both the solid tumour and stroma part (Figure 12 A); further, LUAD sections were stained for IRF9 together with CD68, an established marker for TAMs, showing that TAMs also expressed IRF9 (Figure 12 B). Additionally, tissue microarray was used to study IRF9 expression for several lung cancer classes. Interestingly, it revealed that IRF9 was expressed in all examined classes of lung cancer (Figure 12 C).

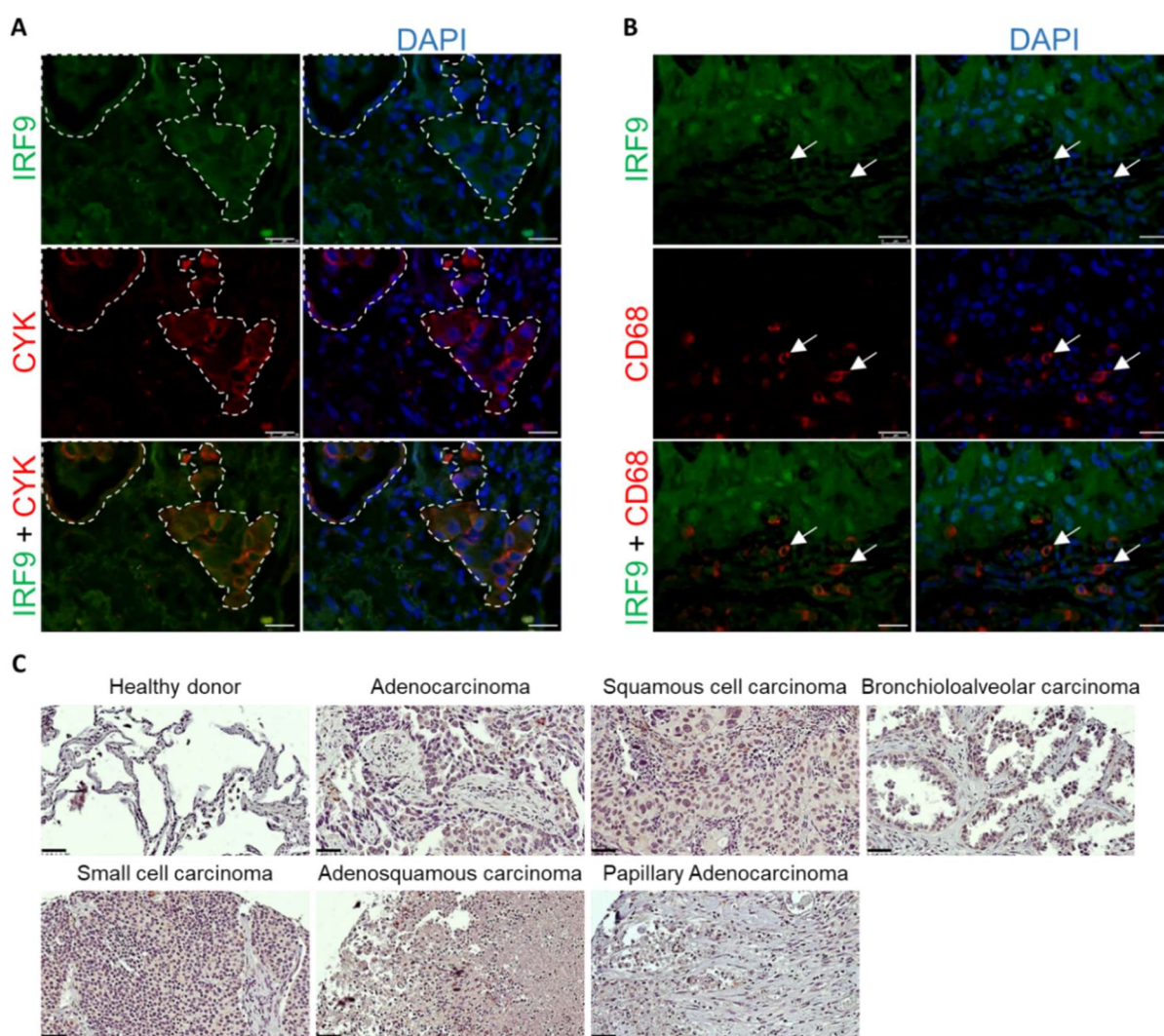


**Figure 12. IRF9 is expressed in different classes of lung cancer in tumour and stromal cells.** Representative immunofluorescence staining of IRF9 and (A) pan-Cytokeratin (CYK) and (B) CD68 in human LUAD, 40X magnification, scale bar 25  $\mu$ m. Lines mark cancer cells; arrows indicate TAMs. (C) Representative immunohistochemistry staining for IRF9 from tissue microarray. Scale bar 100  $\mu$ m.

IRF9 expression could be detected in different classes of lung cancer and in solid tumour tissue as well as in stromal cells – specifically TAMs. High levels of expression are associated with a poor outcome in lung cancer patients, particularly in LUAD patients, where we detected high expression of all three parts of the ISGF3 complex and an absence of STAT1 phosphorylation in the tumour part, indicating a change from canonical IFN signalling towards U-ISGF3 signalling.

#### 4.2. IRF9 is highly expressed in lung and other cancer cell lines

After our findings with regard to lung cancer, we were interested to evaluate the expression of IRF9 in other entities and lung cancer cell lines. Therefore, several cancer cell lines were screened for IRF9 expression detectable in most of them, including the cell lines HepG2 (hepatocellular carcinoma), HCCT116 (colorectal carcinoma), MIA-PaCa2 (pancreatic carcinoma) and MCF7 (breast carcinoma) (Figure 13 A). Interestingly, in DU145, a common prostate cancer cell line, IRF9 and STAT2 could not be detected at the condition sufficient for other cell lines, whereas STAT1 showed significantly weak expression (Figure 13 A).

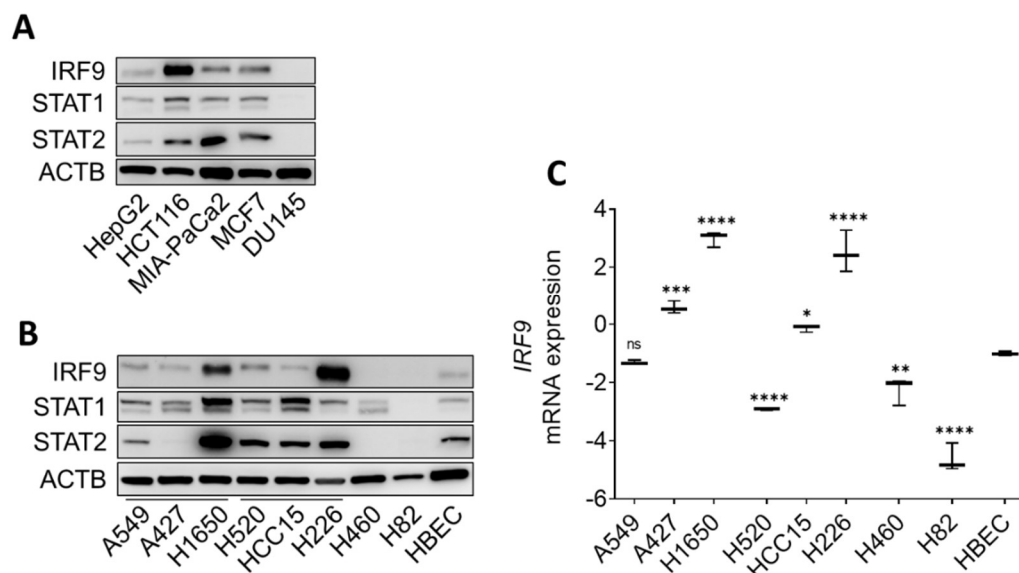


**Figure 13. The expression of ISGF3 members varies in different cancer cell lines.** Protein expression of indicated cancer (A) and lung cancer cell lines (B). Relative mRNA expression of *IRF9* of indicated lung cancer cell lines (C). Data represent mean  $\pm$  SEM ( $n = 3$ ); \*  $p < 0.05$ ; \*\*  $p < 0.01$ ; \*\*\*  $p < 0.001$ ; \*\*\*\*  $p < 0.0001$ ; cell lines were compared to HBEC.

In a protein screening for various lung cancer cell lines from different origins and HBEC (human bronchial epithelial cells), IRF9, STAT1 and STAT2 could be detected in almost all cell lines (Figure 13 B). Notably, the expression level could not be generalised by the lung cancer class. For LUAD cell lines A549, A427 and H1650, as well as for LUSC cell lines H520, HCC15 and H226, we detected immense differences in IRF9 expression within the same cancer class (Figure 13 B). Notably, the cell lines H460 (large cell carcinoma) and H82 (small cell carcinoma) did not express IRF9 and STAT1 or STAT2 at a detectable level, except H460 for STAT1 (Figure 13 B). The available RNA samples of the described cell lines confirmed a high expression level in H1650 and low but detectable expression in H82 (Figure 13 C). It can be noted that the

cell line A549 showed a similar expression of IRF9, STAT1 and STAT2 compared with HBEC (Figure 13 B, C).

In addition to cancer cell line expression, it was interesting to determine whether resistance against anti-proliferative drugs might lead to elevated IRF9 expression, as it was described for other entities (e.g. breast, colon). To answer this question, two LUAD cell lines resistant against Doxorubicin or Paclitaxel were used to evaluate the mRNA level of *IRF9*. In comparison with the parental cell line, which was used as control, significant overexpression could be observed in both cell lines when resistant against Paclitaxel (Figure 14 A, B). The resistance against Doxorubicin led to a moderate but significant increase in *IRF9* expression (Figure 14 A, B).

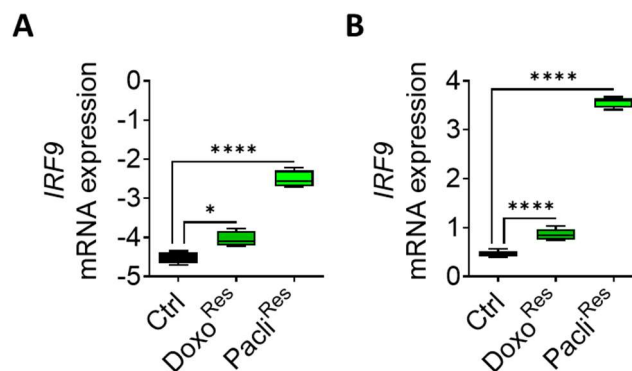


**Figure 14. IRF9 expression is increased in chemoresistant lung cancer cell lines.** Relative mRNA expression of *IRF9* of cell lines A549 (A) and HCC44 (B) resistant against Doxorubicin or Paclitaxel. Data represent mean ± SEM (n = 3); \*  $p < 0.05$ ; \*\*\*\*  $p < 0.0001$ ; cell lines were compared to parental control.

We could prove the expression of IRF9 in several cancer cell lines including LUAD and LUSC cell lines, not necessarily at a comparable level within the same lung cancer class. IRF9 is upregulated in chemoresistant lung cancer cell lines and is most prominent when resistant against Paclitaxel. Adenocarcinoma is the most abundant class in lung cancer and is diagnosed in non-smokers. Since the LUAD cell lines A549 and A427 showed moderate regulation of IRF9, comparable to HBEC, we decided to use those cell lines for further studies to elaborate on the effects of IRF9 manipulation.

### 4.3. Stimulation with type I IFN upregulates IRF9 in cancer cells

One main approach of this study was to activate the expression and function of IRF9 in cancer cells. This was addressed by the stimulation with type I IFN, which is known to enable the expression of ISGs via ISGF3, leading to an increase in IRF9 expression. For this reason, A549 cells were stimulated with IFN in various concentrations for 24 hours. We used RT-qPCR to determine the expression levels of *IRF9*, where we could observe a strong increase even at the lowest concentration but only minor differences between concentrations (Figure 15 A). In contrast, immunofluorescence staining revealed that, with increased concentration, the overall expression of IRF9 increased, and a strong nuclear translocation occurred (Figure 15 B); this nuclear translocation was clearest at a high magnification (Figure 15 C). Thus, we were interested in determining whether the widely used concentration of 100 U/ml IFN was sufficient to activate the transcription complex ISGF3. We transfected the plasmid pGL4.45, which contains 5 ISRE prior to the luciferase gene, into A549. Already after 24 h stimulation with IFN, the luciferase activity showed a 4-fold increase compared to unstimulated cells (Figure 15 D). Through these experiments, we could confirm that 100 U/ml IFN were sufficient to activate the transcriptional effects of IFN and that IRF9 upregulation increased. Hence, for the following experiments, 100 U/ml were used when IFN was applied.

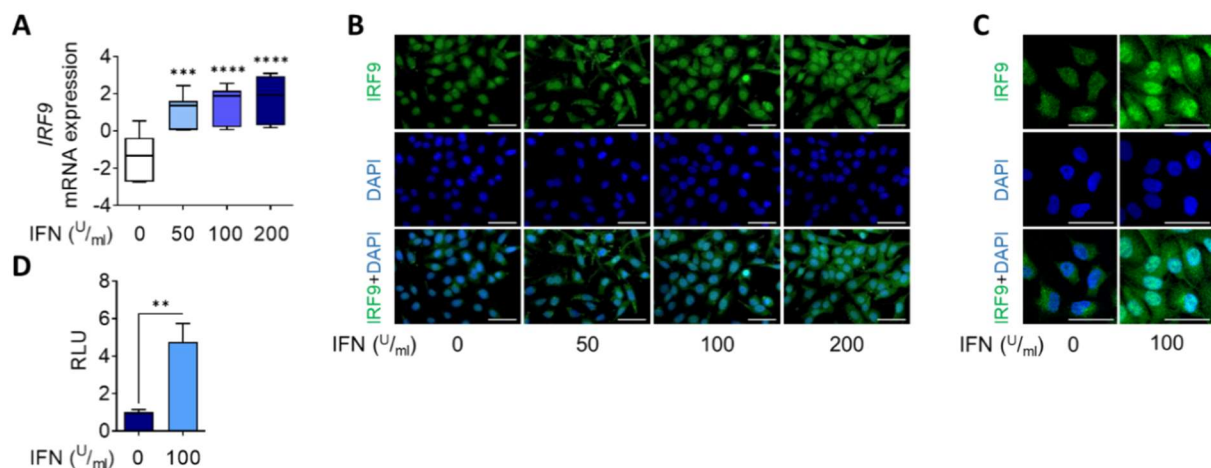


**Figure 15.** IFN stimulation increases expression and nuclear translocation of IRF9 in A549. A549 were stimulated with 0-200 U/ml type I IFN for 24 h. Relative *IRF9* expression was validated via RT-qPCR (A) and immunofluorescence staining with IRF9 and DAPI (B, C). Activity of IRF9 was measured using pGL4.45 luciferase vector (D). Data represent mean  $\pm$  SEM ( $n = 3$ ); \*\*  $p < 0.01$ ; \*\*\*  $p < 0.001$ ; \*\*\*\*  $p < 0.0001$ ; IFN conditions were compared to 0 U/ml. Scale bar 50  $\mu$ m (B, C).

Next, we wanted to study the chronological sequence in A549 after IFN stimulation. In Western Blot analysis, STAT1 and STAT2 are phosphorylated at an early time point, strongest around 30–60 minutes, whereas the overall increase in protein levels of IRF9, STAT1 and STAT2 occurs after several hours, when phosphorylation has mostly diminished (Figure 16 A). Functionally, the antiproliferative effect of IFN cannot be observed after 24 hours of stimulation but rather after 72 hours (Figure 16 B).

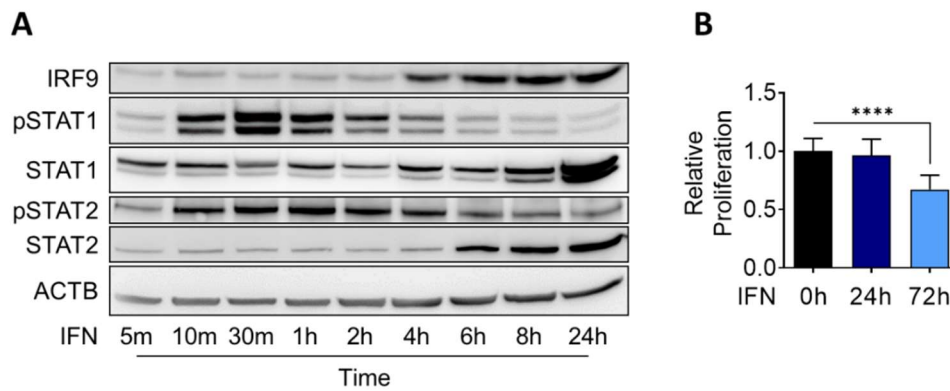


**Figure 16. Time dependent effects of type I IFN in A549.** A549 were stimulated with 100 U/ml type I IFN, and (A) protein expression over time was evaluated; (B) proliferation was evaluated as percentage of 0 h IFN. Data represent mean  $\pm$  SEM ( $n = 3$ ); \*\*\*\*  $p < 0.0001$ ; IFN conditions were compared to 0 h IFN.

Taken together, a concentration of 100 U/ml of IFN for 24 h was sufficient to stimulate A549 and activate ISGF3. STAT phosphorylation occurred at an early time point, whereas the expression levels increased after hours, and the sufficient suppression of proliferation could be observed after 72 h.

#### 4.4. Characterisation of transduction of IRF9 constructs in human lung cancer cell lines

The stimulation with IFN led to an upregulation of IRF9, together with known (STAT1, STAT2) and unknown genes and the involvement of protein phosphorylation. Since our approach was to study the role of IRF9 in lung cancer, we decided to manipulate the expression of IRF9 exclusively. Therefore, we used lentiviral transduction of A549 and A427 cell lines to alter the expression of IRF9; further, we used an overexpressing vector (LV IRF9) and its empty vector as control (LV EV). To knockdown IRF9, we used an shRNA plasmid against IRF9 (shIRF9) or a scramble sequence as control (sh scr). The selection of successfully transduced cells was assured via the application of Puromycin.

##### 4.4.1. Overexpression of IRF9 promotes oncogenic behaviour

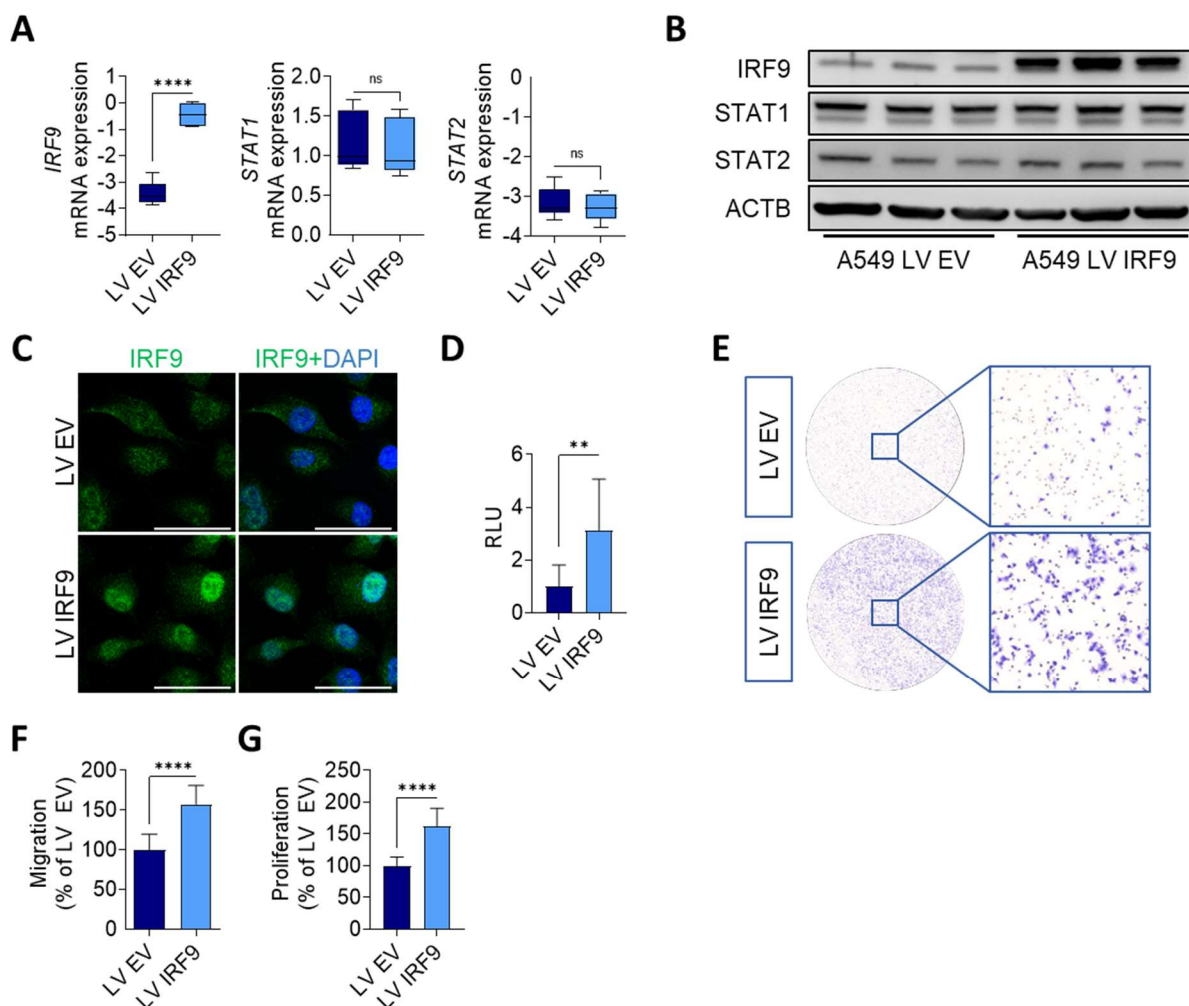


**Figure 17. Overexpression of IRF9 promotes oncogenic behaviour in A549.** A549 were transduced with IRF9-overexpressing (LV IRF9) or control vector (LV EV). Expression of ISGF3 members were evaluated via RT-qPCR ( $n = 4$ ) (A) and Western Blot (B). Expression of IRF9 was assessed via immunofluorescence staining together with DAPI counterstaining (C). Activity of IRF9 was measured using pGL4.45 luciferase vector (D). Migration was evaluated via 8  $\mu$ m transwell membrane assay (E). Quantified migration (F) and proliferation (G) were calculated as percentage of LV EV. Data represent mean  $\pm$  SEM ( $n = 3$ ); \*\*  $p < 0.01$ ; \*\*\*\*  $p < 0.0001$ ; LV IRF9 was compared to LV EV. Scale bar 50  $\mu$ m.

We confirmed the overexpression of IRF9 on mRNA and protein level and observed that STAT1 and STAT2 expression levels were not influenced (Figure 17 A, B); in addition, we detected immunofluorescence staining, the increase of IRF9 expression and an accumulation in the nucleus (Figure 17 C). Next, we wanted to determine whether the nuclear translocation had any effect; thus, we transfected the reporter plasmid pGL4.45 into these cells and confirmed the transcriptional activity of IRF9 after overexpressing in A549 (Figure 17 D). Taken together with the changes in expression, reporter activity and nuclei enrichment, the transductions led to functional changes in A549. In sum, we investigated tumorous behaviour where the overexpression of IRF9 led to an increase in cancer cell migration and proliferation when IRF9 was overexpressed (Figure 17 E-G) and evaluated it by transwell membrane migration and BrdU incorporation, respectively.

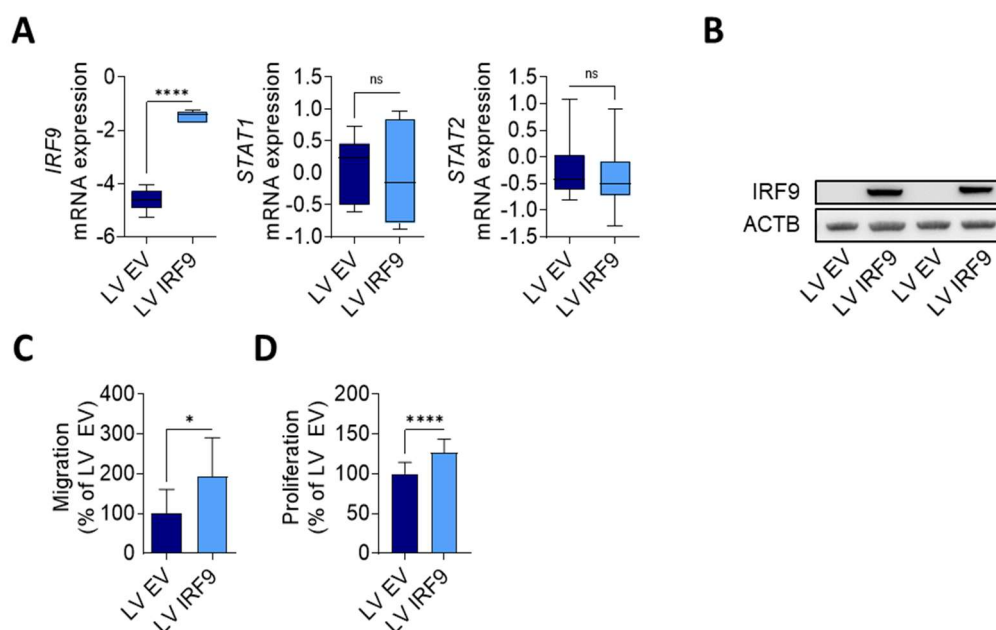


**Figure 18. Overexpression of IRF9 promotes oncogenic behaviour in A427.** A427 were transduced with IRF9-overexpressing (LV IRF9) or control vector (LV EV). Expression of ISGF3 members was evaluated via RT-qPCR (A). Protein expression of IRF9 was evaluated via Western Blot (B). Quantified migration (C) and proliferation (D) were calculated as percentage of LV EV. Data represent mean  $\pm$  SEM ( $n = 4$ ); \*  $p < 0.05$ ; \*\*\*\*  $p < 0.0001$ ; LV IRF9 was compared to LV EV.

To confirm these findings, A427 were transduced in the same way as A549. We detected IRF9 highly overexpressed on mRNA and protein level, whereas STAT1 and STAT2 mRNA expression was not affected (Figure 18 A, B). Consistently, IRF9 overexpression led to an increase in proliferation and migration, confirming the oncogenic effect of IRF9 in lung adenocarcinoma (Figure 18 C, D).

To evaluate whether the present level of IRF9 can additionally influence IFN response, we stimulated transduced A549 for 24h with type I IFN. The expression levels of IRF9 increased even more when high levels were already present (Figure 19 A, B). Then, it can be suggested that IRF9 enables or activates its own expression after IFN stimulation.

In conclusion, IRF9 overexpression alone did not regulate STAT1 or STAT2 expression. It led not only to high but also active IRF9 levels, resulting in increase of luciferase activity, tumour cell migration and proliferation. High IRF9 levels also enhanced the response to IFN.

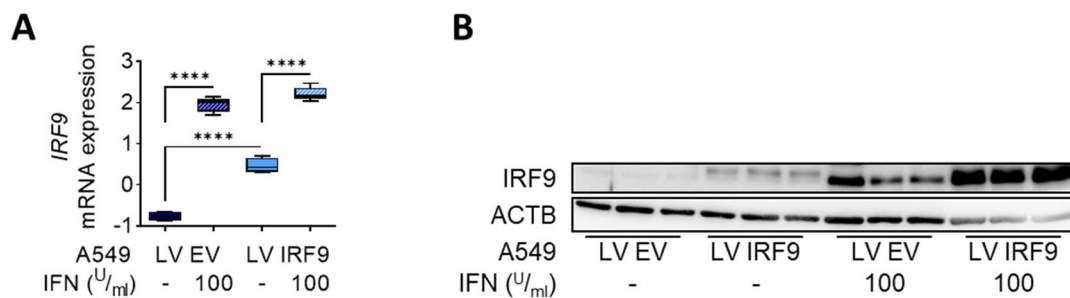


**Figure 19. Overexpression of IRF9 enhances IFN effect.** Transduced A549 were stimulated with 100 U/ml type I IFN for 24 h. IRF9 expression was assessed via RT-qPCR (A) and Western Blot (B). Data represent mean  $\pm$  SEM ( $n = 3$ ); \*\*\*\*  $p < 0.0001$ . Conditions were compared as indicated.

#### 4.4.2. Knockdown of IRF9 reduces migratory and proliferative behaviour

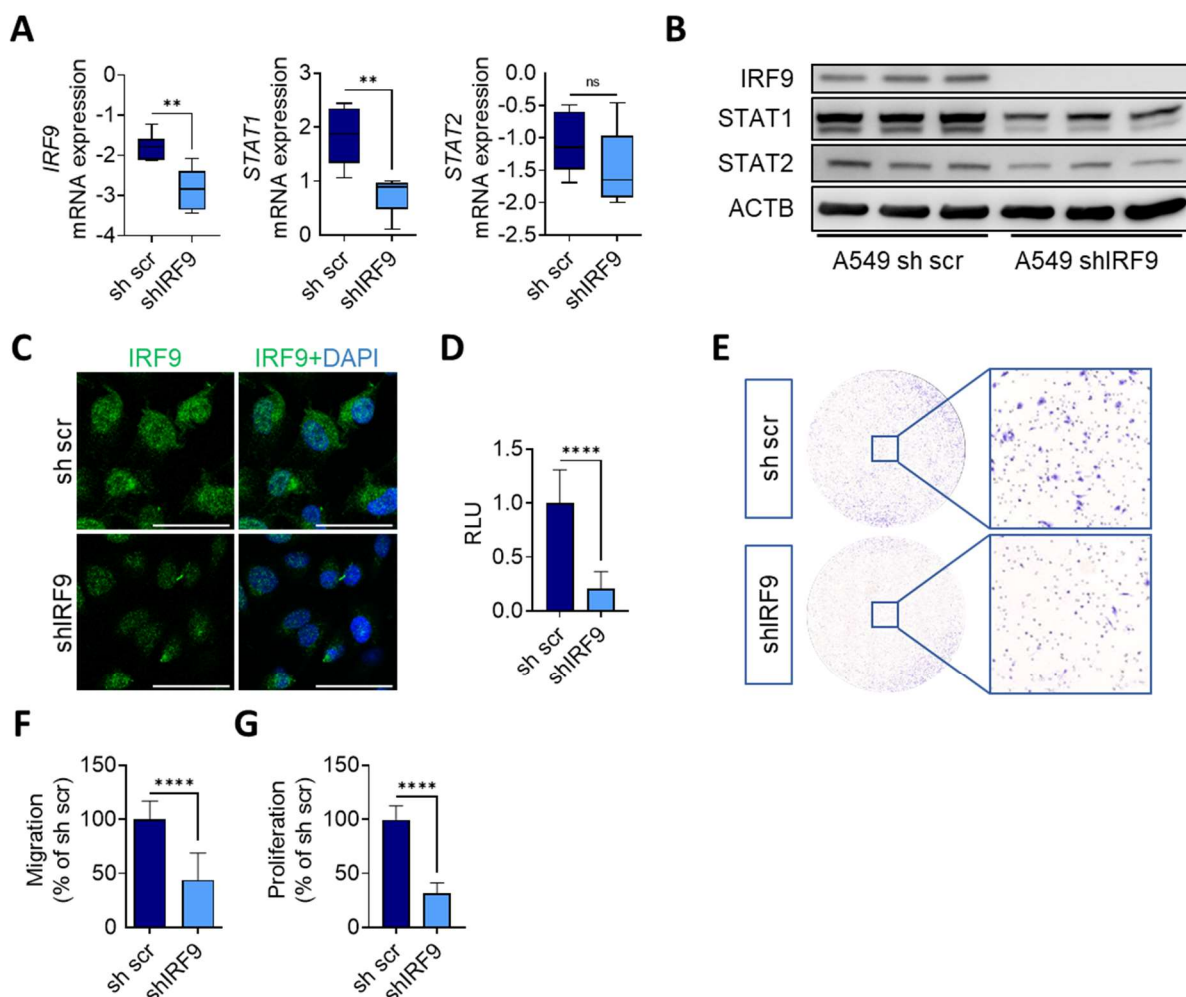


**Figure 20. Knockdown of IRF9 reduces oncogenic features in A549.** A549 were transduced with shRNA constructs against IRF9 (shIRF9) or scramble control (sh scr). Expression of ISGF3 members was evaluated via RT-qPCR (A) and Western Blot (B). Expression of IRF9 was assessed via immunofluorescence staining together with DAPI counterstaining (C). Activity of IRF9 was measured using pGL4.45 luciferase vector (D). Migration was evaluated via 8  $\mu$ m transwell membrane assay (E). Quantified migration (F) and proliferation (G) were calculated as percentage of sh scr. Data represent mean  $\pm$  SEM ( $n = 3$ ); \*\*  $p < 0.01$ ; \*\*\*\*  $p < 0.0001$ ; shIRF9 was compared to sh scr. Scale bar 50  $\mu$ m.

First, we confirmed the knockdown via RT-qPCR and Western Blot analysis (Figure 20 A, B). Despite our findings in overexpressing cells, the knockdown of IRF9 also reduced the expression levels of STAT1 and STAT2 (Figure 20 A, B). The reduction of IRF9 was further confirmed in immunofluorescence staining and additionally resulted in reduced luciferase activity (Figure 20 C, D). As a result of reduced transcriptional activity of IRF9, A549 shIRF9 cells showed a reduction of cancer cell proliferation and migration (Figure 20 E-G).

In A427, the knockdown of IRF9 was confirmed on mRNA and protein level (Figure 21 A, B). On mRNA level, the reduction of *IRF9* appeared to reduce *STAT1* expression, but neither *STAT1* nor *STAT2* expression were significantly regulated (Figure 21 A). At the same time, in A427, the reduction of tumour cell proliferation and migration was observed after shIRF9 transduction (Figure 21 C, D).

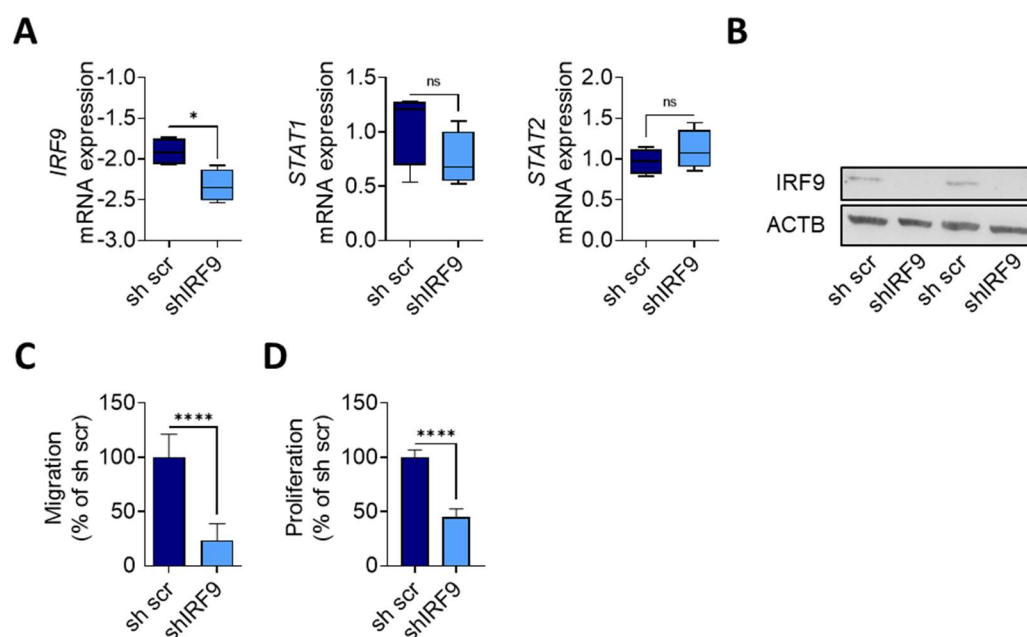


**Figure 21. Knockdown of IRF9 reduces oncogenic features in A427.** A427 were transduced with shRNA constructs against IRF9 (shIRF9) or scramble control (sh scr). Expression of ISGF3 members was evaluated via RT-qPCR (A). Protein expression of IRF9 was evaluated via Western Blot (B). Quantified migration (C) and proliferation (D) were calculated as percentage of sh scr. Data represent mean  $\pm$  SEM ( $n = 4$ ); \*  $p < 0.05$ ; \*\*\*\*  $p < 0.0001$ ; shIRF9 was compared to sh scr.

When A549 shIRF9 cells were stimulated with type I IFN, the upregulation of IRF9 was diminished compared to A549 sh scr cells (Figure 22 A, B). Similar to our findings in A549 LV IRF9, IRF9 expression seemed to be dependent on present IRF9 levels.

Taken together with our results, the knockdown of IRF9 led to a downregulation of co-factors STAT1 and STAT2 depending on the used cell line as well as to the diminution of the oncogenic effects of IRF9, resulting in reduced tumour cell migration, proliferation and transcriptional activity.

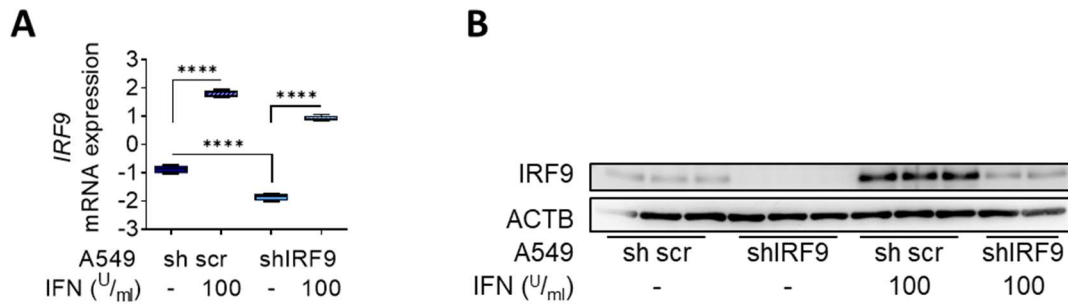


**Figure 22. Knockdown of IRF9 delays IFN effect.** Transduced A549 were stimulated with 100 U/ml type I IFN for 24 h. IRF9 expression was assessed via RT-qPCR (A) and Western Blot (B). Data represent mean  $\pm$  SEM ( $n = 2-3$ ); \*\*\*\*  $p < 0.0001$ . Conditions were compared as indicated.

#### 4.5. Characterisation of transduction of Irf9 constructs in murine lung cancer cell lines

Since the results in human lung adenocarcinoma cell lines A549 and A427 clearly demonstrated that the expression of IRF9 is associated with malignant behaviour, the next aim was to determine whether these findings could be confirmed in another mammalian model. Therefore, we used the murine lung adenocarcinoma cell line CULA to study the effects of murine Irf9. Similarly, we stably transduced CULA cells to overexpress Irf9 (CULA LV Irf9) or to knockdown the expression of Irf9 (CULA shIrf9). Empty vector and scramble sequence were used as controls, respectively (CULA LV EV; CULA sh scr).

First, we analysed mRNA expression, comparing CULA LV Irf9 to CULA LV EV. With the immense overexpression of *Irf9*, transduction was considered successful (Figure 23 A). RT-qPCR also showed the upregulation of *Stat1* and the proliferation marker *Pena*, whereas *Stat2* expression remained unaffected (Figure 23 A).

Next, we analysed the functional effects of Irf9 and observed that similar to our findings in human cell lines A549 and A427, CULA LV Irf9 showed higher proliferation rate (Figure 23 B); further, it led to an increase in migratory behaviour (Figure 23 C). These findings confirmed the oncogenic character of IRF9 in human lung adenocarcinoma.

To knockdown Irf9 efficiently, CULA cells were transduced with five different shRNA constructs provided by an shRNA library. It can be noted that the shRNA-mediated knockdown was relatively low; however, the knockdown efficiency was calculated based on mRNA expression of *Irf9* (Figure 23 D). For shRNA plasmid 2, the transduction or knockdown seemed to have failed; for plasmid 1 and plasmid 6, we observed no significant knockdown (11.3% and 13.4% respectively), and a significant reduction was achieved only for plasmid 3 and plasmid 4 (44.6% and 17.3% respectively; Figure 23 D). Based on the highest knockdown efficiency in CULA cells, shIrf9 plasmid 3 was chosen for transduction and to study the effect of Irf9 knockdown in CULA cells and further referred to as shIrf9.

After repeated transduction of CULA cells, we confirmed the knockdown by a significant downregulation of *Irf9* in CULA shIrf9 (Figure 23 E). Interestingly, we could not observe any changes in *Stat1*, *Stat2* or *Pcna* expression (Figure 23 E). Unlike A549 and A427 shIRF9, CULA shIrf9 cells did not show changes in proliferative or migratory behaviour (Figure 23 F, G). It appeared as if the transduction of *Irf9* had resulted in an isolated knockdown and had not affected other known genes or tumour cell function.

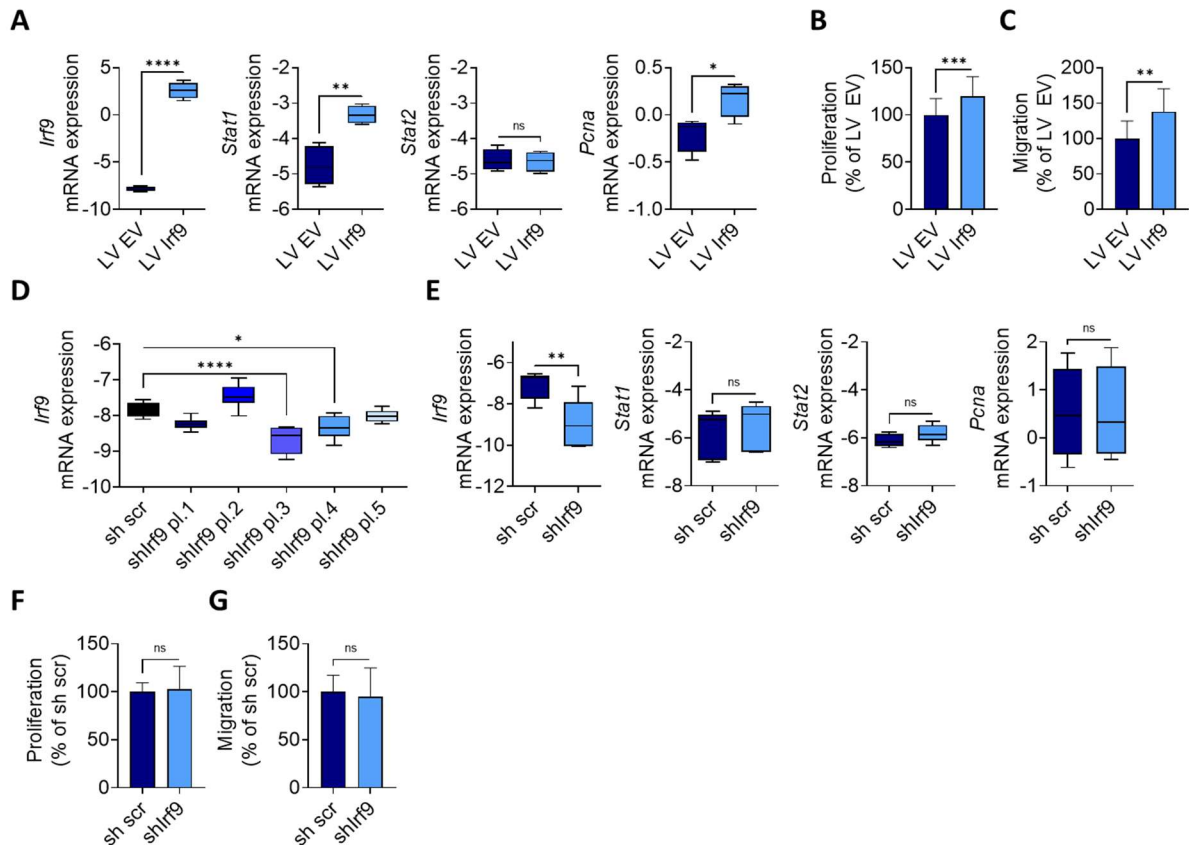


**Figure 23. Irf9 manipulation partially confirms phenotype in CULA.** Murine lung cancer cell line CULA was transduced with *Irf9*-overexpressing (LV *Irf9*) or shRNA constructs against *IRF9* (shIrf9) with respective controls (LV EV or sh scr). mRNA expression was assessed via RT-qPCR (A, D, E). Quantified proliferation (B, F) and migration (C, G) were calculated as percentages of LV EV or sh scr, respectively. Data represent mean  $\pm$  SEM ( $n = 3$ ); \*  $p < 0.05$ ; \*\*  $p < 0.01$ ; \*\*\*  $p < 0.001$ ; \*\*\*\*  $p < 0.0001$ ; LV *Irf9* was compared to LV EV, and shIrf9 constructs were compared to sh scr.

Overexpression of *Irf9* in CULA cells led to changes similar to those seen in human cell lines resulting in increase of malignant behaviour. In contrast, knockdown of *Irf9* did not lead to changes in proliferative or migratory behaviour, suggesting differences in the regulation of *IRF9* in human and murine cells.

#### 4.6. RNA-Sequencing of transduced cells identified VCAN as possible target of IRF9

After identifying IRF9 to promote oncogenic behaviour in tumour cells, we used RNA-Sequencing (RNA-seq) to identify genes that are regulated or altered after IRF9 manipulation. Of each condition, the validated mRNA was isolated and combined with DNase digest, and RNA-seq was performed (Figure 24 A). The results were analysed in a multi-mapping approach, and differentially expressed genes with  $P \leq 0.05$  were considered as significantly regulated (Figure 24 B). The comparison of LV IRF9 and LV EV led to 1544 genes, whereas the number of regulated genes for shIRF9 to sh scr was 662 (Figure 24 C). The analyses revealed the top 25 expression for both sets (Figure 24 D, E).

Since the tumoural behaviour in A549 correlated with the expression level of IRF9, the next step was to reveal one or more genes that were regulated by IRF9 and could enable the functional effects. First, only genes regulated in both sets were considered for further analysis, which narrowed the sample down to 117 genes (Figure 24 C); further, only genes were considered that were regulated in opposite directions (Figure 24 F).

RNA-seq results were validated by RT-qPCR. Therefore, mRNA expression of genes that were identified as significantly regulated in opposite directions was analysed (Figure 25 A, B). Some candidates, such as *DUSP26*, *EMP1*, *IGFBP5*, *SH3TC2* and *VCAN* were expressed in a tendency or as expected from RNA-seq analyses, whereas genes as *ADGRL3*, *GRHL3*, *PADI2*, *SERPINI1* or *TRIM29* were either regulated in one set but not the other or not regulated at all (Figure 25 A, B).

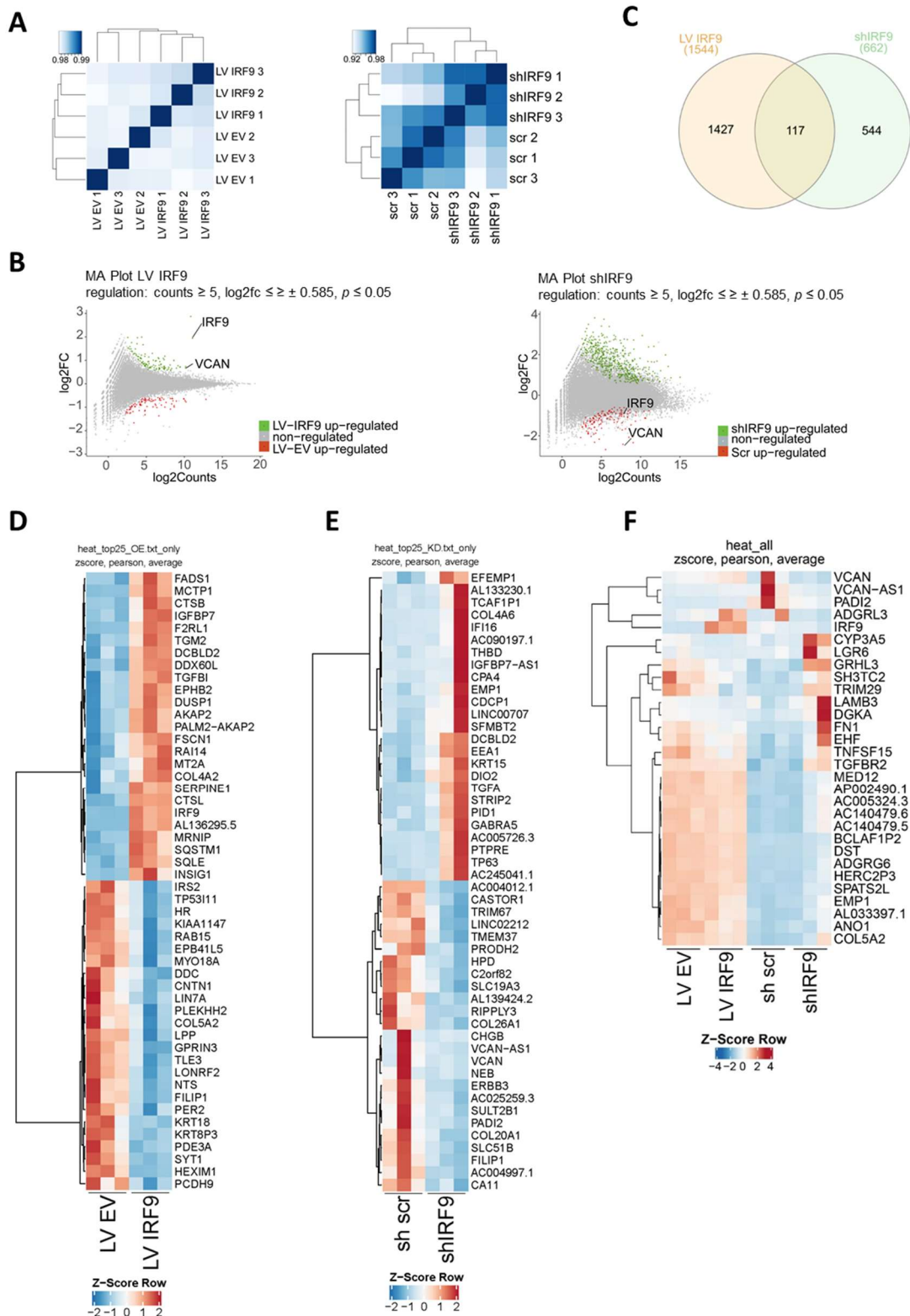


**Figure 24.** RNA-seq of transduced A549 revealed VCAN as top regulated gene. RNA-seq of transduced A549 cells was performed, A549 LV IRF9 were compared to A549 LV EV and A549 shIRF9 to A549 sh scr, respectively ( $n = 3$ ). (A) Correlation of RNA samples. (B) MA Plots of up- and downregulated genes of each set ( $p < 0.05$ ), highlighting *IRF9* and *VCAN*. (C) Venn diagram of genes regulated in LV IRF9 and shIRF9. Heatmap shows significant top 25 up and downregulated genes of LV IRF9 (D) and shIRF9 (E) and top 30 genes, significantly regulated in both sets in opposite directions (F).

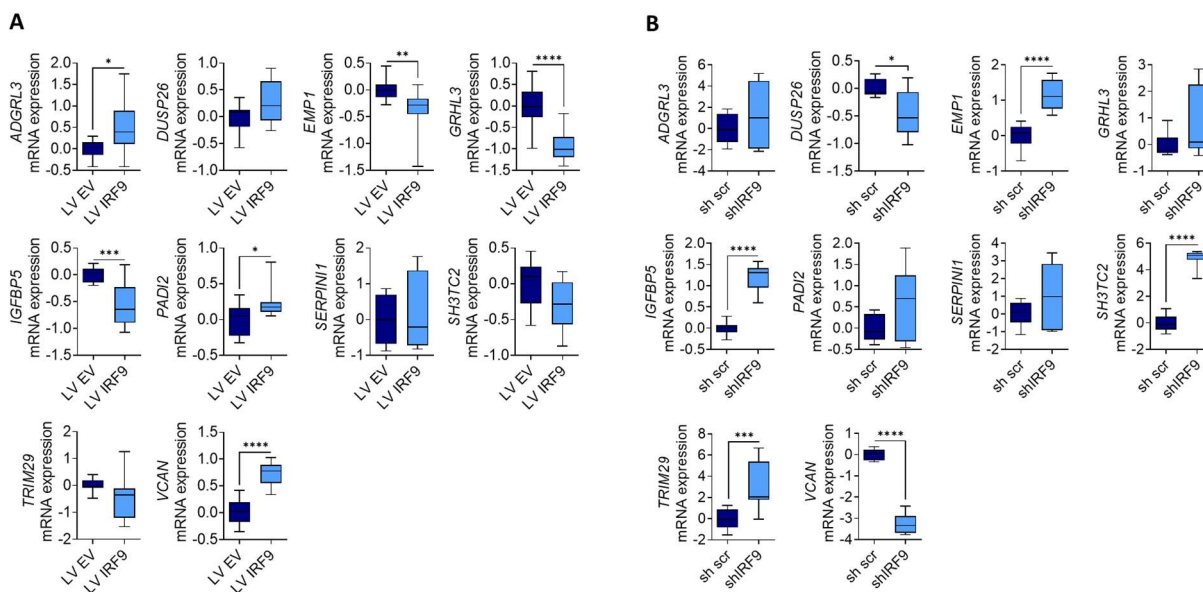


**Figure 25. Evaluation of RNA-seq analysis.** Potential candidates were evaluated via RT-qPCR in IRF9-overexpressing (A) and IRF9-silenced (B) A549. Data represent mean  $\pm$  SEM ( $n = 4$ ); \*  $p < 0.05$ ; \*\*  $p < 0.01$ ; \*\*\*  $p < 0.001$ ; \*\*\*\*  $p < 0.0001$ ; LV IRF9 was compared to LV EV, shIRF9 was compared to sh scr.

RNA-seq revealed overall regulated genes after IRF9 manipulation and 117 genes that were regulated significantly in both sets. RNA-seq results were validated via mRNA analysis, and VCAN was considered as a potential downstream target of IRF9 able to promote the functional effects observed after IRF9 manipulation and analysed in further experiments.

## 4.7. Evaluation of VCAN in lung adenocarcinoma in interaction with IRF9

### 4.7.1. VCAN expression correlates with IRF9 expression in lung cancer patients

VCAN is a known oncogene, and its impact on tumour development and progression varies upon entity. However, we initially studied Kaplan-Meier curves for the survival of lung cancer patients over the expression of *VCAN*. Notably, the findings revealed similarities to those over *IRF9* expression. For lung cancer, high *VCAN* expression was associated with lower overall survival (Figure 26 A; HR = 1.32,  $P = 2.2 \cdot 10^{-5}$ ) and even lower survival for LUAD patients (Figure 26 B; HR = 1.96,  $P = 4.1 \cdot 10^{-8}$ ).

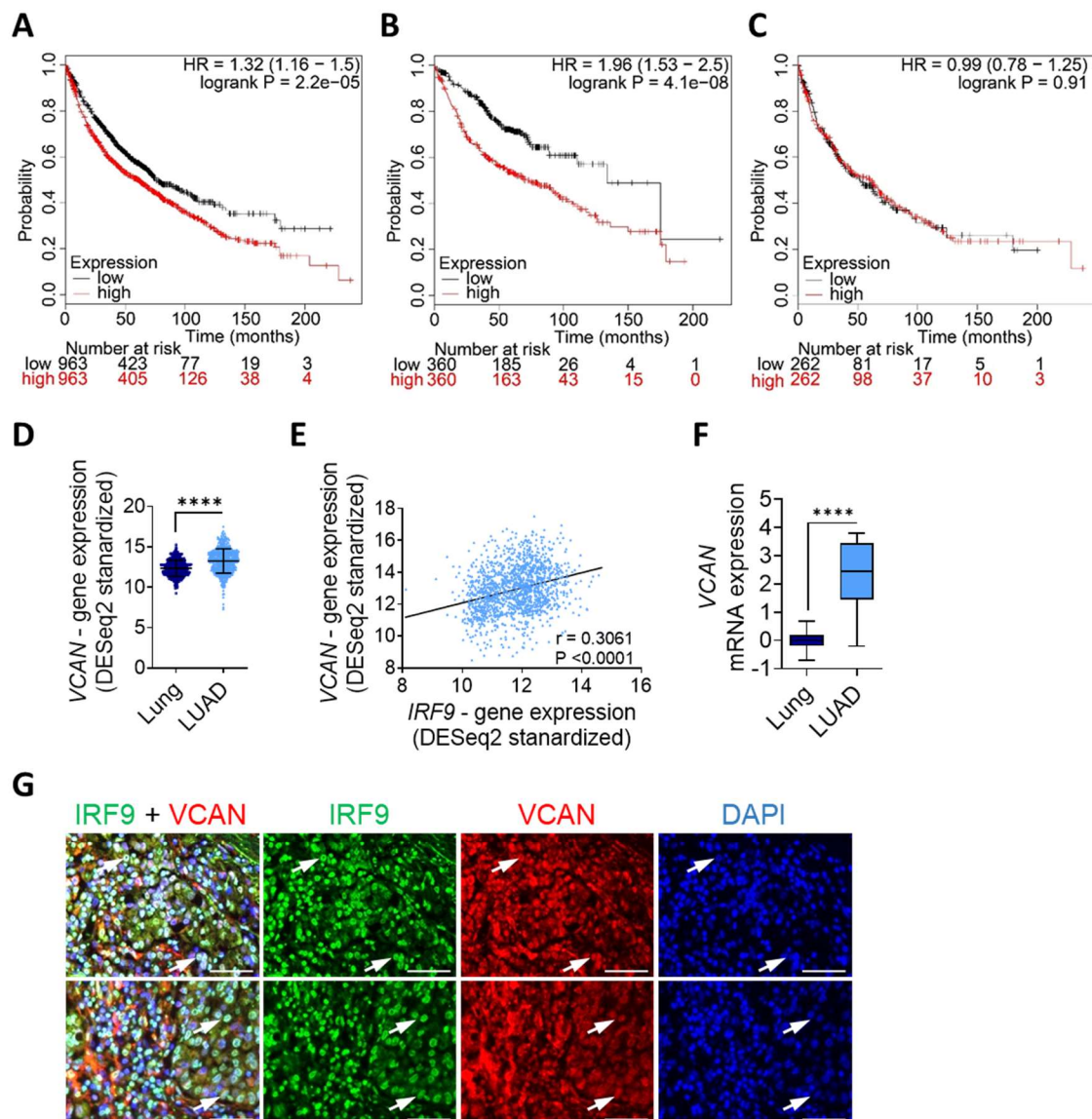


**Figure 26.** IRF9 and VCAN expression correlate and are associated with reduced survival in human lung cancer patients. Kaplan-Meier curves for VCAN levels over the survival of (A) all classes of lung cancer ( $n = 1926$ ), (B) LUAD ( $n = 720$ ), (C) LUSC ( $n = 524$ ) patients; patients were divided by median into high and low expression. (D) Gene expression profile of VCAN in non-tumour lung tissue ( $n = 397$ ) and LUAD patients ( $n = 515$ ) from the TCGA TARGET GTEx study. (E) Scatter plots show the correlation of IRF9 with VCAN expression in 1410 lung tumour samples from a TCGA dataset.  $R$  value and two-tailed  $p$  value was calculated via Pearson's ranking correlation coefficient. (F) mRNA expression of VCAN from LUAD patients and adjacent non-tumour tissue ( $n = 11$ ). (G) Representative immunofluorescence staining of IRF9 and VCAN in human LUAD, scale bar 50  $\mu\text{m}$ . Arrows indicate co-expression.

In LUSC patients, no differences in overall survival could be observed, which followed the findings for IRF9 (Figure 26 C; HR = 0.99,  $P = 0.91$ ). The analysis of TCGA TARGET GTEx study revealed elevated levels of *VCAN* expression in LUAD patients (Figure 26 D). The expression levels of *VCAN* and *IRF9* were correlated moderately in lung cancer patients (Figure 26 E). When analysing RNA samples of LUAD patients, we could confirm the overexpression of *VCAN* compared to adjacent non-tumour lung tissue (Figure 26 F).

Additionally, we performed immunofluorescence staining to identify the expression of the proteoglycan VCAN in LUAD sections (Figure 26 G). It can be noted that VCAN was expressed extracellularly as well as intracellularly, where it was located in or surrounding the nuclei that were also expressing IRF9 (Figure 26 G).

The analyses of human lung adenocarcinoma demonstrated the increased expression of VCAN, correlating with IRF9. High levels of VCAN were associated with patients' lower probability of survival.

#### 4.7.2. VCAN expression is influenced by IRF9 manipulation

Being one of the significantly regulated genes correlating with IRF9 expression after transduction in A549, VCAN was selected for further studies to investigate whether it was responsible for the observed effects. Four splice variants of VCAN are known, with *VCAN [V1]* promoting oncogenic features.

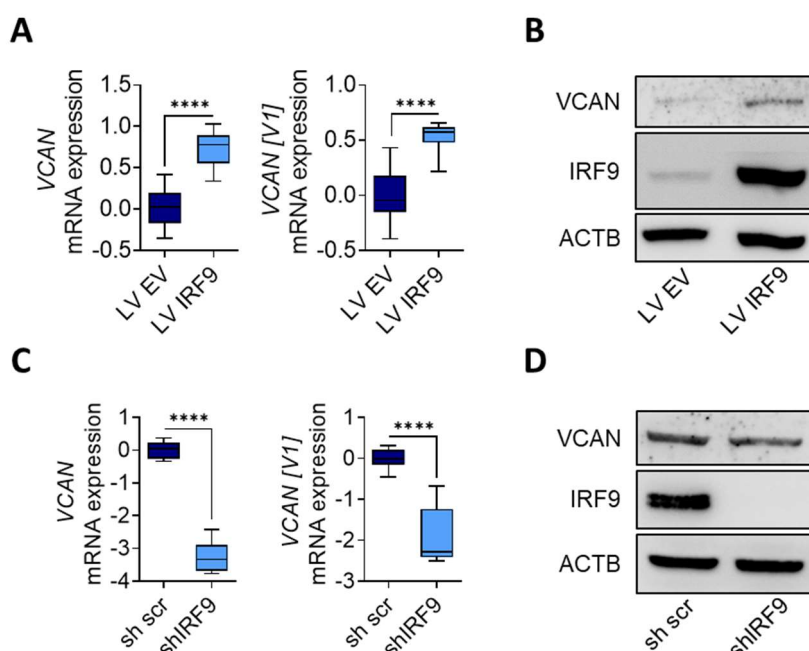


**Figure 27. IRF9 and VCAN expression correlate in transduced A549.** mRNA expression of *VCAN* and *VCAN [V1]* were evaluated via RT-qPCR (A, C). Protein expression of VCAN was evaluated via Western Blot (B, D). Data represent mean  $\pm$  SEM ( $n = 3$ ); \*\*\*\*  $p < 0.0001$ ; LV IRF9 was compared to LV EV, shIRF9 was compared to sh scr.

We analysed the mRNA expression of both, of *VCAN* variants as a whole and *VCAN [V1]* expression, demonstrating that *VCAN* and *VCAN [V1]* in A549 were upregulated when IRF9 was overexpressed and also downregulated when IRF9 was suppressed (Figure 27 A, C). Western Blot analysis also confirmed the correlation of IRF9 and VCAN expression on the protein level (Figure 27 B, D).

In addition to A549, we analysed VCAN expression in other transduced cell lines, where we could confirm our findings. In transduced A427 cells, we detected similar effects with a positive correlation of IRF9 transduction and the expression of VCAN in mRNA and protein expression (Figure 28 A-D). Interestingly, in murine CULA cells, *Irf9* overexpression resulted in a significant upregulation of *Vcan*, but *Irf9* knockdown did not lead to reduced *Vcan* expression (Figure 28 E, F).

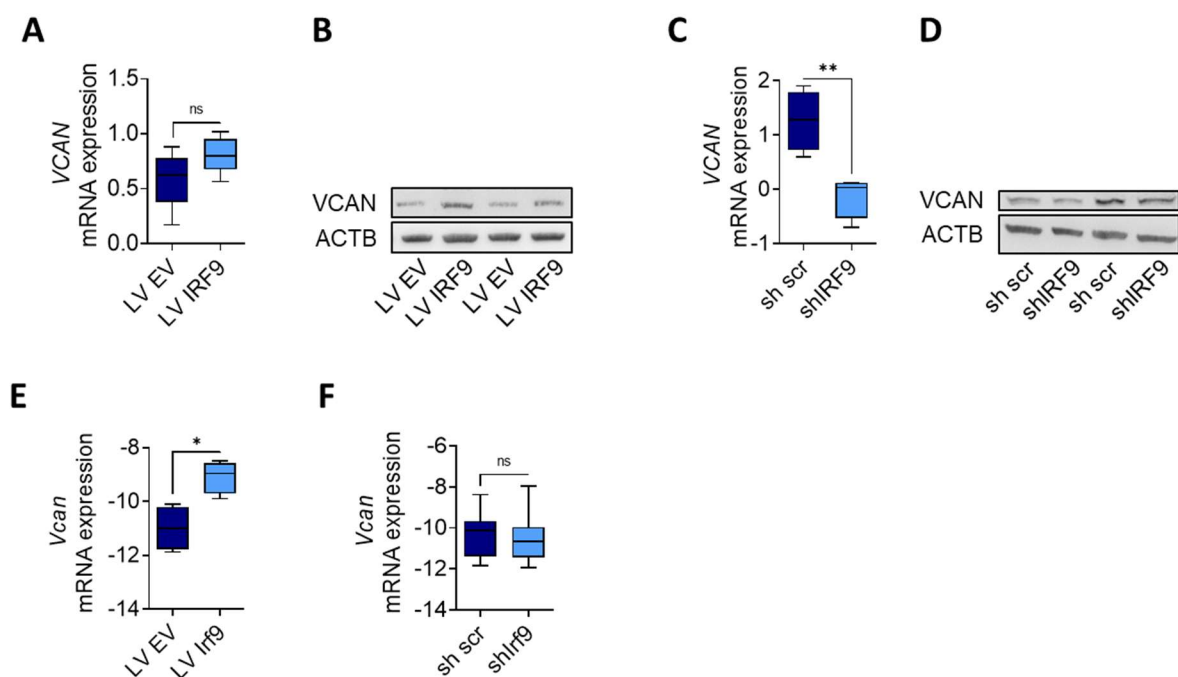


**Figure 28. VCAN expression in transduced A427 and CULA.** Expression of VCAN in human A427 was evaluated via RT-qPCR (A, C) and Western Blot (B, D). mRNA expression of murine *Vcan* in CULA was evaluated via RT-qPCR (E, F). Data represent mean  $\pm$  SEM ( $n = 3$ ); \*  $p < 0.05$ ; \*\*  $p < 0.01$ ; overexpression (LV IRF9; LV Irf9) were compared to LV EV silencing (shIRF9; shIrf9) were compared to sh scr.

Overall, we could show that IRF9 upregulation or knockdown in human LUAD cell lines A427 and A549 led to the regulation of VCAN in the same direction. In CULA LV Irf9, high *Vcan* expression was observed, whereas in CULA shIrf9, *Vcan* expression did not change. This could explain why no changes in malignant behaviour after *Irf9* knockdown were assessed and further fosters the implication that VCAN enables oncogenic features after IRF9 manipulation.

### 4.7.3. VCAN knockdown diminished oncogenic effect of IRF9

As a consequence of VCAN expression analyses, we wanted to study the role of VCAN in the transduced A549 cell lines. Therefore, we used an siRNA approach to sufficiently knockdown the expression of *VCAN* and conduct molecular and functional analyses.

The first experiments were conducted in naïve A549 transfecting two different siRNAs against *VCAN* to validate the knockdown efficiency and to choose which siRNA to use in further experiments. A negative, non-targeting siRNA (si neg) was used as control. After transfection, analysis of mRNA expression showed a sufficient knockdown of *VCAN* and *VCAN [V1]* for both siRNAs (Figure 30 A, B). In particular, siVCAN1 showed a knockdown efficiency of 75.3% for *VCAN* and 80.2% for *VCAN [V1]*, whereas siVCAN2 was able to knockdown *VCAN* to 62.0% and *VCAN [V1]* to 68.2% (Figure 30 A). Interestingly, the knockdown of VCAN led to a mild increase in *IRF9* mRNA and protein levels, questioning whether there might be a feedback loop of IRF9 and VCAN (Figure 30 A, B); however, this could not be confirmed consistently in the following results. When analysing cell proliferation and migration, siVCAN1 resulted in a stronger reduction of tumoural behaviour, which could be supplemented by PCNA downregulation (Figure 30 B-D).

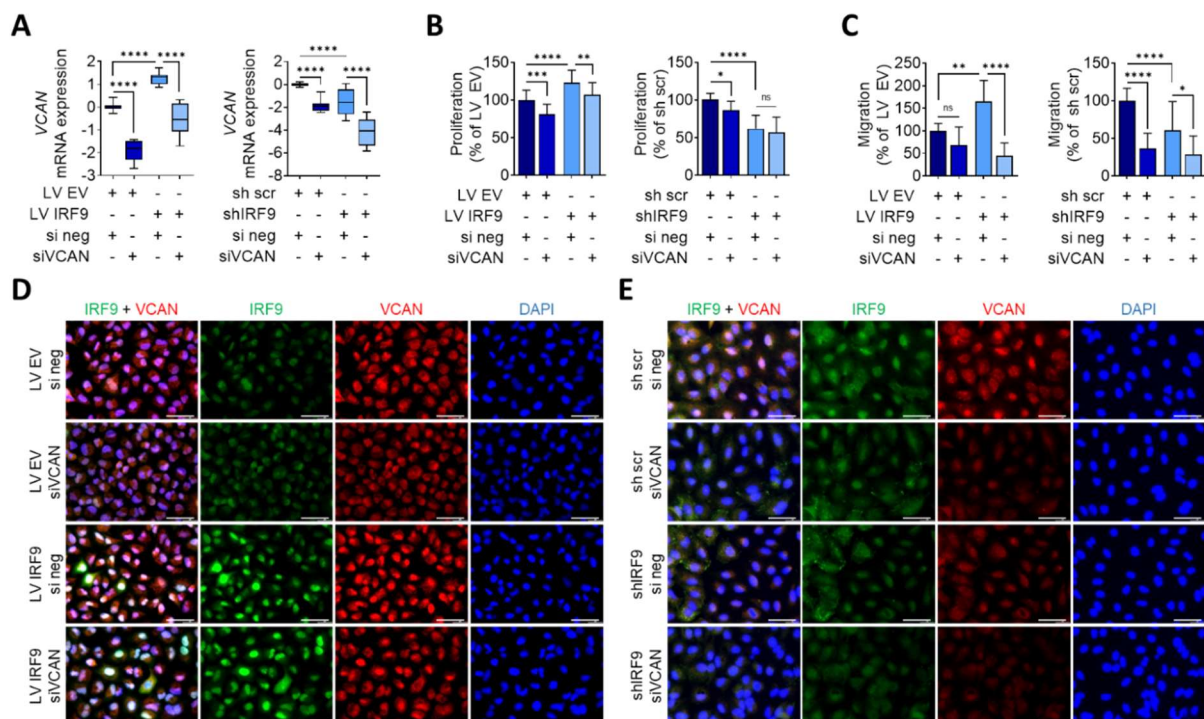


**Figure 29. Knockdown of VCAN diminishes oncogenic phenotype of IRF9.** Transduced A549 were transfected with siRNA against VCAN (siVCAN) or control sequence (si neg). Relative mRNA expression of VCAN was evaluated via RT-qPCR, displayed as  $\Delta\Delta Ct$  of LV EV si neg and sh scr si neg, respectively (A). Quantified proliferation (B) and migration (C) were calculated as percentages of LV EV si neg and sh scr si neg, respectively. Expression of IRF9 and VCAN was assessed via immunofluorescence co-staining together with DAPI counterstaining (D, E). Data represent mean  $\pm$  SEM ( $n = 3$ ); \*  $p < 0.05$ ; \*\*  $p < 0.01$ ; \*\*\*  $p < 0.001$ ; \*\*\*\*  $p < 0.0001$ . Conditions were compared as indicated.

Transfecting siRNA was sufficient to reduce the expression of VCAN and hence the proliferation and migration of A549 tumour cells. Based upon stronger effect and less side effect concerning IRF9 upregulation, we chose to apply siVCAN1 in further siRNA experiments. To ascertain whether VCAN regulation is responsible for the oncogenic behaviour of transduced A549 cells, we used siRNA against *VCAN* in those cells, which were then transfected, and the mRNA expression of genes of interest was evaluated. Additionally, the overall expression of VCAN and IRF9 was studied in immunofluorescence staining, and functional assays to measure cell proliferation and migration were conducted.

RT-qPCR showed that siRNA transfection led to an efficient knockdown of *VCAN* expression in all transfected cell lines (Figure 29 A). In LV IRF9 cells, the knockdown led to similar expression levels of *VCAN* when compared with LV EV si neg (Figure 29 A). Interestingly, the convergence of LV IRF9 siVCAN towards LV EV si neg could be also seen in the changes in proliferation rate (Figure 29 B). Even though the tendency was obvious, the knockdown did not reduce migration significantly in LV EV but did so in IRF9-overexpressing cells (Figure 29 C). Immunofluorescence staining also confirmed the successful knockdown of VCAN (Figure 29 D).

In IRF9-silenced cells, the transfection of siVCAN was able to reduce already low *VCAN* mRNA levels, hence the lowest were observed in the shIRF9 siVCAN condition (Figure 29 A). The siVCAN transfection could reduce the proliferative and migratory behaviour in the sh scr condition. Although it can be stated that the additional reduction of VCAN in shIRF9 cells could not further reduce the already low proliferation rate, it did moderately reduce migration (Figure 29 B, C). Further, the knockdown of VCAN could be demonstrated by immunofluorescence staining (Figure 29 E).

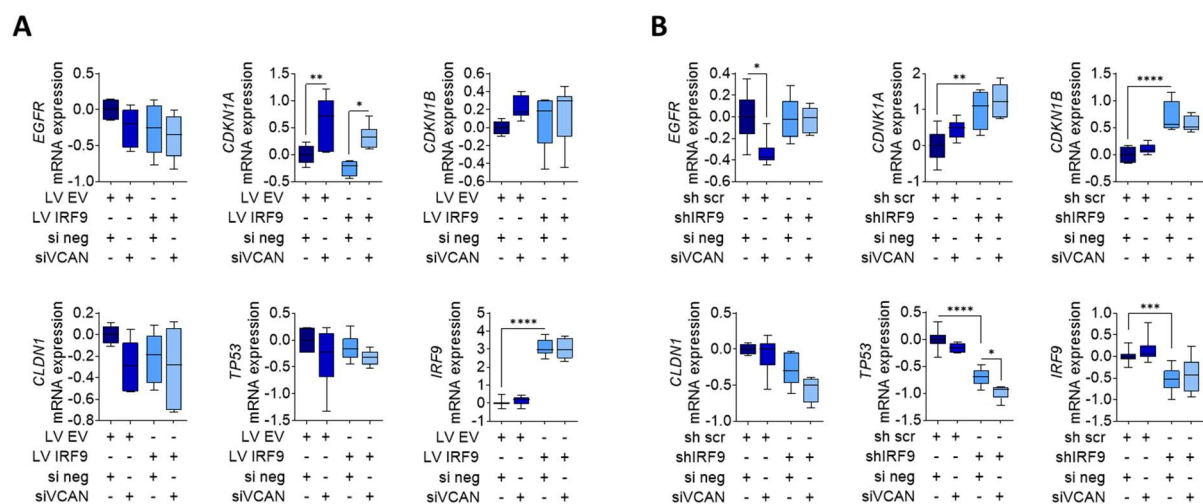


**Figure 31. Knockdown of VCAN increases expression of CDKN1A.** Transduced A549 were transfected with siRNA against VCAN (siVCAN) or control sequence (si neg). Relative mRNA expressions of indicated genes were evaluated via RT-qPCR, displayed as  $\Delta\Delta Ct$  of LV EV si neg (A) and sh scr si neg (B), respectively. Data represent mean  $\pm$  SEM ( $n = 3$ ); \*  $p < 0.05$ ; \*\*  $p < 0.01$ ; \*\*\*  $p < 0.001$ ; \*\*\*\*  $p < 0.0001$ . Conditions were compared as indicated.

Overall, it can be noted that in each transfection scheme, the condition with the lowest mRNA expression of *VCAN* showed the least proliferation – in other words, A549 LV EV siVCAN and A549 shIRF9 siVCAN, respectively (Figure 31 A, B). As it was of great interest to elucidate how VCAN can regulate oncogenic behaviour in A549, several genes known to be associated with VCAN or its EGF-like domain were studied.

We analysed the mRNA expression levels of *EGFR*, as receptor for EGF, and the cell cycle inhibitors *CDKN1A* and *CDKN1B* as potential partners of VCAN. *EGFR* or *CDKN1B* expressions were not altered, whereas *CDKN1A* clearly showed an upregulation after siVCAN transfection in LV EV and LV IRF9 and at least an apparent tendency in sh scr and shIRF9 (Figure 31 A, B). Interestingly, the expression of *CDKN1A* in A549 LV IRF9 si neg compared to LV EV si neg, and shIRF9 si neg compared to sh scr si neg, respectively showed differences as opposite directions of *VCAN* in those conditions (Figure 29 A; Figure 31 A, B). As an important tumour suppressor and known to interact with *CDKN1A* and *CDKN1B*, we studied the expression of *TP53*. In IRF9-overexpressing cells, no changes in expression could be observed, whereas in shIRF9 cells the knockdown of *VCAN* also decreased *TP53* levels, which were already significantly low compared to sh scr cells (Figure 31 A, B). The same tendency could also be observed for the expression of *CLDN1*. Interestingly, the mRNA expression of *IRF9* was not significantly upregulated after siVCAN transfection, unlike previously observed in naïve A549 (Figure 31 A, B).

Altogether, the VCAN knockdown could diminish the oncopromoting effects of IRF9 overexpression by reducing cell proliferation and migration. mRNA analyses showed an involvement of *CDKN1A* in both overexpressing and knockdown cells.

#### 4.8. IRF9 regulates expression of VCAN

After we discovered that IRF9 expression had a strong impact on the tumour cell behaviour of proteoglycan VCAN, we aimed to understand how IRF9 regulated the expression of VCAN. It is not known how IRF9 might bind at the promoter of VCAN and activate its expression. Since IRF9 possesses a DNA-binding domain, we decided to screen the promoter for possible ISREs, notwithstanding of the cofactors that could be involved.

Therefore, we used the IRF9 motif extracted from the online tool HOMER v4.10 (Figure 32 A). The sequence of *VCAN* promoter was taken from the EPD (Eukaryotic Promoter Database) ranging from -1000 bp to +100 bp. Next, we used the online tool FIMO (Find Individual Motif Occurrences) to identify three probable binding sites of the IRF9 motif in the promoter of *VCAN*. One potential ISRE was located between -636 and -625 bp upstream and interestingly, two potential overlapping ISREs between -593 and -576 bp (Figure 32 B).

To confirm the binding, Chromatin-Immunoprecipitation (ChIP) was performed, applying an antibody against IRF9 to the fragmented chromatin of naïve A549. The RT-qPCR of purified chromatin showed that IRF9 specifically bound in the promoter of *VCAN* in the region of the

three presumed ISREs, whereas the analysis of the promoter of *ACTB* did not identify binding (Figure 32 C).

Next, we wanted to prove the regulation of *VCAN* by IRF9 in transduced A549 cells by luciferase assay. The promoter sequence of *VCAN* from -842 to -24 bp was cloned into a pGL3 luciferase vector including all three indicated ISREs (pGL3 *VCAN* 818 bp). The pGL3 *VCAN* 818 bp, or pGL3 basic vector as control, were transfected into transduced A549 cells followed by luciferase measurement. It revealed that in IRF9-overexpressing cells the transcription had significantly increased compared to control cells, whereas transfection in A549 shIRF9 cells did not lead to changes in the transcription (Figure 32 D).

In conclusion, by in-silico analysis we were able to show that the *VCAN* promoter contained three ISRE sites and proved the binding of IRF9 by chromatin analysis. In IRF9-overexpressing cells, this led to increased transcription.

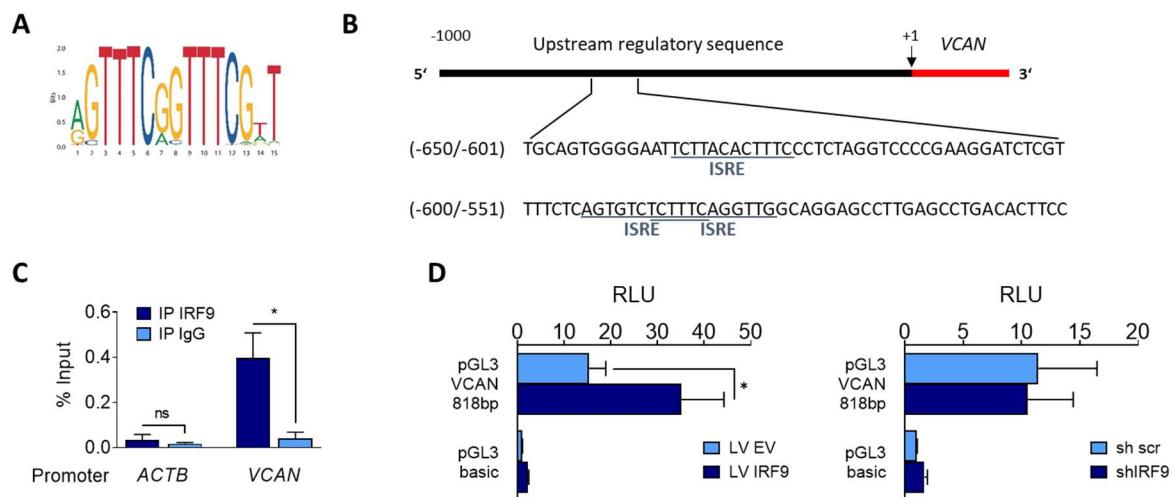


**Figure 32. IRF9 binds to *VCAN* promoter and regulates its expression.** (A) IRF9 binding motif from open-access database JASPAR (matrix ID MA0653.1). (B) Sequence of *VCAN* promoter, potential ISRE based on FIMO search are underlined. (C) Chromatin immunoprecipitation was performed using antibody against IRF9 and the respective IgG in naïve A549 chromatin. Purified DNA was analysed via RT-qPCR in the promoter of *ACTB* and *VCAN*. (D) Luciferase vector containing 818 bp sequence of *VCAN* promoter or empty vector control pGL3 basic were transfected into transduced A549. Luciferase activity was measured, displayed as RLU. Data represent mean  $\pm$  SEM ( $n = 3$ ); \*  $p < 0.05$ ; IP IRF9 was compared to IgG; LV IRF9 was compared to LV EV; shIRF9 was compared to sh scr.

#### 4.9. IRF9 regulates tumour growth in vivo

To study the role of IRF9 in vivo, three strategies were applied. First, in a xenograft model, transduced A549 were injected in BALB/c mice. Second, transduced CULA cells were injected in wildtype mice. Third, global *Irf9* knockout mice (*Irf9*<sup>-/-</sup>) were used in tumour models injecting naïve LLC1 cells.

##### 4.9.1. Subcutaneous tumour models of transduced cell lines

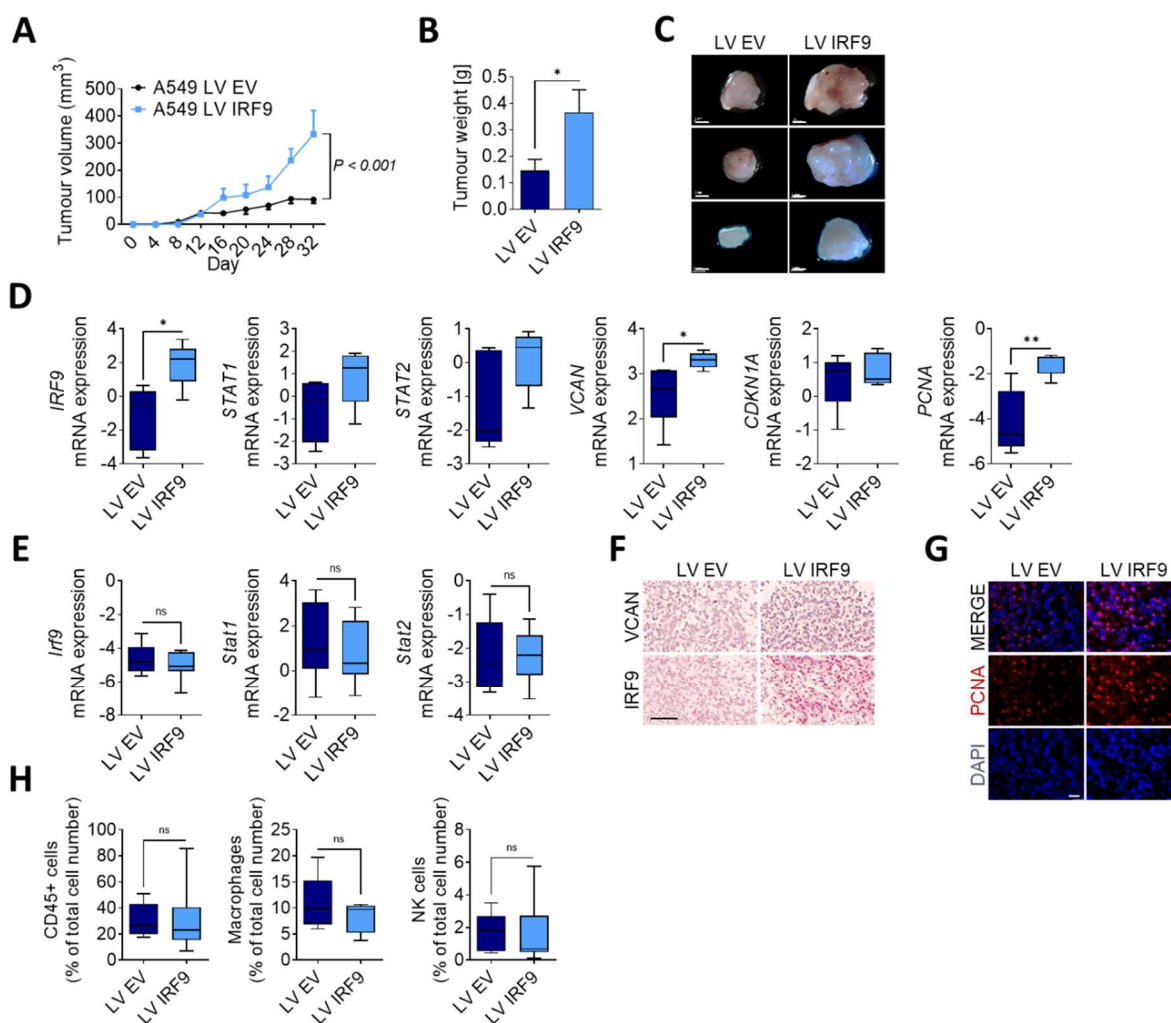


**Figure 33. IRF9 overexpression increases tumour growth in xenograft model.** (A) Transduced A549 were injected subcutaneously, and tumour growth was monitored ( $n = 8$ ). At the endpoint, tumours were excised and weighed (B, C). RNA was isolated and analysed for human (D) and murine gene expression (E) ( $n = 6$ ). Protein expressions of IRF9, VCAN and PCNA in tumour tissue sections were evaluated in (F) immunohistochemical and (G) immunofluorescence staining. (H) Cell composition of the tumour was analysed via flow cytometry ( $n = 5-6$ ). Data represent mean  $\pm$  SEM; \*  $p < 0.05$ ; \*\*  $p < 0.01$ ; LV IRF9 was compared to LV EV. Scale 2mm (C); 100  $\mu$ m (F); 50  $\mu$ m (G).

After the intense characterisation of oncogenic behaviour of IRF9 in human LUAD cell lines A549 and A427, we used the mouse strain BALB/c to study the vivo effects. A549 LV IRF9 and the control A549 LV EV were injected subcutaneously into the flank, and tumour volume was measured every four days (Figure 33 A). At the endpoint, the excised tumours were weighed, and images were taken (Figure 33 B, C). The development of tumour volume of A549 LV IRF9 showed greater tumour growth, and the final tumour mass had significantly increased (Figure 33 A-C). The analyses of mRNA expression revealed that high expression levels of *IRF9*, *VCAN* and *PCNA* were conserved until the endpoint, whereas for *STAT1*, *STAT2* or *CDKN1A*, no significantly altered expression could be observed (Figure 33 D). Interestingly, the injection of these cells did not influence the mRNA expression of host cell-derived murine *Irf9*, *Stat1* or *Stat2* (Figure 33 E). Additional performed immunohistochemical staining confirmed the overexpression of IRF9, VCAN and PCNA in LV IRF9 tumours (Figure 33 F, G). Flow cytometry analysis of excised tumours did not reveal differences in cell composition (Figure 33 H).

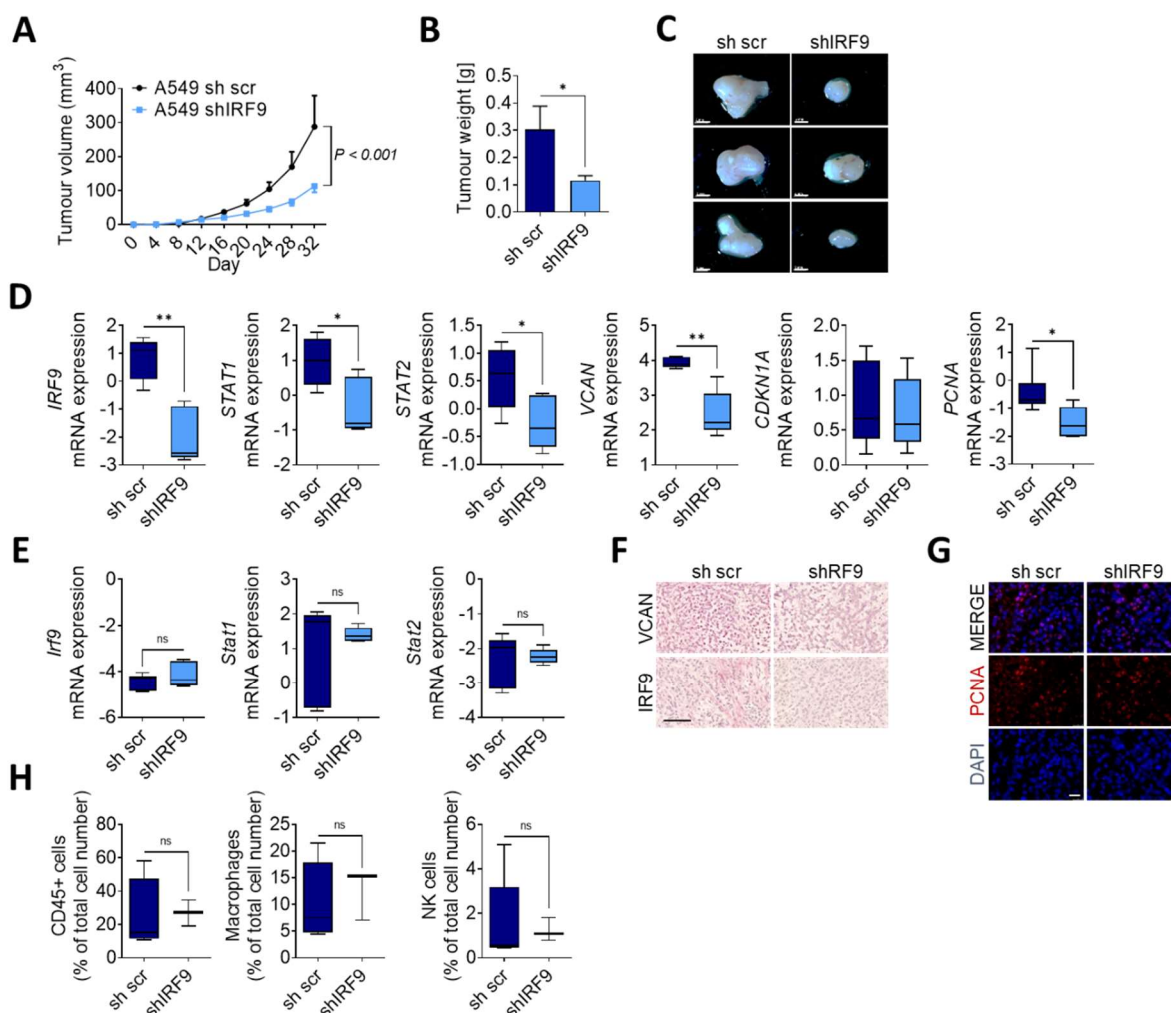


**Figure 34. Knockdown of IRF9 reduces tumour growth in xenograft model.** (A) Transduced A549 were injected subcutaneously, and tumour growth was monitored ( $n = 10$ ). At the endpoint, tumours were excised and weighed (B, C). RNA was isolated and analysed for human (D) and murine gene expression (E) ( $n = 6$ ). Protein expressions of IRF9, VCAN and PCNA in tumour tissue sections were evaluated in (F) immunohistochemical and (G) immunofluorescence staining. (H) Cell composition of the tumour was analysed via flow cytometry ( $n = 3-5$ ). Data represent mean  $\pm$  SEM; \*  $p < 0.05$ ; \*\*  $p < 0.01$ ; shIRF9 was compared to sh scr. Scale 2mm (C); 100  $\mu$ m (F); 50  $\mu$ m (G).

In accordance with the injection of overexpressing cells, we injected A549 shIRF9 and sh scr cells into the flank of BALB/c mice. The tumour model showed a significantly reduced growth of shIRF9 cells compared to the control group, resulting in decreased tumour volume and weight (Figure 34 A-C). When we analysed the mRNA expression, we could confirm the sustainable knockdown of *IRF9* together with reduced mRNA levels of *VCAN* and *PCNA* over the experimental period (Figure 34 D). Similar to in vitro characterisation of A549 shIRF9, *STAT1* and *STAT2* expression was reduced, but *CDKN1A* did not show an altered expression when compared to A549 sh scr tumours (Figure 34 D). The resulting tumours did not show any altered expression of murine *Irf9*, *Stat1* or *Stat2* levels (Figure 34 E). Immunohistochemical analyses of tissue sections could validate mRNA results with decreased IRF9, VCAN and PCNA expression in A549 shIRF9 tumours (Figure 34 F, G), and the flow cytometry analysis of excised tumours did not reveal differences in cell composition (Figure 34 H).

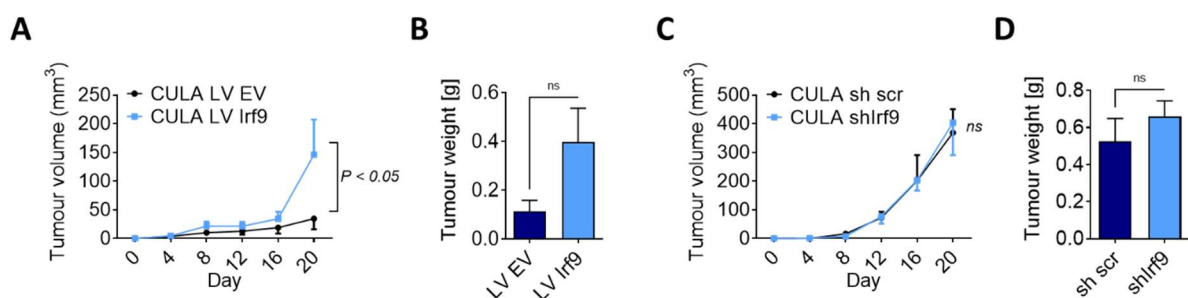


**Figure 35. Overexpression of *Irf9* in CULA influences tumour growth.** Transduced CULA were injected subcutaneously, and tumour growth was monitored (A, C). At the endpoint, tumours were excised and weighed (B, D). Data represent mean  $\pm$  SEM ( $n = 6$ ); \*  $p < 0.05$ ; LV *Irf9* was compared to LV EV; shIrf9 was compared to sh scr.

In addition to subcutaneous injections with A549 IRF9 cells, we injected transduced CULA cells into the flank of C57BL/6N mice despite the non-functional knockdown of *Irf9* in CULA. Tumour growth was monitored until the endpoint was reached where the excised tumours were weighed. The syngeneic model confirmed the influence of elevated *Irf9* levels on tumour progression, with increased tumour volume and mass (Figure 35 A, B). As expected from in vitro analyses, the knockdown of *Irf9* in CULA cells did not affect tumour growth in vitro (Figure 35 C, D).

#### 4.9.2. Tumour models in global *Irf9*-knockout mice

Since IFN cascade and IRF9 are known key players in immunology, one main aim of this study was to reveal the effect of IRF9 in the tumour microenvironment. Therefore, we used global *Irf9*-knockout mice (*Irf9*<sup>-/-</sup>) to study both an intravenous and a subcutaneous tumour model. Wildtype C57BL/6N mice (WT) were compared as control.

LLC1 were injected into the tail vein to study the progression of circulating tumour cells, similar to a metastatic event. Mice reached the endpoint after 16 days; perfused lungs were excised, and the number of tumour nodules in the lungs were counted macroscopically (Figure 36 A, B). No differences in the number of tumour nodules between WT and *Irf9*<sup>-/-</sup> mice could be observed (Figure 36 A). For subcutaneously tumour growth, LLC1 cells were injected into the flank. The

experiment ended after 20 days, but no differences in tumour growth or tumour mass could be assessed (Figure 36 C-E). However, the flow cytometry analysis of tumour homogenate revealed that the composition differed (Figure 36 F). Tumours from *Irf9*<sup>-/-</sup> mice consisted of a higher proportion of tumour cells and a reduced appearance of hematopoietic cells, characterised as CD45+ (Figure 36 F). Additionally, natural killer cells and macrophages were significantly reduced in *Irf9*<sup>-/-</sup> mice, together with their precursors' monocytes (Figure 36 F). As TAMs are one of the main cell types in neoplasms, we used immunofluorescence staining of macrophage marker IBA1 to visualise the reduced presence of macrophages in tumour tissue sections of *Irf9*<sup>-/-</sup> mice (Figure 36 G).

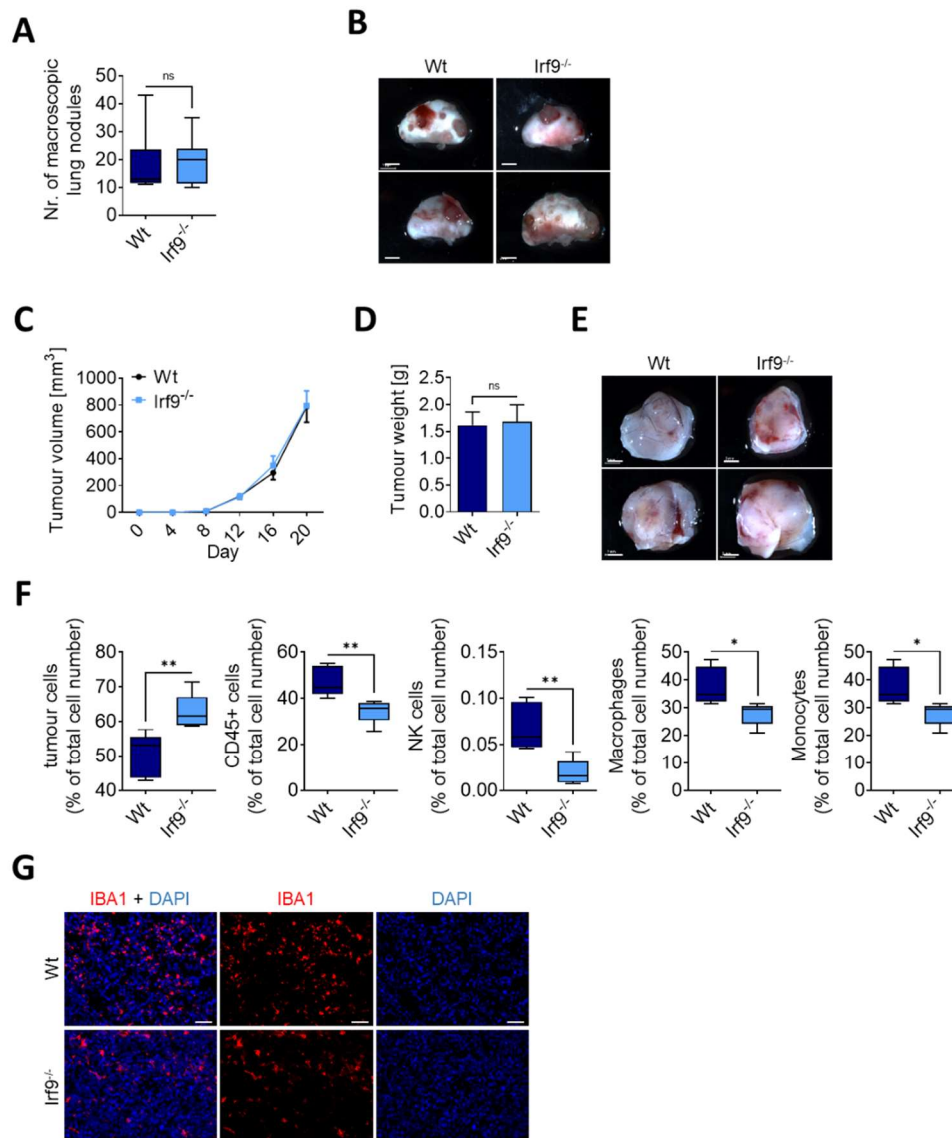


**Figure 36. Loss of *Irf9* alters cell composition in subcutaneous tumours.** LLC1 were injected intravenously into WT or *Irf9*<sup>-/-</sup> mice, and lung tumours were counted macroscopically ( $n = 9-12$ ) (A, B). LLC1 were injected subcutaneously into WT or *Irf9*<sup>-/-</sup> mice, and tumour growth was monitored ( $n = 12$ ) (C). At the endpoint, tumours were excised and weighed (D, E). Cell composition of the tumour was analysed via flow cytometry ( $n = 5$ ) (F). Protein expression of IBA1 in tumour tissue sections counterstained with DAPI (F, G). Data represent mean  $\pm$  SEM; \*  $p < 0.05$ ; \*\*  $p < 0.01$ ; *Irf9*<sup>-/-</sup> were compared to Wt. Scale 25  $\mu$ m.

As we identified numerical differences for TAMs, we used the mRNA analysis of tumour homogenate in order to characterise macrophage phenotype and to identify differences in the regulation and polarisation of TAMs between wildtype and *Irf9*<sup>-/-</sup> mice. Analysing M1-specific markers, such as *Tnf*, *Nos2*, *Il1b* or *Ccl2* (the latter responsible for monocyte chemoattraction), we did not detect differences in mRNA expression (Figure 37). Similarly, the expression of M2 markers *Il10*, *Arg1* or *Chit1* was not altered (Figure 37). Further mRNA analysis revealed reduced mRNA expression of *Irf9*, *Stat1* and *Stat2* in tumours obtained from *Irf9*<sup>-/-</sup> mice as a result of depleted host *Irf9* and naïve *Irf9* expression from LLC1 cells (Figure 37). As expected from similar tumour progression, *Pcna* expression was not altered, whereas *Pdgfra* expression was higher in *Irf9*<sup>-/-</sup> mice (Figure 37). We also analysed the expression of genes involved in immune checkpoint, where we identified *Pdcd1* at similar levels but the ligand *Cd274* as downregulated in tumours of *Irf9*<sup>-/-</sup> mice (Figure 37).

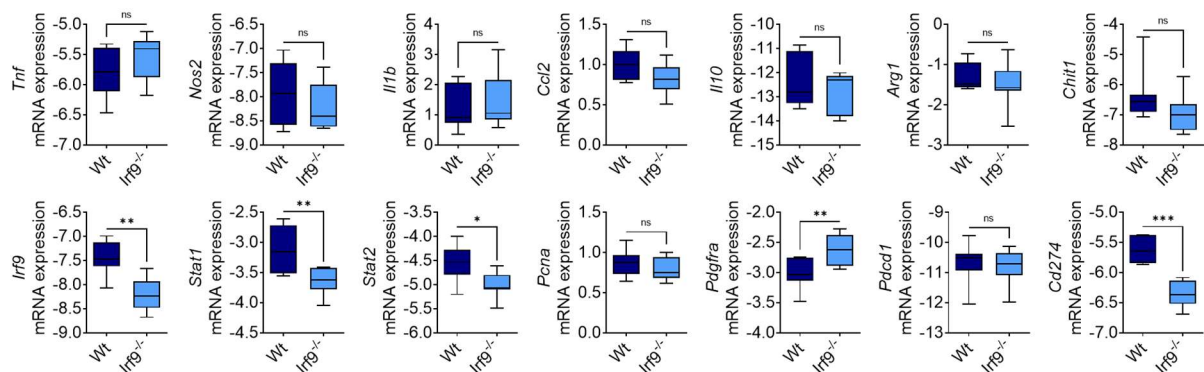


**Figure 37. mRNA expression of subcutaneous LLC1 tumour model.** Subcutaneous tumours after LLC1 injection in WT and *Irf9*<sup>-/-</sup> mice were used to isolate RNA and subsequent analysis of indicated genes via RT-qPCR. Data represent mean  $\pm$  SEM; \*  $p < 0.05$ ; \*\*  $p < 0.01$ ; \*\*\*  $p < 0.001$  ( $n = 7$ ). *Irf9*<sup>-/-</sup> were compared to Wt.

After the reduction of macrophages in *Irf9*<sup>-/-</sup> lungs and tumours suggested an influence of IRF9 in macrophages, we decided to further investigate their role and function. Therefore, we generated bone marrow derived macrophages (BMDM) and polarised them to M1 or M2 phenotype; naïve cells were used as control (M0). The analysis of mRNA confirmed the successful polarisation into M1 phenotype with high expression of *Tnf*, *Nos2* and *Il1b* and M2 phenotype with high expression of *Arg1* and *Chit1*, respectively (Figure 38 A). Based on mRNA expression, no significant differences in the polarisation between wildtype and *Irf9*<sup>-/-</sup> macrophages could be detected (Figure 38 A). Since *Irf9* is not part of the canonical signalling of IFN $\gamma$ , the expression of *Irf9* did not significantly increase in M1 macrophages (Figure 38 A). As a control of *Irf9* depletion, *Irf9* expression was not detectable in *Irf9*<sup>-/-</sup> macrophages (Figure 38 A). Additionally, we analysed the expression of *Vcan* in macrophages, where it was activated more strongly upon IFN $\gamma$  stimulation than upon IL4 treatment; however, we observed no differences between wildtype and *Irf9*<sup>-/-</sup> macrophages (Figure 38 A). Moreover, the conditioned medium of macrophages was collected after polarisation and applied to naïve LLC1 cells. The evaluation of LLC1 proliferation confirmed strong tumour suppressive features of M1 conditional medium for each BMDM source at a similar level and did not allow to determine functional differences of *Irf9*-deletion (Figure 38 B).

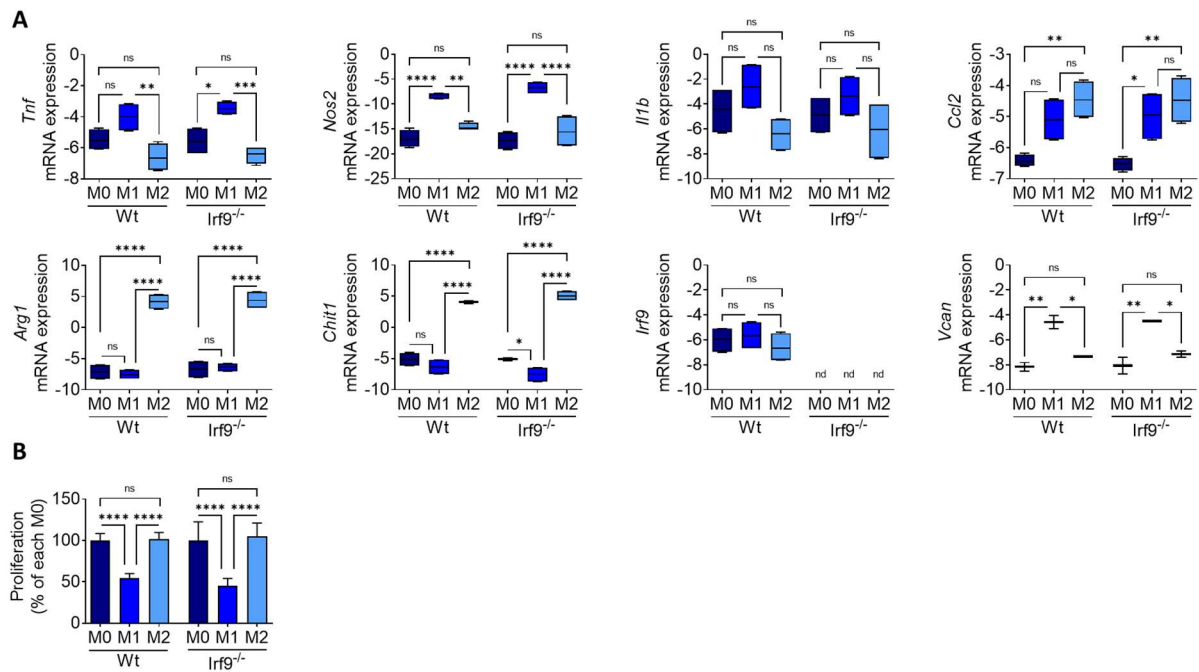


**Figure 38. Deletion of *Irf9* in BMDM does not influence gene expression of macrophage marker.** BMDM of WT and *Irf9*<sup>-/-</sup> mice were generated and polarised into M1 or M2 phenotype. Gene expression of indicated genes were evaluated via RT-qPCR ( $n = 4$ ) (A). Conditioned medium of polarised macrophages was collected and applied to LLC1 cells to evaluate cell proliferation, calculated as percentage of each naïve M0 ( $n = 3$ ) (B). Data represent mean  $\pm$  SEM; \*  $p < 0.05$ ; \*\*  $p < 0.01$ ; \*\*\*  $p < 0.001$ ; \*\*\*\*  $p < 0.0001$ . Conditions were compared as indicated.

Overall, tumour cell injection did not lead to differences in tumour growth or nodule formation but in cell composition, when *Irf9* was absent in the host. The analysis of mRNA expression did not suggest an altered macrophage phenotype, but could detect a downregulation of PD-L1 (*Cd274*). The isolation and investigation of murine macrophages did not reveal differences in polarisation or anti-tumour properties.

## 5. Discussion

### 5.1. Role of IRF9 in lung cancer progression

#### 5.1.1. Relevance of IRF9 in cancer

From the online available data of lung cancer patients, Kaplan-Meier curves showed that the overexpression of IRF9 was associated with reduced survival, which decreased even more significantly in LUAD patients; conversely, in LUSC patients, we observed no effect on patient survival. Supportive survival data confirmed that a low expression of IRF9 was beneficial to lung cancer patients [68]; for other diseases such as breast or renal cancer, the human data are less clear. Renal cell carcinoma patients, with nuclei positive for IRF9, had a better prognosis than those with absent IRF9 expression. Similar to our findings in lung cancer patients, the status of STAT2 did not influence survival in these patients [139]. In triple-negative breast cancer (TNBC), high levels of IRF9 were associated with a better outcome, and IRF9 was considered a prognostic marker for chemotherapy response [187]. Studies showed that the loss of IRF9 in TNBC accompanied a reduced response to intratumoural IFN signalling, whereas the presence of IRF9 could enhance antitumoural immunity and increase patient survival [187]. However, in vitro breast cancer data might differ. In breast cancer cell line MCF7, the overexpression of IRF9 increased the cancer cell's resistance against the chemotherapeutic drug Paclitaxel [90]. The upregulation of STAT1 or STAT2 had no influence in MCF7, hence IRF9 was the key player to mediate the resistance against Paclitaxel, which is in direct contrast to the findings in TNBC. Interestingly, MCF7 did not originate from a triple-negative patient; further, it was able to respond to IFN treatment with reduced proliferation [90]. Based on these findings, it should not be generalised that IRF9 is beneficial to all breast cancer patients. In our results, we could also show that IRF9 was upregulated in lung cancer cell lines when resistant against Doxorubicin or Paclitaxel, but whether manipulation of IRF9 expression influences resistance remains unclear and requires experiments in transduced cell lines accordingly. However, this confirmed the protumoural role of IRF9. Further, the poor outcome over high expression in lung cancer patients could be associated, among other reasons, with therapy resistance. Supportively in colon cancer cell lines, transfection and IRF9 overexpression increased chemoresistance, and further cell crowding in a three-dimensional way led to upregulation of IRF9 and hence resistance [151].

The intrinsic effects of IRF9 in cancer cells seems complex. Some publications demonstrated the tumour suppressive properties of IRF9, such as in the case of prostate cancer cells, where high IRF9 levels as well as artificial overexpression enabled the facilitation of antiproliferative effects of IFN. When IRF9 was expressed at low levels, the response to IFN was poor as well. It was suggested to use the abundance of IRF9 as a prognostic marker for IFN treatment in prostate cancer. Interestingly, the overexpression of IRF9 did not lead to an increase in proliferation, but the knockdown clearly reduced it, which is consistent with our results [137]. In acute myeloid leukaemia, IRF9 also acts as tumour suppressor and is expressed at low levels. The restoration of IRF9 suppressed SIRT1 expression and resulted in a less deacetylated and activated p53 [149].

Moreover, in acute pancreatitis, the silencing of IRF9 inhibited apoptosis via reduced deacetylation of p53 [150]. Similarly, the appearance of ISGF3 complex, even though not in a phosphorylated form, was able to suppress tumour growth in clear cell renal carcinoma. Furthermore, the silencing of IRF9 did not affect proliferation *in vitro*, but significantly increased growth in a xenograft tumour model [139]. Interestingly, the silencing of STAT1 and STAT2 also increased tumour growth, whereas the co-overexpression of IRF9 and STAT1 diminished tumour growth impressively [139].

Our results of IRF9 as oncogenic function were confirmed in other studies. Together with STAT2 and p65, it could bind at the promoter of IL6 and activate its expression [68]. Further, it was shown that the secretion of IL6 and the expression of IRF9 were correlated in human lung cancer cell lines and that the former was reduced after IRF9 knockdown. Furthermore, increased IL6 levels increase tumour growth and are associated with reduced survival in lung cancer patients [188]. The knockdown of IRF9 also led to a reduced cell survival in LUAD cell line HCC827, which confirms our observations in LUAD cell lines A549 and A427 [68]. In accordance with our findings, the silencing of IRF9 reduced the migration of AR42J cells [150].

Human cancer data from different entities seem to suggest that high IRF9 expression is associated with resistance against chemotherapy or radiotherapy but that it could, however, improve the response to stromal or therapeutic IFN. Whether high or low expression of IRF9 is beneficial to cancer patients might depend on the tumour type, and in lung cancer, such expression is associated with a reduced survival prognosis.

### **5.1.2. Non-canonical/IFN-independent upregulation of IRF9 promotes oncogenic features**

In our study, IRF9 clearly promoted proliferation, migration, and tumour growth. It is clear that in lung cancer, amongst others, stromal cells secrete IFNs to activate immune defence and inhibit tumour growth, as previously described [77]. In support of findings that long-term stimulation with IFNs reduces canonical signalling [85], we observed the reduced phosphorylation status of STATs together with elevated IRF9 levels in tumour areas. It encourages our hypothesis that the loss of canonical ISGF3 signalling towards an activation of U-ISGF3 plays a relevant role in lung cancer. With the loss of IFN sensitivity, IRF9 is no longer able to facilitate the antiproliferative effects of IFN; consequently, the downstream profile of IRF9 changes. In these circumstances, it is reasonable that Kaplan–Meier curves showed lower survival in lung cancer patients when IRF9 expression was high.

U-ISGF3 was shown to play a role in breast cancer to activate the expression of IRDS (IFN-related DNA damage resistance). Cell lines deriving from radiotherapy and chemotherapy-resistant tumours showed upregulation of IRDS gene signature and a more aggressive phenotype. Moreover, the knockdown of STAT1 was able to reduce their expression and subsequently their phenotype [189]. In another study focusing on TNBC, the relevance of U-ISGF3 and IRDS could be confirmed. Moreover, it was shown that cells with mesenchymal, hence more aggressive,

phenotype overexpressed U-ISGF3 including IRF9. The knockdown of IRF9 reduced the migration of these cells, whereas cell proliferation was not influenced [105]. Additionally, experiments in breast cancer cells showed that receptor RIG-I was activated by stromal exosomes to increase IFN-related response, which resulted in a STAT1- and NOTCH3-mediated activation of therapy resistant tumour-initiating cells [190]. The upregulation of IRDS was also shown in colon cancer to increase chemoresistance [151].

We observed upregulation of IRF9 in Doxorubicin-resistant cells and even greater upregulation in Paclitaxel-resistant cells. How important it is to target IRF9 or U-ISGF3 and to restore sensitivity against Doxorubicin was demonstrated by the knockdown of IRF9 and STAT1 [85]. This is in line with the observations in colon cancer, where IRF9 overexpression led to resistance against Docetaxel, amongst others [151]. Even though further experiments are needed to confirm the restored sensitivity in resistant lung cancer cells, we could show that IRF9 and thus U-ISGF3 is involved in chemoresistance in lung cancer.

In both human IRF9-overexpressing lung cancer cell lines, IRF9 overexpression could not influence STAT1 or STAT2 expression, which echoes published work [151]. Only in murine cells, Stat1 expression was increased after Irf9 overexpression; moreover, we observed decreased expression of STAT1 and STAT2 in IRF9-silenced human lung cancer cell line, which was similarly observed in colon cancer cells [151]. Even though STAT1 and STAT2 expression are dependent on ISRE activation at their promoter, and reduction of IRF9 also reduced STAT1 and STAT2; the excess of IRF9, able to bind to ISREs, did not necessarily lead to STAT1 or STAT2 overexpression. Since IRF9 is the DNA-binding part and co-opts STATs, it is possible that a feedback mechanism recognises whether the activity of (U-)ISGF3 is already sufficient or further STAT upregulation is required. However, the reduced IRF9 level in A549 resulted in decreased STATs expression due to lacking activity at STAT promoter. If we consider this model, the correlation of IRF9 with STAT1 and STAT2 in human lung cancer patients would not fit perfectly. Nevertheless, it should also be considered that IRF9 expression in patients might not be the source but rather the consequence of long-term IFN stimulation originating from tumour stroma and is therefore upregulated together with STAT1 and STAT2. The findings in HCT116 cells were similar, when IRF9 upregulation did not influence STAT expression, but a 3D cell culture model induced IRF9 together with STAT1 and STAT2, even though functional effects were caused by IRF9 induction [151].

Further, we observed differences when comparing lung cancer cell lines A549 and A427. Both cell lines originated from lung adenocarcinoma with moderate and comparable IRF9 and STAT1 expression, differing in almost no detectable STAT2 expression in A427. However, both cell lines showed similar oncogenic behaviour and upregulation of VCAN after IRF9 overexpression. Based on our findings, it cannot be stated whether STAT1 or STAT2 build a complex with IRF9, but it can be presumed that IRF9 can recruit its partner, and even small amounts are sufficient to form an active complex. Supportive data showed that once U-ISGF3 complex was formed, it was highly stable, even when the mRNA expression of IRF9, STAT1 and STAT2 decreased [105].

The upregulation of IRF9 after IFN stimulation was obvious. The phosphorylation of STATs at an early timepoint activated first response and may have also activated the expression of IRF9 and STATs [85]. The increases after 24 h were massive; yet, differences in proliferation were observed only after 72 h. The literature has suggested that IRF9 enables the antiproliferative effects of IFN [148], which might be beneficial to increase IRF9 in order to enhance the antiproliferative effect of IFN. Nevertheless, STATs also increased together with IRF9; thus, it could be explained why solely IRF9 overexpression increases proliferation, as in the case of the study by Cheon et al., where the expression of canonical and non-canonical IFN were different [85]. It would have been of interest to investigate the response of our transduced cell lines to IFN treatment in respect to proliferation as we could have enlightened whether the oncopromoting effect of IRF9 or the increased response to antiproliferative IFN would dominate. Since present IRF9 levels influence the response of IRF9 itself to IFN, we would assume a stronger and/or faster reduction of proliferation for LV IRF9 and a reduced or slowed response for shIRF9. It would be possible that the shift towards non-canonical signalling would not regulate proliferation as expected.

The sequencing of transduced A549 IRF9 cells revealed differences in the expression pattern between overexpression and silencing of IRF9. Overall, more genes were regulated after IRF9 overexpression than after silencing in A549. Interestingly, IRF9 was in top 25 upregulated genes in A549 LV IRF9, whereas it was not top downregulated in A549 shIRF9. Consequently, the effects of IRF9 knockdown can be more extensive than the knockdown itself, resulting in by far stronger knockdown of other genes.

RNA-seq of IRF9-overexpressing cells revealed the upregulation of genes that are reported to support pro-tumoural behaviour in lung cancer, such as DUSP1 (Dual-specificity phosphatase 1), FSCN1 (Fascin actin-binding protein 1), CTSL (Cathepsin L) and CTSB (Cathepsin B). Particularly, DUSP1 was reported to promote migration in lung cancer cell line H460 and downregulation reduced VEGFC production [191]. Beside lung cancer, high expression of DUSP1 was associated with poor prognosis for cancer patients [192]. FSCN1 is overexpressed in NSCLC patients and correlated with progression and lower survival [193], and it was shown to regulate migration and invasion in NSCLC [194]. Focusing on both upregulated CTSB and CTSL, Chen et al. showed that they were enriched in sera of lung cancer patients, and CTSB, in particular, was associated with lower survival probability [195, 196]. Interestingly, tumour suppressor genes such as IGFBP7 (insulin like growth factor binding protein 7) were also upregulated in LV IRF9, which was reported to be downregulated or inactivated in lung cancer patients and might be regulated by tumour suppressor p53 [197]; further analysis also showed a suppressing role in colorectal cancer [198].

From those genes that were downregulated in LV IRF9, HEXIM1 (Hexamethylene-bis-acetamide-inducible protein 1) is in line with the observed effects; it can inhibit cell migration and invasion and seems beneficial to breast cancer patients by enhancing chemotherapy response [199, 200]. We also observed a reduction of PDE3A (Phosphodiesterase 3A), which is downregulated in NSCLC cells and associated with chemotherapy resistance; PER2 (period circadian regulator 2) and TLE3 (Transducin-like enhancer of Split 3), which were shown to inhibit proliferation in A549 and colon cancer cell lines, respectively [201-203]. In contrast, RNA-seq showed downregulation

of NTS (Neurotensin) and KRT18 (Keratin 18), which are associated with NSCLC progression as well as CNTN1 (Contactin 1), an oncogene that was shown to increase chemotherapy sensitivity after downregulation in NSCLC [204-207].

The regulated genes in IRF9-silencing A549 were less compared to IRF9 overexpression and tended to have a less homogeneous distribution. This can be explained by the sequencing depth and level of alteration of IRF9 levels in cell lines. However, upregulated genes were in line with observed reduction of tumour cell proliferation and migration such as EFEMP1 (EGF-containing fibulin-like extracellular matrix protein 1) and TP63 (Tumour protein 63) reducing tumoural behaviour of NSCLC and other entities, respectively [208, 209]. At the same time, the genes CDCP1 (CUB domain containing protein 1) and TGFA (transforming growth factor alpha) were upregulated, which are known to drive proliferation and migration in lung cancer [210, 211]. Downregulated genes in A549 shIRF9, such as PRODH2 (Proline dehydrogenase), HPD (4-hydroxyphenylpyruvate dioxygenase) and ERBB3 (Receptor tyrosine-protein kinase erbB-3), supported the functional changes in these cells. It was demonstrated that the knockdown of PRODH2 and HPD, respectively reduced the tumoural phenotype in NSCLC cells, whereas ERBB3 as RTK is a promising target for lung cancer treatment [212-214]. It is to mention that the low expression of CASTOR1 (Cytosolic Arginine Sensor for MTORC1 Subunit 1) in LUAD patients is associated with poor survival, contrary to the phenotype in A549 shIRF9 [215].

Overall, the RNA-seq of transduced A549 could show that the top regulated genes in overexpressing and knockdown cells were in line with the oncogenic phenotype of IRF9; however, we detected contradictory genes in each set. Since the oncogenic phenotype of IRF9 dominated, resulting in the observed phenotype after overexpression or knockdown, the regulation of these contradictory genes could be a cellular counteraction, albeit unsuccessful. For this purpose, we analysed genes that were commonly regulated in each set and in opposite directions. Genes revealed by the RNA-seq were further validated via RT-qPCR, which demonstrated that DUSP26 (dual-specificity phosphatase 26), EMP1 (epithelial membrane protein 1), GRHL3 (grainyhead like transcription factor 3), IGFBP5 (insulin like growth factor binding protein 5), SH3TC2 (SH3 domain and tetratricopeptide repeats 2), TRIM29 (Tripartite motif-containing 29) and VCAN were associated with IRF9 expression in each set, respectively.

Beside the well-known oncogene VCAN, DUSP26 was regulated in the same direction as IRF9, and even though literature reports are less consistent, they show that it acts in an oncogenic manner in some entities [216, 217]. Other genes were regulated in a way opposite to IRF9 and could be characterised mainly as tumour suppressors; an example was EMP1, for which it was demonstrated that loss or downregulation was associated with a reduced cell proliferation, higher apoptosis in colon cancer and breast cancer cells and with a lower survival rate among breast cancer patients [218, 219]. Little is known about GRHL3, ranging from suppressing properties in squamous cell carcinoma, anti-proliferative and pro-apoptotic in colorectal cancer cells to pro-migratory and invasive in MCF7 cells [220-222]. IGFBP5 is characterised more in detail. For lung cancer, it was shown that high IGFBP5 expression in LUSC was associated with a better survival probability, and overexpression in breast cancer cells reduced proliferation and migration [223-225]. The function

of SH3TC2 in cancer is poorly investigated, functioning as tumour suppressor in glioma and renal cancer but also enabling oncogenic properties in breast cancer and leukaemia [226-229]. Despite the genes reviewed so far, the research on TRIM29 revealed its function as an oncogene regulated by  $\beta$ -catenin and its mechanism to enhance chemoresistance against cisplatin [230, 231].

Overall, the RNA-seq analysis of IRF9-overexpressing cells identified upregulation of predominantly oncogenic genes or downregulation of tumour suppressors, whereas the knockdown of IRF9 resulted in opposite effects. However, some genes that were not in line with the observed phenotype were regulated. The results of the analysis of commonly regulated genes mostly matched the phenotype of transduced A549 IRF9 cells, even though the RT-qPCR validation did not confirm significant regulation for all genes or sets. Based on these analyses and on the literature, we chose VCAN to further investigate its IRF9-regulated role in lung cancer.

### **5.1.3. VCAN elicits oncogenic feature after IRF9 manipulation**

RNA-seq, RT-qPCR validation, and the literature indicated that VCAN could be a potential downstream target of IRF9 to facilitate oncogenic phenotype. A further analysis of VCAN in human lung cancer patients revealed that expression increased and that the high expression of VCAN was associated with lower survival, particularly among LUAD patients, which is in line with IRF9 data. Further, we could detect a mild positive correlation of IRF9 and VCAN expression in lung cancer patients, which could hint at a regulation by IRF9. Immunohistological analysis showed cells with a strong nuclear enrichment of both IRF9 and VCAN, together with additional expression in the ECM of the proteoglycan VCAN.

Functionally different splice variants of VCAN are known, with VCAN [V1] as the oncogenic variant. Since protein and immunohistochemical analyses can only detect the overall VCAN, we used RT-qPCR of A549 IRF9 cells to confirm that the detected expression of VCAN also covered the expression of VCAN [V1]. Similarly, we assured that validating the total VCAN expression was sufficient to explain the observed functional effects by confirming that the siRNA approach efficiently silenced the VCAN [V1] variant as well. It would have been of interest to analyse other splice variants and whether they were influenced by either IRF9 transduction or siVCAN transfection. It could be possible that in the used cancer cell lines A549 and A427, VCAN is mainly spliced into V1 variant, and therefore, transcriptional changes of VCAN result in VCAN [V1]. Additional siRNA experiments against different splice variants could prove both, whether VCAN [V1] is acting oncogenic in LUAD cell lines and whether the effect of IRF9 transduction is specific for VCAN [V1].

In CULA cells, Irf9 overexpression led to both upregulation of Vcan and oncogenic phenotype, whereas no changes could be observed after Irf9 knockdown. The discrepancy of Vcan regulation between human and murine cells could be explained by different cofactors involved in the regulation. In addition, it appears reasonable that the knockdown of Irf9 was less efficient than in human cells, which could be seen when several shRNA plasmids failed to knockdown successfully. Despite intense optimisation, the strongest knockdown efficiency did not exceed 50%. Other

approaches, such as siRNA transfection, CRISPR/Cas9-mediated deletion of *Irf9* or isolation of epithelial cells or fibroblasts from *Irf9*<sup>-/-</sup> mice could be helpful to investigate whether the absent regulation of *Vcan* in CULA shIrf9 depended on weak *Irf9* knockdown and whether it could be more successful with one of the aforementioned methods.

However, it can be noted that in human and murine cells, the IRF9-dependent regulation of VCAN led to a change in oncogenic behaviour, and the absent downregulation in CULA shIrf9 demonstrated that VCAN could be directly responsible for enabling the oncogenic properties of IRF9. Although it is widely accepted as oncogene, previous studies in A549 did not identify VCAN knockdown as reducing tumoural behaviour *in vitro* but in an *in vivo* xenograft model [232]. This is in clear contrast to our findings as well as studies where in murine lung cancer cells VCAN silencing reduced tumour cell proliferation [233].

We could demonstrate that siVCAN transfection efficiently reduced the oncogenic effects of IRF9 that were sustained by VCAN upregulation when the proliferation levels of A549 LV IRF9 siVCAN and LV EV si neg were similar. Similarly, the migratory behaviour of IRF9 overexpressing cells were diminished by VCAN silencing. With already reduced VCAN expression, siVCAN experiments in A549 shIRF9 moderately reduced migration but not proliferation. Within each experimental setup, the lowest *VCAN* mRNA level was connected to the lowest proliferation rate and vice versa. To further demonstrate the role of VCAN, experiments with VCAN overexpression would be beneficial, particularly in shIRF9, to restore proliferation and migration.

Since the G3 domain of VCAN with its EGF motifs is responsible for proliferation, we studied the mRNA expression of the responsible receptor but could not detect changes in EGFR mRNA expression. We also followed published studies where the oncogenic variant VCAN [V1] was reported to alter the activation and phosphorylation of p27 to enhance proliferation [159]. Even though the mRNA expression of its encoded gene *CDKN1B* was already elevated in IRF9-silenced cells, we were not able to detect changes after VCAN knockdown. Nevertheless, protein expression and phosphorylation status should be studied to fully understand whether changes in mRNA expression were functional. Further, we checked the related cell-cycle inhibitor p21, encoded by *CDKN1A*. As we have seen in siRNA experiments, the knockdown of *VCAN* led to an increase in *CDKN1A* expression and correlated negatively with *VCAN* mRNA levels. The interplay of VCAN with its EGF-like domain, p53 and p21 was shown to be dependent on oncogenic mutations in EGFR [234, 235]. Where EGFR is mutated, the ligand EGF leads to an unexpected upregulation of originally tumour suppressor p21, enabling further proliferation and tumour progression [234, 235]. This is confirmed particularly in lung cancer patients, where high levels of p21 but wildtype EGFR status show better survival, whereas the p21 expression in patients with oncogenic EGFR mutations correlate with a poor outcome [15]. In the case of p53 null mutation, p21 activity does not lead to senescence but further promotes cancerous behaviour [236, 237]. In our case, A549 cells carry both EGFR and p53 wildtype, in which p21 can act in its function as cyclin-dependent kinase inhibitor, and the siVCAN-dependent upregulation of p21 might explain the observed reduction of proliferation and migration. In human breast tumours, VCAN was enriched in proliferating tumour areas, particularly in HA-rich portions [238]. When the HA-

binding affinity of VCAN was impaired, p21 expression was upregulated, eventually resulting in cellular senescence [163]. IRF9 was not reported to influence the cell cycle progression in cancer cells, but it had a link with p21. In AML, where IRF9 acts as tumour suppressor, the overexpression of IRF9 did not only increase p53 activity but also the expression of p21 [149]. The influence of IRF9 on cell cycle regulation in the context of p21 and p53 should be studied. Additionally, the role of IRF9 in a VCAN-dependent manner in cell lines with mutated p53 or EGFR status would be of further interest.

Another interesting aspect is a potential feedback loop of IRF9 and VCAN, which was observed in naïve A549 after siVCAN transfection by a mild upregulation of *IRF9*. In already transduced A549, this feedback mechanism could not be confirmed, and regardless of the cell set, the mRNA levels of *IRF9* did not increase after the knockdown of VCAN.

Our work is the first that both described ISRE and proved the direct binding of IRF9 in the promoter of *VCAN*. Chang et al. described that stimulation of BMDM with type I IFN, but not with type II IFN, clearly increased mRNA expression of VCAN in a concentration-dependent manner by activating the respective receptor IFNAR1 [160]. The authors suggested that upon infection, LPS could induce expression and secretion of type I IFN, which stimulates VCAN to further enable immune cell invasion and host defence [160]. Although the authors were not investigating the underlying mechanism, our results suggest the involvement of IRF9. Interestingly, type I IFN stimulation in A549 did not increase VCAN expression, which suggests that the differences in signalling transduction are dependent on the cell-specific presence of other factors. However, the regulation could be more complex since polarisation of BMDM led to the upregulation of VCAN, unimpressed by *Irf9*-deletion. We presume that LPS is involved in VCAN upregulation as well. Purposive experiments with different cell types (e.g. A549, human and murine macrophages) and stimulation with type I IFN, type II IFN and LPS could clarify the regulation, and TLR involvement should be considered.

In silico promoter analysis of VCAN calculated three ISRE in the area of -1000 bp to +100 upstream of *VCAN*, of which two were overlapping. It is to mention that the extracted binding motif of IRF9 was based mostly on classical ISGF3 signalling with IRF9 as DNA-binding factor. Cheon et al. demonstrated that the ISRE consensus sequences of ISGF3 and U-ISGF3 mostly concurred but that the up- and down-stream sequences of the established consensus sequence differed [85]. Indeed, the sequence of VCAN promoter from -598 to -572 bp had more additional matches with U-ISGF3 consensus sequence than with ISGF3. According to the aforementioned work, these subtle differences were responsible for differential expression signature and could explain why VCAN was not expressed upon type I IFN stimulation but by sole IRF9 manipulation in the used lung cancer cell lines [85].

When performing promoter analyses, ChIP experiments could detect binding of IRF9 in the proposed region of *VCAN* promoter with those three ISREs. Since we focused mainly on the functional effects of IRF9 and VCAN, it would be of great interest to investigate the regulation in detail. Claiming U-ISGF3 to be responsible for the VCAN regulation together with proven binding

of IRF9 in absence of phosphorylation cannot verify that claim without any doubt. Overall co-immunoprecipitations with IRF9 in cells with manipulated expression could enlighten how IRF9 is recruited in this context, and further ChIP experiments (e.g. against STAT1, STAT2) are necessary to clarify in which complex IRF9 binds to the DNA and whether other factors are responsible for it, as described for p65 [68]. In silico analysis of the promoter of murine *Vcan* and ChIP experiments in murine cells – regardless of insufficient antibodies at present – could clarify the regulation of *Vcan* by *Irf9*.

For luciferase experiments, we cloned an adequate promoter sequence of *VCAN* into the pGL3 basic plasmid. The higher luciferase expression in A549 LV IRF9 was congruent with mRNA and ChIP analysis and confirmed the regulation of *VCAN* by IRF9. However, in A549 shIRF9, no significant differences were detected. Whether this observation might be based on technical circumstances, such as the pGL3 backbone, side effects by transfection agents or the selected sequence of the promoter, further and more intense experiments could improve the significance of *VCAN* regulation in A549 shIRF9. Additional luciferase experiments with the according sequence in CULA shIrf9 could explain whether the absent downregulation of *Vcan* was specific to murine lung cancer cells.

Focusing on IFN-induced regulation of *VCAN* and the role of IRF9, this study contributes to understanding the underlying mechanism. IRF9 changes oncogenic phenotype by regulating *VCAN* expression in human lung cancer.

## 5.2. Relevance of IRF9 in TME

### 5.2.1. Effects of IRF9 in stromal cells

As previously mentioned, this study focused mainly on the role of IRF9 in human lung adenocarcinoma. The in vitro results were confirmed when IRF9-transduced A549 were injected subcutaneously into BALB/c mice. This xenograft model is well established to study tumour development of primary tumours but misses out on the metastatic potential of A549 [239]. To study and confirm the metastatic potential of human cells, other models that form less dense tumours and allow metastasis studies, such as the use of NSG (NOD scid gamma) mice, are recommended [239]. Another disadvantage of xenograft models (including BALB/c) is immunodeficiency. Even though it is necessary to tolerate applications of human cells, the interaction between tumour and stromal cells and their secreted proteins is limited. Hence, we could not identify differences in the recruitment of immune cells in subcutaneous tumours or differences in the expression of murine *Irf9*, Stat1 or Stat2. For intense studies on TME, it is almost indispensable to use syngeneic tumour models. However, the results from subcutaneous CULA tumours in wildtype mice were limited and confirmed the cancer phenotype of CULA LV *Irf9*. This experiment should be continued if *Irf9* silencing could be gained more efficiently with in vitro effects as it would analyse how *Irf9* influences cancer cells recruit or activate the TME. The influence of tumoural *Irf9* on the production and secretion of cytokines would be of particular interest.

Since IRF9 takes a vital role in the immune system, it is of great importance to study its influence on TME. In infectious diseases, it is essential for viral clearance mainly via T cell activation and enables the effects of pro-inflammatory IFN [99, 142, 148]; further, a loss of IRF9 leads to protection from inflammation in mice together with the downregulation or impaired activation of the cytokines CXCL9 and CXCL10 [240]. Additionally, reduced levels of CXCR3 – the receptor for both cytokines – might reduce the chemotaxis of immune cells and the overall immune response [240-242]. Indeed, we could detect that the depletion of *Irf9* led to a reduction of the lymphocyte proportion in subcutaneous tumours, particularly monocytes and macrophages. Together with DCs, macrophages are important for antigen procession and presentation [243]. As previously described, tumour-infiltrating DCs and macrophages were associated with poor outcome, but we were not able to conclude whether the reduction in these cell types supports or suppresses tumour growth [51, 52, 115]. In studies on the brains of *Irf9*<sup>-/-</sup> mice, Il18 was downregulated, affecting the activation of NK cells [244]. We were indeed able to observe a reduction of NK cells in subcutaneous tumours *Irf9*<sup>-/-</sup> mice. Further, it would be interesting to know whether Il18 is also affected in our *Irf9*<sup>-/-</sup> model and how it could influence lymphocyte attraction.

However, we were not able to show differences in tumour development or growth in the subcutaneous or intravenous models. Considering the relevance of *Irf9* in infection models, where the loss of *Irf9* might not be lethally crucial but undoubtedly of great importance in host defence, immunosurveillance and eventually viral clearance, we presume that increasing the time between tumour implantation and endpoint could be effective to demonstrate the effects of *Irf9*. A tumour relapse model, where the initial subcutaneous tumour is removed and the metastasis formation in the lung can be evaluated, would be suitable [185].

The role of IRF9 in the TME seems complex. Based on our results, it does not influence the development and progression, even though changes in immune cell infiltration could be observed. Since the loss of IRF9 did not result in a clear phenotype, we suggest working with cell-specific transgenic models to reveal the role of IRF9, particularly in the TME. In the absence of conditional knockout animals, we analysed the regulation of macrophages in subcutaneous tumours and ex vivo but could not detect differences in the expression of M1 or M2 markers. Additionally, the conditioned medium of *Irf9*<sup>-/-</sup> macrophages had similar effects on tumour cell proliferation as a wildtype conditioned medium. The activity and polarisation might not be affected by *Irf9* depletion, but the downregulation of Pd-11 (*Cd274*) suggests that the function of macrophages as antigen-presenting cells might be affected. It was reported that IRF9 is involved in the type I IFN-mediated upregulation of PD-L1 and that macrophages can induce PD-L1 expression [35, 243]. Based upon the reduced *Cd274* expression in *Irf9*<sup>-/-</sup> tumours, the involvement and relevance of IRF9 in immune checkpoints as well as the distribution and expression of PD-1 and PD-L1 via flow cytometry should be investigated.

### 5.2.2. Effects of VCAN in stromal cells

In this study, we showed the regulation of VCAN by IRF9 in tumour cells and the influence on tumour progression. The role of VCAN in the TME can act in two ways: (i) IRF9-mediated production and secretion to the ECM; (ii) IRF9-mediated activity of VCAN in stromal cells. By interacting with other components of the ECM, such as HA or fibronectin, VCAN can modify the ECM to enhance leukocyte attraction and adhesion [245, 246]. It was reported that VCAN and HA were activated and enriched upon viral nucleic acids, which increased the adhesion of monocytes in the ECM. VCAN further stimulated macrophages towards M1 polarisation to produce pro-inflammatory cytokines IL6 and TNF $\alpha$  [164]. Nevertheless, crosstalk between macrophages and ovarian cancer cells revealed that tumoural VCAN suppressed anti-tumour macrophages and promoted tumour cell proliferation and angiogenesis [164, 233]. It is rather unlikely that human VCAN from A549 influences the ECM in a xenograft to modify immune response of murine host defence. Therefore, the syngeneic tumour model, with CULA LV *Irf9* overexpressing *Vcan*, is suitable to study the effects of tumoural *Vcan* on tumour stroma.

We focused on in vivo effects in *Irf9*-deficient mice but less on how *Vcan* is regulated in these. It can be assumed that the mechanism of how IRF9 activates VCAN expression is highly dependent on the organism or cell type. Since we have proven the activation of VCAN in cancer cells but not in leukocytes, we are unable to answer this question with certainty, even though other

studies suggested so [160]. In *Irf9*-deficient macrophages, whether naïve or polarised, we were not able to observe differences in the expression of *Vcan* indicating an *Irf9*-independent regulation in macrophages. However, VCAN expression increased after M1 polarisation, and the M1 conditioned medium efficiently reduced tumour cell proliferation. Since stromal VCAN can induce neoangiogenesis and metastasis, we suggest purposive experiments with conditional knockout animals to study stromal VCAN.

### 5.3. Conclusion

High expression of IRF9 was identified and associated with lower survival in lung adenocarcinoma patients. Canonically, IRF9 is upregulated upon type I IFN stimulation, where it elicits the antiproliferative properties of IFN. We could demonstrate that an IFN-independent overexpression of IRF9 increased tumour cell proliferation and migration. In a non-canonical U-ISGF3 manner, IRF9 directly bound at ISRE in the promoter of the proteoglycan VCAN and increased its expression. The expression of IRF9 and VCAN correlated positively and the oncogenic phenotype of IRF9 was confirmed in a xenograft tumour model. The interference of VCAN expression diminished the IRF9-mediated oncogenic effects via cell cycle inhibitor p21.

Nevertheless, the role of IRF9 in the tumour microenvironment is intriguing. Several tumour models indicated that effects of IRF9 do not reflect in an immediate response but rather come into effect with tumour progression. Immune cells and host defence might forfeit partial efficiency in absence of IRF9 – presumably the adaptive immune defence – but are still capable of an adequate response through the innate immune system. Macrophages are a highly important cell type within the tumour microenvironment and are mostly associated with poor survival. IRF9 is associated with the number of TAMs and NK cells. However, whether the function of these cell types is affected and thereby influences tumour development remains elusive.

Tumour cell-specific inhibition of IRF9 is suggested as a novel treatment strategy in lung cancer to enable higher specificity over a global inhibition of JAK-STAT pathway by bypassing collateral harm to beneficial environmental IFN. Stromal IRF9 would not be affected, and the suppression of the host defence would be avoided.

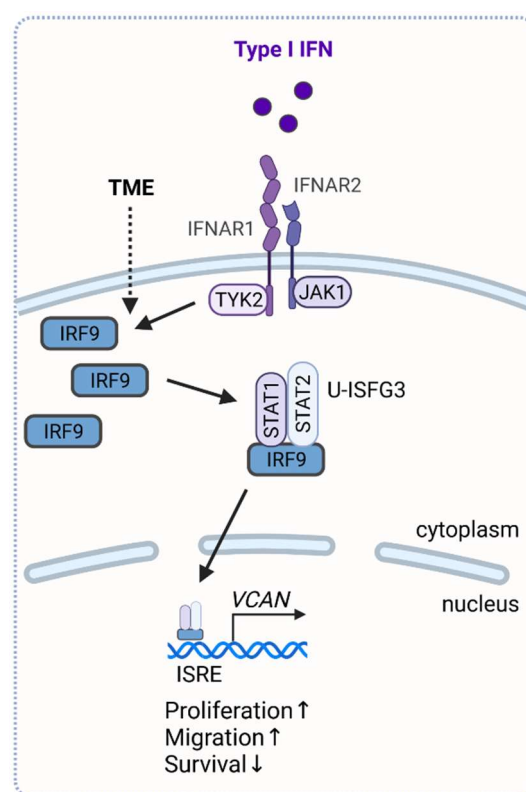


**Figure 39. Conclusion figure.** The TME provides high levels of IFN, eventually leading to increased IRF9 levels in tumour cells. IRF9 recruits transcriptional complexes (such as U-ISGF3) binding at ISRE in the promoter of VCAN to activate the expression. VCAN upregulation results in an oncogenic phenotype.

#### 5.4. Future Perspectives / Outlook

Further investigations should focus on the phenotype characterisation of IRF9 in cancer cells. In addition to the used cell lines, particularly lung cancer cell lines with already high (e.g. H1650, H226) or low IRF9 expression (e.g. H460, H82) should be considered for further IRF9 transduction experiments. The characterisation could confirm its influence on cancer cell proliferation and migration. Since high expression levels of IRF9 were not associated with poor prognosis in LUSC patients, LUSC cell lines should be included to determine whether this effect varies depending on the cancer class. Additionally, future studies should analyse the expression of IRF9 in LUSC patients, and in case of similar expression, whether overexpression could still influence the oncogenic phenotype; however, if IRF9 levels were elevated, the relevance of IRF9 for tumour progression in LUSC would be unlikely and highly dependent on the cancer class. Furthermore, cytostatic drugs Paclitaxel and Doxorubicin should be administered to transduced cells, and response or resistance as a function of IRF9 expression should be investigated.

By investigating the secretome of IRF9-overexpressing and IRF9-silencing cells, it would be possible to identify other factors that enhance tumour progression in a paracrine way or factors that can modulate immune response. These factors could serve as druggable targets in patients and an alternative to laborious tumour-specific inhibition of IRF9. It would be of further interest, to study the secretome of both tumour cells as well as leukocytes, namely macrophages, natural killer cells and dendritic cells.

Another aspect is the transcriptional mechanism of IRF9. Co-immunoprecipitations would enlighten the interaction partners of IRF9. Further, it is suggested to conduct combined experiments with IRF9 overexpression and silencing of STAT1 or STAT2, allowing to identify both how IRF9 activates transcription and a binding partner specific gene signature. Along the same line are experiments based on the available RNA-seq results which study why regulated genes after IRF9 overexpression and silencing differ by number and genes, why the number of matching genes is relatively low and why distinct genes are regulated in the same way, even though IRF9 is expressed in opposition. Furthermore, RNA-seq revealed several potential target genes that could elicit the oncogenic phenotype of IRF9 as well, such as IGFBP5, potentially proving that IRF9 could suppress transcription of a tumour suppressor.

Additional studies should be performed to validate the IRF9-dependent regulation of VCAN, such as CHIP analyses with STATs, to understand which molecules are recruited by IRF9; promote the study of Vcan in mouse since *Irf9*-silencing did not affect Vcan expression and tumour phenotype; investigate the correlation of VCAN and IRF9 in other malignancies where IRF9 is associated with better outcome (e.g. leukaemia); and evaluate luciferase assay of VCAN after mutations in ISRE. Furthermore, the secretion of VCAN (e.g. via ELISA) of IRF9-manipulated cells or of isolated cells from *Irf9*<sup>-/-</sup> mice should be analysed.

*Irf9*<sup>-/-</sup> mice represent a powerful model to investigate the effects of IRF9 in the TME. Tumour relapse models can consider the long-term effects of *Irf9*-deletion, and conditional *Irf9*<sup>-/-</sup> models are a useful approach to study the role of *Irf9* in the immune cell type of interest. Adding other genetic mutations, such as *Tp53* or *Kras* would allow to investigate the role of *Irf9* in the full oncogenic process. Particularly in lung cancer, the *Kras*-driven tumour model should be observed for a defined time and the number and area of lung tumour nodules should be evaluated. Further, a survival study should be considered to discover the influence of *Irf9* on the overall survival.

## 6. List of Abbreviations

-/-	Knockout of indicated gene
$\alpha$	alpha
A	Adenin
a.a.	Amino acid
ABC	ATP-binding cassette
ADAMTS	A disintegrin and metalloproteinase with thrombospondin motif
ADGRL3	Adhesion G protein-coupled receptor L3
AJCC	American Joint Committee on Cancer
ALK	ALK receptor tyrosine kinase
ARG1	Arginase 1
$\beta$	beta
BAP1	Suppressor and deubiquitinating enzyme
BCL2	BCL2 apoptosis regulator
BRAF	B-Raf proto-oncogene, serine/threonine kinase
BSA	Bovine Serum Albumin
$\gamma$	gamma
C	Cytosine
CAF	Cancer-associated fibroblasts
CASP	Caspase
CASTOR1	Cytosolic Arginine Sensor For mTORC1 Subunit 1
CCL	C-C motif chemokine ligand
CD	Cluster of differentiation
CDCP1	CUB domain containing protein 1
CDKN1A	Cyclin dependent kinase inhibitor 1A (p21)
CDKN1B	Cyclin dependent kinase inhibitor 1B
ChIP	Chromatin Immunoprecipitation
CHIT1	Chitinase 1
CLDN1	Claudin 1
CNTN1	Contactin 1
CSF1	Cytokine colony stimulating factor 1
Ct	Cycle Threshold
CTSB/L	Cathepsin B/L
CXCL	C-X-C motif chemokine ligand
Cyk	Cytokeratin
DAPI	4',6-Diamidino-2-phenylindol
DBD	DNA-binding domain
DC	Dendritic cells
DEPC	Diethyl-pyrocabonate
DMEM	Dulbecco's Modified Eagle Medium
DNA	Deoxyribonucleic acid
DUSP	Dual-specificity phosphatase
e.g.	for example (exempli gratia)
ECM	Extracellular matrix

EDTA	Ethylenediaminetetraacetic acid
EFEMP1	EGF-containing fibulin-like extracellular matrix protein 1
EGFR	Epidermal growth factor receptor
ELISA	Enzyme-linked immunosorbent assay
EMP1	Epithelial membrane protein 1
ERBB3	Receptor tyrosine-protein kinase erbB-3
FAK	Protein tyrosine kinase 2
FAS	Fas cell surface death receptor
FFPE	Formalin-Fixed Paraffin-Embedded
FGF	Fibroblast growth factors
FGFR1	Fibroblast growth factor receptor 1
FOXP3	Forkhead box P3
FSCN1	Fascin actin-binding protein 1
G	Guanin
GAF	IFN $\gamma$ -activated factor
GAG	G2 domain with glycosaminoglycan binding regions
GAS	IFN $\gamma$ -activation sites
GDP	Guanosine diphosphate
GRHL3	Grainyhead like transcription factor 3
GTP	Guanosine triphosphate
H&E	Haematoxylin & Eosin
HA	Hyaluronan
HABR	Hyaluronan binding region
HER2	Erb-b2 receptor tyrosine kinase 2 (ERBB2)
HEXIM1	Hexamethylene-bis-acetamide-inducible protein 1
HIF	Hypoxia-inducible factor
HPD	4-hydroxyphenylpyruvate dioxygenase
HPRT	Hypoxanthine guanine phosphoribosyl transferase
IAD	IRF-associated domain
IBA1	Induction of brown adipocytes 1
ICC	Immunocytochemistry
IFN	Interferon
IFNAR	IFN $\alpha/\beta$ receptor complex
IFNGR	Interferon gamma receptor
IFNLR1	Interferon lambda receptor 1
IGFBP	Insulin like growth factor binding protein
IgG	Immunoglobulin G
IHC	Immunohistochemistry
IL	Interleukin
IL10R $\beta$	Interleukin 10 receptor subunit beta
IMRT	Intensity-modulated radiotherapy
IRDS	IFN-related DNA damage resistance
IRF	Interferon regulatory factor
ISFG3	Interferon-stimulated gene factor 3

ISG	Interferon-stimulated genes
ISRE	Interferon-stimulated response elements
IVC	Individual ventilated cages
JAK	Janus kinase
KDM5C	Lysine demethylase 5C
Kras	Kirsten rat sarcoma
KRT	Keratin 18
λ	lambda
LAR II	Luciferase Assay Reagent II
LCC	Large cell carcinoma
LCMV	Lymphotic choriomeningitis virus
LPS	Lipopolysaccharides
LUAD	Lung adenocarcinoma
LUSC	Lung squamous carcinoma
LV EV	Empty vector
LV IRF9	IRF9-overexpressing vector
MDA5	melanoma differentiation-associated protein 5
MMP	metalloprotease
MYC	MYC proto-oncogene
N	IUPAC symbol for any nucleotide: G,A,C oder T
NF1	Neurofibromin 1
NK cells	Natural killer cells
NO	Nitric oxide
NOS2	Nitric oxide synthase 2
NSCLC	Non-small-cell lung carcinoma
NSG	NOD scid gamma
NTC	Non-template control
NTS	Neurotensin
OAS1	Oligoadenylate synthases
PADI2	Peptidyl arginine deiminase 2
PCNA	Proliferating cell nuclear antigen
PCR	Polymerase chain reaction
PDCD1	Programmed cell death 1 (PD-1)
PDE3A	Phosphodiesterase 3A
PDGF	Platelet-derived growth factor
PDGFRA	Platelet derived growth factor receptor alpha
PD-L1	Programmed death-ligand 1 (CD274)
PER2	Period circadian regulator 2
PFA	Paraformaldehyde
PIAS	Protein inhibitors of activated STATs
PIK3CA	Phosphatidylinositol-4,5-bisphosphate 3-kinase catalytic subunit alpha
PKR	Protein kinase RNA-activated
PRODH2	Proline dehydrogenase
PTEN	Phosphatase and tensin homolog

PVDF	Polyvinylidene difluoride
RIG-I	Retinoic acid-inducible gene I
RL	Renilla luciferase
RLU	Relative light units
RMP1	Roswell Park Memorial Institute (Medium)
RNA	Ribonucleic acid
RNase L	Ribonuclease L
RNA-seq	RNA-Sequencing
ROS	Reactive oxygen species
RTK	Receptor tyrosine kinase
RT-qPCR	Realtime quantitative PCR
SABR	Stereotactic ablative body radiotherapy
SCLC	Small cell lung carcinoma
SDS	Sodium dodecyl sulphate
SEM	Standard error of the mean
SERPINI1	Serpin family I member 1
sh scr	Scrambled shRNA vector
SH3TC2	SH3 domain and tetratricopeptide repeats 2
shIRF9	ShRNA vector against IRF9
siRNA	Small interfering RNA
SIRT1	Sirtuin
SOCS	Suppressor of cytokine signalling
STAT	Signal transducer and activator of transcription
T	Thymin
TAMs	Tumour-associated macrophages
TBST	Tris-buffered saline (TBS) and Polysorbate 20
TGFA	Transforming growth factor alpha
TGFβ	Transforming growth factor β
T <sub>H</sub> 1/2/9/17	T helper 1/2/9/17 cell
TierSchG	Tierschutzgesetz
TKI	Tyrosine kinase inhibitor
TLE3	Transducin-like enhancer of Split3
TLR	Toll-like receptors
TMA	Tissue microarray
TME	Tumour microenvironment
TNBC	Triple-negative breast cancer
TNF	Tumor necrosis factor
TP53	Tumor protein p53
TP63	Tumour protein 63
T <sub>REG</sub>	Regulatory T cell
TRIM29	Tripartite motif-containing 29
Tris	Tris(hydroxymethyl)aminomethane
TYK2	Tyrosine kinase 2
UICC	Union Internationale Contre le Cancer

U-ISFG3	Unphosphorylated interferon-stimulated gene factor 3
VCAN	Versican
VEGFR	Vascular endothelial growth factor receptor
VSMC	Vascular smooth muscle cells
Wt	Wildtype

## 7. List of Figures and Tables

### 7.1. List of Figures

Figure 1. Distribution of worldwide cancer incidence in 2020. ....	8
Figure 2. Distribution of worldwide cancer mortality in 2020. ....	9
Figure 3. Impact of microenvironmental cells on tumour development. ....	15
Figure 4. Canonical signalling of interferon types I, II and III. ....	20
Figure 5. Non-canonical signalling of type I and type II interferons. ....	22
Figure 6. Structure of IRF family members IRF1-9. ....	25
Figure 7. Structure of Versican splicing variants. ....	31
Figure 8. Hypothesis and aim of the study. ....	33
Figure 9. Genotyping of <i>Irf9</i> <sup>-/-</sup> offspring. ....	46
Figure 10. IRF9 expression is associated with a decreased survival in lung cancer patients. ....	49
Figure 11. Expression of U-ISGF3 members is upregulated and correlated in human lung cancer patients. ....	50
Figure 12. IRF9 is expressed in different classes of lung cancer in tumour and stromal cells. ....	51
Figure 13. The expression of ISGF3 members varies in different cancer cell lines. ....	52
Figure 14. IRF9 expression is increased in chemoresistant lung cancer cell lines. ....	53
Figure 15. IFN stimulation increases expression and nuclear translocation of IRF9 in A549. ....	54
Figure 16. Time dependent effects of type I IFN in A549. ....	55
Figure 17. Overexpression of IRF9 promotes oncogenic behaviour in A549. ....	56
Figure 18. Overexpression of IRF9 promotes oncogenic behaviour in A427. ....	57
Figure 19. Knockdown of IRF9 reduces oncogenic features in A549. ....	58
Figure 20. Overexpression of IRF9 enhances IFN effect. ....	58
Figure 21. Knockdown of IRF9 reduces oncogenic features in A427. ....	59
Figure 22. Knockdown of IRF9 delays IFN effect. ....	60
Figure 23. <i>Irf9</i> manipulation partially confirms phenotype in CULA. ....	61
Figure 24. RNA-seq of transduced A549 revealed VCAN as top regulated gene. ....	63
Figure 25. Evaluation of RNA-seq analysis. ....	64
Figure 26. IRF9 and VCAN expression correlate and are associated with reduced survival in human lung cancer patients. ....	65
Figure 27. IRF9 and VCAN expression correlate in transduced A549. ....	66
Figure 28. VCAN expression in transduced A427 and CULA. ....	67
Figure 29. Knockdown of VCAN diminishes oncogenic phenotype of IRF9. ....	68
Figure 30. Knockdown of VCAN inhibits proliferation and migration in A549. ....	69
Figure 31. Knockdown of VCAN increases expression of CDKN1A. ....	69
Figure 32. IRF9 binds to VCAN promoter and regulates its expression. ....	71
Figure 33. IRF9 overexpression increases tumour growth in xenograft model. ....	72
Figure 34. Knockdown of IRF9 reduces tumour growth in xenograft model. ....	73
Figure 35. Overexpression of <i>Irf9</i> in CULA influences tumour growth. ....	74
Figure 36. Loss of <i>Irf9</i> alters cell composition in subcutaneous tumours. ....	75
Figure 37. mRNA expression of subcutaneous LLC1 tumour model. ....	76
Figure 38. Deletion of <i>Irf9</i> in BMDM does not influence gene expression of macrophage marker. ....	77
Figure 39. Conclusion figure. ....	90

## 7.2. List of Tables

Table 1. Lung cancer stage grouping based on TNM classification, 8 <sup>th</sup> Edition. ....	10
Table 2. Frequencies of genetic alterations in lung cancer, divided by classes. ....	11
Table 3. Average 5-year overall survival of lung cancer patients [%] divided by clinical and pathological stage grouping. ....	12
Table 4. List of primers used for RT-qPCR of human mRNA. ....	37
Table 5. List of primers used for RT-qPCR of murine mRNA. ....	38
Table 6. List of primers used for RT-qPCR of human promoter sequences. ....	42
Table 7. List and composition of used buffers for Chromatin Immunoprecipitation. ....	43
Table 8. List of primers used for mouse genotyping. ....	46

## 8. Literature

1. Sung, H., et al., *Global Cancer Statistics 2020: GLOBOCAN Estimates of Incidence and Mortality Worldwide for 36 Cancers in 185 Countries*. CA Cancer J Clin, 2021. **71**(3): p. 209-249.
2. Ferlay, J., et al., *Cancer incidence and mortality patterns in Europe: Estimates for 40 countries and 25 major cancers in 2018*. Eur J Cancer, 2018. **103**: p. 356-387.
3. Eurostat. *Causes and occurrence of deaths in the EU 2016* 16.07.2019; Available from: <https://ec.europa.eu/eurostat/web/products-eurostat-news/-/DDN-20190716-1>.
4. Detterbeck, F.C., et al., *The Eighth Edition Lung Cancer Stage Classification*. CHEST, 2017. **151**(1): p. 193-203.
5. Latimer, K.M. and T.F. Mott, *Lung cancer: diagnosis, treatment principles, and screening*. Am Fam Physician, 2015. **91**(4): p. 250-6.
6. Collins, L.G., et al., *Lung cancer: diagnosis and management*. Am Fam Physician, 2007. **75**(1): p. 56-63.
7. Nasim, F., B.F. Sabath, and G.A. Eapen, *Lung Cancer*. Medical Clinics of North America, 2019. **103**(3): p. 463-473.
8. Malhotra, J., et al., *Risk factors for lung cancer worldwide*. European Respiratory Journal, 2016. **48**(3): p. 889.
9. Hecht, S.S., *Lung carcinogenesis by tobacco smoke*. International journal of cancer, 2012. **131**(12): p. 2724-2732.
10. Kenfield, S.A., et al., *Comparison of aspects of smoking among the four histological types of lung cancer*. Tobacco control, 2008. **17**(3): p. 198-204.
11. O'Callaghan, D.S., et al., *The Role of Inflammation in the Pathogenesis of Non-small Cell Lung Cancer*. Journal of Thoracic Oncology, 2010. **5**(12): p. 2024-2036.
12. Chen, Z., et al., *Non-small-cell lung cancers: a heterogeneous set of diseases*. Nat Rev Cancer, 2014. **14**(8): p. 535-46.
13. Tan, W.L., et al., *Novel therapeutic targets on the horizon for lung cancer*. Lancet Oncol, 2016. **17**(8): p. e347-e362.
14. von Marschall, Z., et al., *Effects of interferon alpha on vascular endothelial growth factor gene transcription and tumor angiogenesis*. J Natl Cancer Inst, 2003. **95**(6): p. 437-48.
15. Na, I., et al., *The survival outcomes of patients with resected non-small cell lung cancer differ according to EGFR mutations and the P21 expression*. Lung Cancer, 2007. **57**(1): p. 96-102.
16. Ferrer, I., et al., *KRAS-Mutant non-small cell lung cancer: From biology to therapy*. Lung Cancer, 2018. **124**: p. 53-64.
17. Liu, P., Y. Wang, and X. Li, *Targeting the untargetable KRAS in cancer therapy*. Acta Pharmaceutica Sinica B, 2019. **9**(5): p. 871-879.
18. Gibbons, D.L., L.A. Byers, and J.M. Kurie, *Smoking, p53 Mutation, and Lung Cancer*. Molecular Cancer Research, 2014. **12**(1): p. 3.
19. Lackey, A. and J.S. Donington, *Surgical management of lung cancer*. Seminars in interventional radiology, 2013. **30**(2): p. 133-140.
20. Vinod, S.K. and E. Hau, *Radiotherapy treatment for lung cancer: Current status and future directions*. Respirology, 2020. **25**(S2): p. 61-71.
21. Rajeswaran, A., et al., *Efficacy and side effects of cisplatin- and carboplatin-based doublet chemotherapeutic regimens versus non-platinum-based doublet chemotherapeutic regimens as first line treatment of metastatic non-small cell lung carcinoma: a systematic review of randomized controlled trials*. Lung Cancer, 2008. **59**(1): p. 1-11.
22. Socinski, M.A., et al., *Weekly nab-paclitaxel in combination with carboplatin versus solvent-based paclitaxel plus carboplatin as first-line therapy in patients with advanced non-small-cell lung cancer: final results of a phase III trial*. J Clin Oncol, 2012. **30**(17): p. 2055-62.

23. Wang, D. and S.J. Lippard, *Cellular processing of platinum anticancer drugs*. Nature Reviews Drug Discovery, 2005. **4**(4): p. 307-320.
24. Lai, G.-M., et al., *Effect of Glutathione on DNA Repair in Cisplatin-Resistant Human Ovarian Cancer Cell Lines*. JNCI: Journal of the National Cancer Institute, 1989. **81**(7): p. 535-539.
25. Zeng-Rong, N., et al., *Elevated DNA Repair Capacity Is Associated with Intrinsic Resistance of Lung Cancer to Chemotherapy*. Cancer Research, 1995. **55**(21): p. 4760.
26. Kasahara, K., et al., *Metallothionein content correlates with the sensitivity of human small cell lung cancer cell lines to cisplatin*. Cancer Res, 1991. **51**(12): p. 3237-42.
27. Blair, H.A. and E.D. Deeks, *Albumin-Bound Paclitaxel: A Review in Non-Small Cell Lung Cancer*. Drugs, 2015. **75**(17): p. 2017-24.
28. Kavallaris, M., *Microtubules and resistance to tubulin-binding agents*. Nat Rev Cancer, 2010. **10**(3): p. 194-204.
29. Tacar, O., P. Sriamornsak, and C.R. Dass, *Doxorubicin: an update on anticancer molecular action, toxicity and novel drug delivery systems*. Journal of Pharmacy and Pharmacology, 2013. **65**(2): p. 157-170.
30. Melguizo, C., et al., *Enhanced antitumoral activity of doxorubicin against lung cancer cells using biodegradable poly(butylcyanoacrylate) nanoparticles*. Drug design, development and therapy, 2015. **9**: p. 6433-6444.
31. Vatsyayan, R., et al., *Role of RLIP76 in doxorubicin resistance in lung cancer*. International journal of oncology, 2009. **34**(6): p. 1505-1511.
32. Mazzarella, L., A. Guida, and G. Curigliano, *Cetuximab for treating non-small cell lung cancer*. Expert Opin Biol Ther, 2018. **18**(4): p. 483-493.
33. Yang, S., Z. Zhang, and Q. Wang, *Emerging therapies for small cell lung cancer*. J Hematol Oncol, 2019. **12**(1): p. 47.
34. Zhou, Z.-J., P. Zhan, and Y. Song, *PD-L1 over-expression and survival in patients with non-small cell lung cancer: a meta-analysis*. Translational Lung Cancer Research; Vol 4, No 2 (April 2015): Translational Lung Cancer Research (Molecular Genetics of Lung Cancer) 1, 2015.
35. Cai, J., et al., *The role of PD-1/PD-L1 axis and macrophage in the progression and treatment of cancer*. Journal of Cancer Research and Clinical Oncology, 2019. **145**(6): p. 1377-1385.
36. Hanahan, D. and R.A. Weinberg, *Hallmarks of cancer: the next generation*. Cell, 2011. **144**(5): p. 646-74.
37. Anderson, N.M. and M.C. Simon, *The tumor microenvironment*. Current Biology, 2020. **30**(16): p. R921-R925.
38. Pullamsetti, S.S., et al., *Phosphodiesterase-4 promotes proliferation and angiogenesis of lung cancer by crosstalk with HIF*. Oncogene, 2013. **32**(9): p. 1121-1134.
39. Carmeliet, P., *VEGF as a key mediator of angiogenesis in cancer*. Oncology, 2005. **69** Suppl 3: p. 4-10.
40. Ferrara, N., *Pathways mediating VEGF-independent tumor angiogenesis*. Cytokine Growth Factor Rev, 2010. **21**(1): p. 21-6.
41. Anderberg, C. and K. Pietras, *On the origin of cancer-associated fibroblasts*. Cell Cycle, 2009. **8**(10): p. 1461-2.
42. Bremnes, R.M., et al., *The Role of Tumor Stroma in Cancer Progression and Prognosis: Emphasis on Carcinoma-Associated Fibroblasts and Non-small Cell Lung Cancer*. Journal of Thoracic Oncology, 2011. **6**(1): p. 209-217.
43. Umansky, V. and A. Sevko, *Tumor microenvironment and myeloid-derived suppressor cells*. Cancer Microenviron, 2013. **6**(2): p. 169-77.
44. Banat, G.A., et al., *Immune and Inflammatory Cell Composition of Human Lung Cancer Stroma*. PLoS One, 2015. **10**(9): p. e0139073.
45. Liu, J., et al., *Mast cell: insight into remodeling a tumor microenvironment*. Cancer Metastasis Rev, 2011. **30**(2): p. 177-84.
46. Carlini, M.J., et al., *Mast cell phenotypes and microvessels in non-small cell lung cancer and its prognostic significance*. Hum Pathol, 2010. **41**(5): p. 697-705.

47. Tran Janco, J.M., et al., *Tumor-infiltrating dendritic cells in cancer pathogenesis*. J Immunol, 2015. **194**(7): p. 2985-91.
48. Cortez-Retamozo, V., et al., *Origins of tumor-associated macrophages and neutrophils*. Proc Natl Acad Sci U S A, 2012. **109**(7): p. 2491-6.
49. Noy, R. and Jeffrey W. Pollard, *Tumor-Associated Macrophages: From Mechanisms to Therapy*. Immunity, 2014. **41**(1): p. 49-61.
50. Rhee, I., *Diverse macrophages polarization in tumor microenvironment*. Arch Pharm Res, 2016. **39**(11): p. 1588-1596.
51. Zheng, X., et al., *Redirecting tumor-associated macrophages to become tumoricidal effectors as a novel strategy for cancer therapy*. Oncotarget; Vol 8, No 29, 2017.
52. Ma, J., et al., *The M1 form of tumor-associated macrophages in non-small cell lung cancer is positively associated with survival time*. BMC Cancer, 2010. **10**: p. 112.
53. Savai, R., et al., *Evaluation of angiogenesis using micro-computed tomography in a xenograft mouse model of lung cancer*. Neoplasia (New York, N.Y.), 2009. **11**(1): p. 48-56.
54. Guillerey, C., N.D. Huntington, and M.J. Smyth, *Targeting natural killer cells in cancer immunotherapy*. Nat Immunol, 2016. **17**(9): p. 1025-36.
55. Besse, B., et al., *Dendritic cell-derived exosomes as maintenance immunotherapy after first line chemotherapy in NSCLC*. Oncoimmunology, 2015. **5**(4): p. e1071008-e1071008.
56. Kiraz, Y., Y. Baran, and A. Nalbant, *T cells in tumor microenvironment*. Tumour Biol, 2016. **37**(1): p. 39-45.
57. Chin, Y., et al., *Phenotypic analysis of tumor-infiltrating lymphocytes from human breast cancer*. Anticancer Res, 1992. **12**(5): p. 1463-6.
58. Salazar, Y., et al., *Microenvironmental Th9 and Th17 lymphocytes induce metastatic spreading in lung cancer*. The Journal of Clinical Investigation, 2020. **130**(7): p. 3560-3575.
59. Petersen, R.P., et al., *Tumor infiltrating Foxp3+ regulatory T-cells are associated with recurrence in pathologic stage I NSCLC patients*. Cancer, 2006. **107**(12): p. 2866-72.
60. Raskov, H., et al., *Cytotoxic CD8+ T cells in cancer and cancer immunotherapy*. British Journal of Cancer, 2020.
61. Henke, E., R. Nandigama, and S. Ergün, *Extracellular Matrix in the Tumor Microenvironment and Its Impact on Cancer Therapy*. Frontiers in Molecular Biosciences, 2020. **6**: p. 160.
62. Noël, A., *New and Paradoxical Roles of Matrix Metalloproteinases in the Tumor Microenvironment*. Frontiers in Pharmacology, 2012. **3**: p. 140.
63. Brisse, M. and H. Ly, *Comparative Structure and Function Analysis of the RIG-I-Like Receptors: RIG-I and MDA5*. Frontiers in immunology, 2019. **10**: p. 1586-1586.
64. Isaacs, A. and J. Lindenmann, *Virus interference. I. The interferon*. Proc R Soc Lond B Biol Sci, 1957. **147**(927): p. 258-67.
65. Lee, A.J. and A.A. Ashkar, *The Dual Nature of Type I and Type II Interferons*. Frontiers in Immunology, 2018. **9**: p. 2061.
66. Lazear, H.M., J.W. Schoggins, and M.S. Diamond, *Shared and Distinct Functions of Type I and Type III Interferons*. Immunity, 2019. **50**(4): p. 907-923.
67. Aaronson, D.S. and C.M. Horvath, *A road map for those who don't know JAK-STAT*. Science, 2002. **296**(5573): p. 1653-5.
68. Nan, J., et al., *IRF9 and unphosphorylated STAT2 cooperate with NF-kappaB to drive IL6 expression*. Proc Natl Acad Sci U S A, 2018. **115**(15): p. 3906-3911.
69. Shuai, K., *Modulation of STAT signaling by STAT-interacting proteins*. Oncogene, 2000. **19**(21): p. 2638-44.
70. Krebs, D.L. and D.J. Hilton, *SOCS proteins: negative regulators of cytokine signaling*. Stem Cells, 2001. **19**(5): p. 378-87.
71. McNab, F., et al., *Type I interferons in infectious disease*. Nature Reviews Immunology, 2015. **15**(2): p. 87-103.
72. Majoros, A., et al., *Canonical and Non-Canonical Aspects of JAK-STAT Signaling: Lessons from Interferons for Cytokine Responses*. Frontiers in immunology, 2017. **8**: p. 29-29.

73. Hemann, E.A., M. Gale, and R. Savan, *Interferon Lambda Genetics and Biology in Regulation of Viral Control*. *Frontiers in Immunology*, 2017. **8**: p. 1707.
74. Zhou, Z., et al., *Type III interferon (IFN) induces a type I IFN-like response in a restricted subset of cells through signaling pathways involving both the Jak-STAT pathway and the mitogen-activated protein kinases*. *Journal of virology*, 2007. **81**(14): p. 7749-7758.
75. Lasfar, A., et al., *IFN- $\lambda$  cancer immunotherapy: new kid on the block*. *Immunotherapy*, 2016. **8**(8): p. 877-888.
76. Yan, Y., et al., *Inhibition of lung adenocarcinoma transfected with interleukin 28A recombinant adenovirus (Ad-mIFN- $\lambda$ 2) in vivo*. *Cancer Biother Radiopharm*, 2013. **28**(2): p. 124-30.
77. Cheon, H., E.C. Borden, and G.R. Stark, *Interferons and Their Stimulated Genes in the Tumor Microenvironment*. *Seminars in Oncology*, 2014. **41**(2): p. 156-173.
78. Parkin, J. and B. Cohen, *An overview of the immune system*. *The Lancet*, 2001. **357**(9270): p. 1777-1789.
79. Yang, X., et al., *Targeting the Tumor Microenvironment with Interferon- $\beta$  Bridges Innate and Adaptive Immune Responses*. *Cancer Cell*, 2014. **25**(1): p. 37-48.
80. Borden, E.C., *Interferons  $\alpha$  and  $\beta$  in cancer: therapeutic opportunities from new insights*. *Nat Rev Drug Discov*, 2019. **18**(3): p. 219-234.
81. Conlon, K.C., M.D. Miljkovic, and T.A. Waldmann, *Cytokines in the Treatment of Cancer*. *Journal of Interferon & Cytokine Research*, 2018. **39**(1): p. 6-21.
82. Cheon, H. and G.R. Stark, *Unphosphorylated STAT1 prolongs the expression of interferon-induced immune regulatory genes*. *Proc Natl Acad Sci U S A*, 2009. **106**(23): p. 9373-8.
83. Lou, Y.-J., et al., *IRF-9/STAT2 Functional Interaction Drives Retinoic Acid-Induced Gene G Expression Independently of STAT1*. *Cancer Research*, 2009. **69**(8): p. 3673.
84. Bluysen, H.A. and D.E. Levy, *Stat2 is a transcriptional activator that requires sequence-specific contacts provided by stat1 and p48 for stable interaction with DNA*. *J Biol Chem*, 1997. **272**(7): p. 4600-5.
85. Cheon, H., et al., *IFN $\beta$ -dependent increases in STAT1, STAT2, and IRF9 mediate resistance to viruses and DNA damage*. *EMBO J*, 2013. **32**(20): p. 2751-63.
86. Testoni, B., et al., *Chromatin dynamics of gene activation and repression in response to interferon alpha (IFN( $\alpha$ )) reveal new roles for phosphorylated and unphosphorylated forms of the transcription factor STAT2*. *J Biol Chem*, 2011. **286**(23): p. 20217-27.
87. Fink, K., et al., *IFN $\beta$ /TNF $\alpha$  synergism induces a non-canonical STAT2/IRF9-dependent pathway triggering a novel DUOX2 NADPH oxidase-mediated airway antiviral response*. *Cell Res*, 2013. **23**(5): p. 673-90.
88. Brierley, M.M., et al., *Identification of GAS-dependent interferon-sensitive target genes whose transcription is STAT2-dependent but ISGF3-independent*. *Febs j*, 2006. **273**(7): p. 1569-81.
89. Ghislain, J.J., et al., *The interferon-inducible Stat2:Stat1 heterodimer preferentially binds in vitro to a consensus element found in the promoters of a subset of interferon-stimulated genes*. *J Interferon Cytokine Res*, 2001. **21**(6): p. 379-88.
90. Luker, K.E., et al., *Overexpression of IRF9 confers resistance to antimicrotubule agents in breast cancer cells*. *Cancer Res*, 2001. **61**(17): p. 6540-7.
91. Begitt, A., et al., *STAT1-cooperative DNA binding distinguishes type 1 from type 2 interferon signaling*. *Nat Immunol*, 2014. **15**(2): p. 168-76.
92. Stetson, D.B. and R. Medzhitov, *Type I interferons in host defense*. *Immunity*, 2006. **25**(3): p. 373-81.
93. Beutler, B.A., *TLRs and innate immunity*. *Blood*, 2009. **113**(7): p. 1399-1407.
94. Luthra, P., et al., *Activation of IFN- $\gamma$ ; expression by a viral mRNA through RNase L and MDA5*. *Proceedings of the National Academy of Sciences of the United States of America*, 2011. **108**(5): p. 2118-2123.

95. Harding, H.P., et al., *Transcriptional and translational control in the Mammalian unfolded protein response*. *Annu Rev Cell Dev Biol*, 2002. **18**: p. 575-99.
96. Zhu, Z., et al., *Type I interferon-mediated immune response against influenza A virus is attenuated in the absence of p53*. *Biochem Biophys Res Commun*, 2014. **454**(1): p. 189-95.
97. Zhang, X., et al., *Potent and selective stimulation of memory-phenotype CD8+ T cells in vivo by IL-15*. *Immunity*, 1998. **8**(5): p. 591-9.
98. Nguyen, K.B., et al., *Coordinated and distinct roles for IFN-alpha beta, IL-12, and IL-15 regulation of NK cell responses to viral infection*. *J Immunol*, 2002. **169**(8): p. 4279-87.
99. Hofer, M.J., et al., *Mice deficient in STAT1 but not STAT2 or IRF9 develop a lethal CD4+ T-cell-mediated disease following infection with lymphocytic choriomeningitis virus*. *J Virol*, 2012. **86**(12): p. 6932-46.
100. Cho, H.Y., et al., *Interferon-sensitive response element (ISRE) is mainly responsible for IFN-alpha-induced upregulation of programmed death-1 (PD-1) in macrophages*. *Biochim Biophys Acta*, 2008. **1779**(12): p. 811-9.
101. Sandler, N.G., et al., *Type I interferon responses in rhesus macaques prevent SIV infection and slow disease progression*. *Nature*, 2014. **511**(7511): p. 601-5.
102. Paolicelli, D., V. Drenzo, and M. Trojano, *Review of interferon beta-1b in the treatment of early and relapsing multiple sclerosis*. *Biologics : targets & therapy*, 2009. **3**: p. 369-376.
103. Parker, B.S., J. Rautela, and P.J. Hertzog, *Antitumour actions of interferons: implications for cancer therapy*. *Nature Reviews Cancer*, 2016. **16**(3): p. 131-144.
104. Hobeika, A.C., P.S. Subramaniam, and H.M. Johnson, *IFNalpha induces the expression of the cyclin-dependent kinase inhibitor p21 in human prostate cancer cells*. *Oncogene*, 1997. **14**(10): p. 1165-70.
105. Doherty, M.R., et al., *Interferon-beta represses cancer stem cell properties in triple-negative breast cancer*. *Proceedings of the National Academy of Sciences*, 2017. **114**(52): p. 13792.
106. Takaoka, A., et al., *Integration of interferon-alpha/beta signalling to p53 responses in tumour suppression and antiviral defence*. *Nature*, 2003. **424**(6948): p. 516-23.
107. Raig, E.T., et al., *VEGF secretion is inhibited by interferon-alpha in several melanoma cell lines*. *J Interferon Cytokine Res*, 2008. **28**(9): p. 553-61.
108. Spaapen, R.M., et al., *Therapeutic activity of high-dose intratumoral IFN-beta requires direct effect on the tumor vasculature*. *J Immunol*, 2014. **193**(8): p. 4254-60.
109. Oh, S.S., et al., *Adenovirally delivered IFN-beta exerts antitumor effects through transient T-lymphocyte depletion and Ag-specific T-cell proliferation*. *Int J Mol Med*, 2012. **29**(6): p. 1153-7.
110. Swann, J.B., et al., *Type I IFN Contributes to NK Cell Homeostasis, Activation, and Antitumor Function*. *The Journal of Immunology*, 2007. **178**(12): p. 7540.
111. Chang, L.C., et al., *IFNAR1 is a predictor for overall survival in colorectal cancer and its mRNA expression correlated with IRF7 but not TLR9*. *Medicine (Baltimore)*, 2014. **93**(29): p. e349.
112. Koromilas, A.E. and V. Sexl, *The tumor suppressor function of STAT1 in breast cancer*. *JAKSTAT*, 2013. **2**(2): p. e23353.
113. Bidwell, B.N., et al., *Silencing of Irf7 pathways in breast cancer cells promotes bone metastasis through immune escape*. *Nat Med*, 2012. **18**(8): p. 1224-31.
114. Sisirak, V., et al., *Plasmacytoid dendritic cells deficient in IFNalpha production promote the amplification of FOXP3(+) regulatory T cells and are associated with poor prognosis in breast cancer patients*. *Oncoimmunology*, 2013. **2**(1): p. e22338.
115. Treilleux, I., et al., *Dendritic cell infiltration and prognosis of early stage breast cancer*. *Clin Cancer Res*, 2004. **10**(22): p. 7466-74.
116. Bradley, J.D., et al., *A phase III comparison of radiation therapy with or without recombinant beta2-interferon for poor-risk patients with locally advanced non-small-cell lung cancer (RTOG 93-04)*. *International Journal of Radiation Oncology, Biology, Physics*, 2002. **52**(5): p. 1173-1179.

117. Mattson, K., et al., *Interferon Maintenance Therapy for Small Cell Lung Cancer: Improvement in Long-Term Survival*. Journal of Interferon & Cytokine Research, 1997. **17**(2): p. 103-105.
118. Tamura, T., et al., *The IRF family transcription factors in immunity and oncogenesis*. Annu Rev Immunol, 2008. **26**: p. 535-84.
119. Yanai, H., H. Negishi, and T. Taniguchi, *The IRF family of transcription factors: Inception, impact and implications in oncogenesis*. Oncoimmunology, 2012. **1**(8): p. 1376-1386.
120. Chistiakov, D.A., et al., *The impact of interferon-regulatory factors to macrophage differentiation and polarization into M1 and M2*. Immunobiology, 2018. **223**(1): p. 101-111.
121. Huang, J.X., et al., *IRF1 Negatively Regulates Oncogenic KPNA2 Expression Under Growth Stimulation and Hypoxia in Lung Cancer Cells*. Onco Targets Ther, 2019. **12**: p. 11475-11486.
122. Chan, Y.C., et al., *Overexpression of PSAT1 promotes metastasis of lung adenocarcinoma by suppressing the IRF1-IFN $\gamma$  axis*. Oncogene, 2020. **39**(12): p. 2509-2522.
123. Guichard, C., et al., *Integrated analysis of somatic mutations and focal copy-number changes identifies key genes and pathways in hepatocellular carcinoma*. Nat Genet, 2012. **44**(6): p. 694-8.
124. Liang, C., et al., *MicroRNA-18a-5p functions as an oncogene by directly targeting IRF2 in lung cancer*. Cell Death Dis, 2017. **8**(5): p. e2764.
125. Liu, F., et al., *Upregulation of microRNA-450 inhibits the progression of lung cancer in vitro and in vivo by targeting interferon regulatory factor 2*. Int J Mol Med, 2016. **38**(1): p. 283-90.
126. Honda, K. and T. Taniguchi, *IRFs: master regulators of signalling by Toll-like receptors and cytosolic pattern-recognition receptors*. Nat Rev Immunol, 2006. **6**(9): p. 644-58.
127. Csumita, M., et al., *Specific enhancer selection by IRF3, IRF5 and IRF9 is determined by ISRE half-sites, 5' and 3' flanking bases, collaborating transcription factors and the chromatin environment in a combinatorial fashion*. Nucleic Acids Res, 2020. **48**(2): p. 589-604.
128. Qian, Y., et al., *Interferon regulatory factor 4 (IRF4) is overexpressed in human non-small cell lung cancer (NSCLC) and activates the Notch signaling pathway*. Mol Med Rep, 2017. **16**(5): p. 6034-6040.
129. Bailey, C.M., et al., *Interferon regulatory factor 6 promotes cell cycle arrest and is regulated by the proteasome in a cell cycle-dependent manner*. Mol Cell Biol, 2008. **28**(7): p. 2235-43.
130. Liu, Y., et al., *Interferon regulatory factor 6 correlates with the progression of non-small cell lung cancer and can be regulated by miR-320*. J Pharm Pharmacol, 2021. **73**(5): p. 682-691.
131. Ning, S., J.S. Pagano, and G.N. Barber, *IRF7: activation, regulation, modification and function*. Genes Immun, 2011. **12**(6): p. 399-414.
132. Liang, J., et al., *IRF8 induces senescence of lung cancer cells to exert its tumor suppressive function*. Cell Cycle, 2019. **18**(23): p. 3300-3312.
133. Kimura, T., et al., *Essential and non-redundant roles of p48 (ISGF3  $\gamma$ ) and IRF-1 in both type I and type II interferon responses, as revealed by gene targeting studies*. Genes Cells, 1996. **1**(1): p. 115-24.
134. Paul, A., T.H. Tang, and S.K. Ng, *Interferon Regulatory Factor 9 Structure and Regulation*. Front Immunol, 2018. **9**: p. 1831.
135. Gupta, S., M. Jiang, and A.B. Pernis, *IFN- $\alpha$  activates Stat6 and leads to the formation of Stat2:Stat6 complexes in B cells*. J Immunol, 1999. **163**(7): p. 3834-41.
136. Weihua, X., et al., *Interleukin-6 modulates interferon-regulated gene expression by inducing the ISGF3 $\gamma$  gene using CCAAT/enhancer binding protein-beta (C/EBP- $\beta$ )*. Biochimica et Biophysica Acta (BBA) - Gene Structure and Expression, 2000. **1492**(1): p. 163-171.
137. Erb, H.H.H., et al., *IL6 sensitizes prostate cancer to the antiproliferative effect of IFN $\alpha$ 2 through IRF9*. Endocrine-related cancer, 2013. **20**(5): p. 677-689.
138. Matikainen, S., et al., *Retinoic acid induces signal transducer and activator of transcription (STAT) 1, STAT2, and p48 expression in myeloid leukemia cells and enhances their responsiveness to interferons*. 1997. **8**(6): p. 687-698.
139. Liao, L., et al., *Multiple tumor suppressors regulate a HIF-dependent negative feedback loop via ISGF3 in human clear cell renal cancer*. Elife, 2018. **7**.

140. Ganta Vijay, C., et al., *A MicroRNA93–Interferon Regulatory Factor-9–Immunoresponse Gene-1–Itaconic Acid Pathway Modulates M2-Like Macrophage Polarization to Revascularize Ischemic Muscle*. *Circulation*, 2017. **135**(24): p. 2403-2425.
141. Smith, S., et al., *MicroRNA-302d targets IRF9 to regulate the IFN-induced gene expression in SLE*. *Journal of Autoimmunity*, 2017. **79**: p. 105-111.
142. Huber, M., et al., *IRF9 Prevents CD8<sup>+</sup> T Cell Exhaustion in an Extrinsic Manner during Acute Lymphocytic Choriomeningitis Virus Infection*. *Journal of Virology*, 2017. **91**(22): p. e01219-17.
143. Fink, K. and N. Grandvaux, *STAT2 and IRF9: Beyond ISGF3*. *Jakstat*, 2013. **2**(4): p. e27521.
144. Suprunenko, T. and M.J. Hofer, *The emerging role of interferon regulatory factor 9 in the antiviral host response and beyond*. *Cytokine & Growth Factor Reviews*, 2016. **29**: p. 35-43.
145. Hernandez, N., et al., *Life-threatening influenza pneumonitis in a child with inherited IRF9 deficiency*. *J Exp Med*, 2018. **215**(10): p. 2567-2585.
146. Hofer, M.J., et al., *The type I interferon-alpha mediates a more severe neurological disease in the absence of the canonical signaling molecule interferon regulatory factor 9*. *J Neurosci*, 2010. **30**(3): p. 1149-57.
147. Oliver-Martos, B., et al., *Gene expression in IFN $\beta$  signalling pathway differs between monocytes, CD4 and CD8 T cells from MS patients*. *Journal of Neuroimmunology*, 2011. **230**(1): p. 153-159.
148. Tsuno, T., et al., *IRF9 is a key factor for eliciting the antiproliferative activity of IFN-alpha*. *J Immunother*, 2009. **32**(8): p. 803-16.
149. Tian, W.-L., et al., *The IRF9-SIRT1-P53 axis is involved in the growth of human acute myeloid leukemia*. *Experimental Cell Research*, 2018. **365**(2): p. 185-193.
150. Xue, B.H., et al., *A novel function of IRF9 in acute pancreatitis by modulating cell apoptosis, proliferation, migration, and suppressing SIRT1-p53*. *Mol Cell Biochem*, 2020.
151. Kolosenko, I., et al., *Cell crowding induces interferon regulatory factor 9, which confers resistance to chemotherapeutic drugs*. *Int J Cancer*, 2015. **136**(4): p. E51-61.
152. Zhang, S.-M., et al., *Interferon regulatory factor 9 is critical for neointima formation following vascular injury*. *Nature Communications*, 2014. **5**(1): p. 5160.
153. Chen, H.Z., et al., *A critical role for interferon regulatory factor 9 in cerebral ischemic stroke*. *J Neurosci*, 2014. **34**(36): p. 11897-912.
154. Zhang, Y., et al., *Interferon regulatory factor 9 is an essential mediator of heart dysfunction and cell death following myocardial ischemia/reperfusion injury*. *Basic Res Cardiol*, 2014. **109**(5): p. 434.
155. Wang, P.-X., et al., *Interferon regulatory factor 9 is a key mediator of hepatic ischemia/reperfusion injury*. *Journal of Hepatology*, 2015. **62**(1): p. 111-120.
156. Rahmani, M., et al., *Versican: signaling to transcriptional control pathways*. *Can J Physiol Pharmacol*, 2006. **84**(1): p. 77-92.
157. Naso, M.F., D.R. Zimmermann, and R.V. Iozzo, *Characterization of the complete genomic structure of the human versican gene and functional analysis of its promoter*. *J Biol Chem*, 1994. **269**(52): p. 32999-3008.
158. Wight, T.N., *Versican: a versatile extracellular matrix proteoglycan in cell biology*. *Current Opinion in Cell Biology*, 2002. **14**(5): p. 617-623.
159. Sheng, W., et al., *The roles of versican V1 and V2 isoforms in cell proliferation and apoptosis*. *Mol Biol Cell*, 2005. **16**(3): p. 1330-40.
160. Chang, M.Y., et al., *Versican is produced by Trif- and type I interferon-dependent signaling in macrophages and contributes to fine control of innate immunity in lungs*. *Am J Physiol Lung Cell Mol Physiol*, 2017. **313**(6): p. L1069-L1086.
161. LaPierre, D.P., et al., *The ability of versican to simultaneously cause apoptotic resistance and sensitivity*. *Cancer Res*, 2007. **67**(10): p. 4742-50.
162. Ricciardelli, C., et al., *The biological role and regulation of versican levels in cancer*. *Cancer and Metastasis Reviews*, 2009. **28**(1): p. 233.

163. Suwan, K., et al., *Versican/PG-M Assembles Hyaluronan into Extracellular Matrix and Inhibits CD44-mediated Signaling toward Premature Senescence in Embryonic Fibroblasts*. *Journal of Biological Chemistry*, 2009. **284**(13): p. 8596-8604.
164. Wight, T.N., I. Kang, and M.J. Merrilees, *Versican and the control of inflammation*. *Matrix Biology*, 2014. **35**: p. 152-161.
165. Du, W.W., W. Yang, and A.J. Yee, *Roles of versican in cancer biology--tumorigenesis, progression and metastasis*. *Histol Histopathol*, 2013. **28**(6): p. 701-13.
166. Pirinen, R., et al., *Versican in nonsmall cell lung cancer: relation to hyaluronan, clinicopathologic factors, and prognosis*. *Human Pathology*, 2005. **36**(1): p. 44-50.
167. Du, W.W., et al., *The role of versican G3 domain in regulating breast cancer cell motility including effects on osteoblast cell growth and differentiation in vitro - evaluation towards understanding breast cancer cell bone metastasis*. *BMC Cancer*, 2012. **12**: p. 341.
168. Asano, K., et al., *Stromal Versican Regulates Tumor Growth by Promoting Angiogenesis*. *Scientific Reports*, 2017. **7**(1): p. 17225.
169. Yang, W. and A.J. Yee, *Versican V2 isoform enhances angiogenesis by regulating endothelial cell activities and fibronectin expression*. *FEBS Letters*, 2013. **587**(2): p. 185-192.
170. Giopanou, I., et al., *Tumor-derived osteopontin isoforms cooperate with TRP53 and CCL2 to promote lung metastasis*. *Oncolmmunology*, 2017. **6**(1): p. e1256528.
171. Agalioti, T., et al., *Mutant KRAS promotes malignant pleural effusion formation*. *Nat Commun*, 2017. **8**: p. 15205.
172. Livak, K.J. and T.D. Schmittgen, *Analysis of Relative Gene Expression Data Using Real-Time Quantitative PCR and the 2- $\Delta\Delta$ CT Method*. *Methods*, 2001. **25**(4): p. 402-408.
173. Bioinformatics, B., *FastQC: a quality control tool for high throughput sequence data*. Cambridge, UK: Babraham Institute, 2011.
174. Davis, M.P.A., et al., *Kraken: a set of tools for quality control and analysis of high-throughput sequence data*. *Methods (San Diego, Calif.)*, 2013. **63**(1): p. 41-49.
175. Dobin, A., et al., *STAR: ultrafast universal RNA-seq aligner*. *Bioinformatics*, 2012. **29**(1): p. 15-21.
176. Liao, Y., G.K. Smyth, and W. Shi, *featureCounts: an efficient general purpose program for assigning sequence reads to genomic features*. *Bioinformatics*, 2013. **30**(7): p. 923-930.
177. Love, M.I., W. Huber, and S. Anders, *Moderated estimation of fold change and dispersion for RNA-seq data with DESeq2*. *Genome Biology*, 2014. **15**(12): p. 550.
178. *Activities at the Universal Protein Resource (UniProt)*. *Nucleic Acids Res*, 2014. **42**(Database issue): p. D191-8.
179. Gyorffy, B., et al., *Online survival analysis software to assess the prognostic value of biomarkers using transcriptomic data in non-small-cell lung cancer*. *PLoS One*, 2013. **8**(12): p. e82241.
180. Goldman, M.J., et al., *Visualizing and interpreting cancer genomics data via the Xena platform*. *Nature Biotechnology*, 2020. **38**(6): p. 675-678.
181. Heinz, S., et al., *Simple combinations of lineage-determining transcription factors prime cis-regulatory elements required for macrophage and B cell identities*. *Mol Cell*, 2010. **38**(4): p. 576-89.
182. Dreos, R., et al., *The Eukaryotic Promoter Database: expansion of EPDnew and new promoter analysis tools*. *Nucleic Acids Res*, 2015. **43**(Database issue): p. D92-6.
183. Grant, C.E., T.L. Bailey, and W.S. Noble, *FIMO: scanning for occurrences of a given motif*. *Bioinformatics*, 2011. **27**(7): p. 1017-8.
184. Savai, R., et al., *Pro-proliferative and inflammatory signaling converge on FoxO1 transcription factor in pulmonary hypertension*. *Nat Med*, 2014. **20**(11): p. 1289-300.
185. Schmall, A., et al., *Macrophage and cancer cell cross-talk via CCR2 and CX3CR1 is a fundamental mechanism driving lung cancer*. *Am J Respir Crit Care Med*, 2015. **191**(4): p. 437-47.

186. Olesch, C., et al., *MPGES-1-derived PGE2 suppresses CD80 expression on tumor-associated phagocytes to inhibit anti-tumor immune responses in breast cancer*. *Oncotarget*, 2015. **6**(12): p. 10284-10296.
187. Brockwell, N.K., et al., *Tumor inherent interferon regulators as biomarkers of long-term chemotherapeutic response in TNBC*. *npj Precision Oncology*, 2019. **3**(1): p. 21.
188. Qu, Z., et al., *Interleukin-6 Prevents the Initiation but Enhances the Progression of Lung Cancer*. *Cancer research*, 2015. **75**(16): p. 3209-3215.
189. Weichselbaum, R.R., et al., *An interferon-related gene signature for DNA damage resistance is a predictive marker for chemotherapy and radiation for breast cancer*. *Proceedings of the National Academy of Sciences*, 2008. **105**(47): p. 18490.
190. Boelens, Mirjam C., et al., *Exosome Transfer from Stromal to Breast Cancer Cells Regulates Therapy Resistance Pathways*. *Cell*, 2014. **159**(3): p. 499-513.
191. Moncho-Amor, V., et al., *DUSP1/MKP1 promotes angiogenesis, invasion and metastasis in non-small-cell lung cancer*. *Oncogene*, 2011. **30**(6): p. 668-78.
192. Shen, J., et al., *Role of DUSP1/MKP1 in tumorigenesis, tumor progression and therapy*. *Cancer medicine*, 2016. **5**(8): p. 2061-2068.
193. Luo, A., et al., *The clinical significance of FSCN1 in non-small cell lung cancer*. *Biomedicine & Pharmacotherapy*, 2015. **73**: p. 75-79.
194. Zhang, Y., et al., *MicroRNA-145 inhibits migration and invasion via inhibition of fascin 1 protein expression in non-small-cell lung cancer cells*. *Mol Med Rep*, 2015. **12**(4): p. 6193-8.
195. Gong, F., et al., *Cathepsin B as a potential prognostic and therapeutic marker for human lung squamous cell carcinoma*. *Molecular Cancer*, 2013. **12**(1): p. 125.
196. Chen, Q., et al., *Detection of cathepsin B, cathepsin L, cystatin C, urokinase plasminogen activator and urokinase plasminogen activator receptor in the sera of lung cancer patients*. *Oncology letters*, 2011. **2**(4): p. 693-699.
197. Chen, Y., et al., *IGFBP7 is a p53 target gene inactivated in human lung cancer by DNA hypermethylation*. *Lung Cancer*, 2011. **73**(1): p. 38-44.
198. Ruan, W., et al., *IGFBP7 plays a potential tumor suppressor role in colorectal carcinogenesis*. *Cancer Biol Ther*, 2007. **6**(3): p. 354-9.
199. Ketchart, W., et al., *Inhibition of metastasis by HEXIM1 through effects on cell invasion and angiogenesis*. *Oncogene*, 2013. **32**(33): p. 3829-3839.
200. Lin, X., et al., *HEXIM1 as a Robust Pharmacodynamic Marker for Monitoring Target Engagement of BET Family Bromodomain Inhibitors in Tumors and Surrogate Tissues*. *Molecular Cancer Therapeutics*, 2017. **16**(2): p. 388.
201. Tian, F.M., et al., *PDE3A is hypermethylated in cisplatin resistant non-small cell lung cancer cells and is a modulator of chemotherapy response*. *Eur Rev Med Pharmacol Sci*, 2017. **21**(11): p. 2635-2641.
202. Xiang, R., et al., *Circadian clock gene Per2 downregulation in non-small cell lung cancer is associated with tumour progression and metastasis*. *Oncol Rep*, 2018. **40**(5): p. 3040-3048.
203. Yang, R.-W., et al., *TLE3 represses colorectal cancer proliferation by inhibiting MAPK and AKT signaling pathways*. *Journal of experimental & clinical cancer research : CR*, 2016. **35**(1): p. 152-152.
204. Younes, M., et al., *Neurotensin (NTS) and its receptor (NTSR1) causes EGFR, HER2 and HER3 over-expression and their autocrine/paracrine activation in lung tumors, confirming responsiveness to erlotinib*. *Oncotarget*, 2014. **5**(18): p. 8252-8269.
205. Zhang, J., S. Hu, and Y. Li, *KRT18 is correlated with the malignant status and acts as an oncogene in colorectal cancer*. *Bioscience reports*, 2019. **39**(8): p. BSR20190884.
206. Zhang, R., et al., *Increased sensitivity of human lung adenocarcinoma cells to cisplatin associated with downregulated contactin-1*. *Biomed Pharmacother*, 2015. **71**: p. 172-84.
207. Chen, N., et al., *Overexpression of Contactin 1 promotes growth, migration and invasion in Hs578T breast cancer cells*. *BMC Cell Biology*, 2018. **19**(1): p. 5.

208. Lang, Y., et al., [*EFEMP1 suppresses growth and invasion of lung cancer cells by downregulating matrix metalloproteinase-7 expression*]. *Zhongguo Fei Ai Za Zhi*, 2015. **18**(2): p. 92-7.
209. Bergholz, J. and Z.-X. Xiao, *Role of p63 in Development, Tumorigenesis and Cancer Progression*. *Cancer microenvironment : official journal of the International Cancer Microenvironment Society*, 2012. **5**(3): p. 311-322.
210. Chiu, K.-L., et al., *ADAM9 enhances CDCP1 protein expression by suppressing miR-218 for lung tumor metastasis*. *Scientific Reports*, 2015. **5**(1): p. 16426.
211. Liu, X., et al., *MiR-137 and its target TGFA modulate cell growth and tumorigenesis of non-small cell lung cancer*. *Eur Rev Med Pharmacol Sci*, 2017. **21**(3): p. 511-517.
212. Liu, Y., et al., *Cancer progression is mediated by proline catabolism in non-small cell lung cancer*. *Oncogene*, 2020. **39**(11): p. 2358-2376.
213. Shan, C., et al., *4-hydroxyphenylpyruvate dioxygenase promotes lung cancer growth via pentose phosphate pathway (PPP) flux mediated by LKB1-AMPK/HDAC10/G6PD axis*. *Cell Death Dis*, 2019. **10**(7): p. 525.
214. Guo, R., et al., *Discovery of ERBB3 inhibitors for non-small cell lung cancer (NSCLC) via virtual screening*. *J Mol Model*, 2016. **22**(6): p. 135.
215. Zhou, X., et al., *CASTOR1 suppresses the progression of lung adenocarcinoma and predicts poor prognosis*. *J Cell Biochem*, 2018. **119**(12): p. 10186-10194.
216. Kim, H., et al., *The DUSP26 phosphatase activator adenylate kinase 2 regulates FADD phosphorylation and cell growth*. *Nature communications*, 2014. **5**: p. 3351-3351.
217. Yu, W., et al., *A novel amplification target, DUSP26, promotes anaplastic thyroid cancer cell growth by inhibiting p38 MAPK activity*. *Oncogene*, 2007. **26**(8): p. 1178-1187.
218. Sun, G.G., et al., *Epithelial membrane protein 1 negatively regulates cell growth and metastasis in colorectal carcinoma*. *World J Gastroenterol*, 2014. **20**(14): p. 4001-10.
219. Sun, G.G., et al., *EMP1, a member of a new family of antiproliferative genes in breast carcinoma*. *Tumour Biol*, 2014. **35**(4): p. 3347-54.
220. Darido, C., et al., *Targeting of the tumor suppressor GRHL3 by a miR-21-dependent proto-oncogenic network results in PTEN loss and tumorigenesis*. *Cancer Cell*, 2011. **20**(5): p. 635-48.
221. Wang, X.-k., et al., *Knockdown of GRHL3 inhibits activities and induces cell cycle arrest and apoptosis of human colorectal cancer cells*. *Current Medical Science*, 2017. **37**(6): p. 880-885.
222. Zhao, P., et al., *Grhl3 induces human epithelial tumor cell migration and invasion via downregulation of E-cadherin*. *Acta biochimica et biophysica Sinica*, 2016. **48**(3): p. 266-274.
223. Wang, J., et al., *Gene expression and prognosis of insulin-like growth factor-binding protein family members in non-small cell lung cancer*. *Oncology reports*, 2019. **42**(5): p. 1981-1995.
224. Akkiprik, M., et al., *The subcellular localization of IGFBP5 affects its cell growth and migration functions in breast cancer*. *BMC Cancer*, 2009. **9**(1): p. 103.
225. Sureshbabu, A., et al., *IGFBP5 induces cell adhesion, increases cell survival and inhibits cell migration in MCF-7 human breast cancer cells*. *Journal of Cell Science*, 2012. **125**(7): p. 1693.
226. Yu, P., et al., *High Expression of the SH3TC2-DT/SH3TC2 Gene Pair Associated With FLT3 Mutation and Poor Survival in Acute Myeloid Leukemia: An Integrated TCGA Analysis*. *Frontiers in Oncology*, 2020. **10**: p. 829.
227. Fils-Aimé, N., et al., *MicroRNA-584 and the protein phosphatase and actin regulator 1 (PHACTR1), a new signaling route through which transforming growth factor- $\beta$  Mediates the migration and actin dynamics of breast cancer cells*. *The Journal of biological chemistry*, 2013. **288**(17): p. 11807-11823.
228. Wang, X.-P., X.-L. Deng, and L.-Y. Li, *MicroRNA-584 functions as a tumor suppressor and targets PTTG1IP in glioma*. *International journal of clinical and experimental pathology*, 2014. **7**(12): p. 8573-8582.

229. Ueno, K., et al., *Tumour suppressor microRNA-584 directly targets oncogene Rock-1 and decreases invasion ability in human clear cell renal cell carcinoma*. British Journal of Cancer, 2011. **104**(2): p. 308-315.
230. Luo, S., et al., *Long non-coding RNA TP73-AS1 accelerates the progression and cisplatin resistance of non-small cell lung cancer by upregulating the expression of TRIM29 via competitively targeting microRNA-34a-5p*. Mol Med Rep, 2020. **22**(5): p. 3822-3832.
231. Zhou, Z.-Y., et al., *Significance of TRIM29 and  $\beta$ -catenin expression in non-small-cell lung cancer*. Journal of the Chinese Medical Association, 2012. **75**(6): p. 269-274.
232. Creighton, C.J., et al., *Analysis of Tumor-Host Interactions by Gene Expression Profiling of Lung Adenocarcinoma Xenografts Identifies Genes Involved in Tumor Formation*. Molecular Cancer Research, 2005. **3**(3): p. 119.
233. Wang, Z., et al., *Versican silencing improves the antitumor efficacy of endostatin by alleviating its induced inflammatory and immunosuppressive changes in the tumor microenvironment*. Oncol Rep, 2015. **33**(6): p. 2981-2991.
234. Moerkens, M., et al., *Epidermal growth factor receptor signalling in human breast cancer cells operates parallel to estrogen receptor  $\alpha$  signalling and results in tamoxifen insensitive proliferation*. BMC Cancer, 2014. **14**(1): p. 283.
235. Sheng, G., et al., *Epidermal growth factor receptor-mediated proliferation of enterocytes requires p21waf1/cip1 expression*. Gastroenterology, 2006. **131**(1): p. 153-64.
236. Georgakilas, A.G., O.A. Martin, and W.M. Bonner, *p21: A Two-Faced Genome Guardian*. Trends Mol Med, 2017. **23**(4): p. 310-319.
237. Galanos, P., et al., *Chronic p53-independent p21 expression causes genomic instability by deregulating replication licensing*. Nat Cell Biol, 2016. **18**(7): p. 777-89.
238. Nara, Y., et al., *Immunohistochemical localization of extracellular matrix components in human breast tumours with special reference to PG-M/versican*. Histochem J, 1997. **29**(1): p. 21-30.
239. Harris, J.E., Jr., et al., *A murine xenograft model of spontaneous metastases of human lung adenocarcinoma*. The Journal of surgical research, 2011. **171**(1): p. e75-e79.
240. Rauch, I., et al., *Noncanonical Effects of IRF9 in Intestinal Inflammation: More than Type I and Type III Interferons*. Molecular and cellular biology, 2015. **35**(13): p. 2332-2343.
241. Ohri, C.M., et al., *Chemokine receptor expression in tumour islets and stroma in non-small cell lung cancer*. BMC Cancer, 2010. **10**(1): p. 172.
242. Groom, J.R. and A.D. Luster, *CXCR3 ligands: redundant, collaborative and antagonistic functions*. Immunol Cell Biol, 2011. **89**(2): p. 207-15.
243. Morimoto, Y., et al., *Interferon- $\beta$  signal may up-regulate PD-L1 expression through IRF9-dependent and independent pathways in lung cancer cells*. Biochemical and Biophysical Research Communications, 2018. **507**(1): p. 330-336.
244. Fabbi, M., G. Carbotti, and S. Ferrini, *Context-dependent role of IL-18 in cancer biology and counter-regulation by IL-18BP*. J Leukoc Biol, 2015. **97**(4): p. 665-75.
245. Evanko, S.P., et al., *Hyaluronan and versican in the control of human T-lymphocyte adhesion and migration*. Matrix Biology, 2012. **31**(2): p. 90-100.
246. Potter-Perigo, S., et al., *Polyinosine-polycytidylic acid stimulates versican accumulation in the extracellular matrix promoting monocyte adhesion*. Am J Respir Cell Mol Biol, 2010. **43**(1): p. 109-20.

## 9. Statement of Authenticity

“I declare that I have completed this dissertation single-handedly without the unauthorized help of a second party and only with the assistance acknowledged therein. I have appropriately acknowledged and cited all text passages that are derived verbatim from or are based on the content of published work of others, and all information relating to verbal communications. I consent to the use of an anti-plagiarism software to check my thesis. I have abided by the principles of good scientific conduct laid down in the charter of the Justus Liebig University Giessen “Satzung der Justus-Liebig-Universität Gießen zur Sicherung guter wissenschaftlicher Praxis” in carrying out the investigations described in the dissertation.”

---

Name

---

Signature

## 10. Acknowledgement

I would like to express my sincere gratitude to everyone contributing to this thesis.

First, I would like to thank Prof. Dr. Werner Seeger for giving me the opportunity to perform my studies in his department at the Max-Planck-Institute for Heart and Lung Research in Bad Nauheim.

I would like to express my gratitude to my supervisor Prof. Dr. Reinhard Dammann for his friendly support and interest during my thesis.

I am truly grateful to Prof. Dr. Rajkumar Savai for welcoming me in his lab group and the chance to start my studies. My PhD would not have been possible without his support throughout my years at the institute. I appreciate the discussions and exchanges we had and the freedom to develop scientifically.

Within my studies, I received scientific support from many scientists, therefore, I would like to thank Prof. Dr. Soni Pullamsetti for her valuable input, Prof. Dr. Magdalena Huber for her expertise in the IRF family, and Prof. Dr. Andreas Weigert for the FACS analyses. Prof. Dr. Georgios Stathopoulos for the expertise around VCAN, Dr. Stefan Günther for the RNA-Seq analysis and PD Dr. Thomas Böttger for his support in the PhD committee.

I would like to thank the faculty of the post-graduate programme Molecular Biology and Medicine of the Lung (MBML) for the excellent training and inspiring retreats, especially Prof. Dr. Rory Morty and Jun.-Prof. Dr. Elie El Agha.

My warmest thanks goes to my lab mates and all colleagues from our department for the great time together, especially Dr. Kati Turkowski, Annika Karger, Xiang Zheng, Siavash Mansouri, Dr. Stephanie Dobersch, Dr. Nefertiti El-Nikhely, Dr. Ylia Salazar, Martin Schreck, Vanessa Golchert, Marianne Hoeck, Yanina Knepper, Jeannette Knepper, and Monika Haselbauer. You have been valuable help in all lab-related matters as well as in all non-lab-related matters and made lonely poster sessions appear shorter than they were.

Finally, my deepest gratitude goes to my friends and family, especially to my parents for their constant support and understanding. I would like to thank my wife Daniela in particular. Thank you for your unconditional love, unshakeable faith and all the patience you had to have with me.

## **11. Curriculum Vitae**

Curriculum Vitae has been removed from digital version.

Curriculum Vitae has been removed from digital version.

Curriculum Vitae has been removed from digital version.